Molecular Photovoltaic Systems Based on Phospholipids/Alkanethiol Hybrid Bilayer Membranes: Photocurrent Generation and Modulation

by

Hong Xie

A dissertation submitted to the Graduate Faculty of
Auburn University
in partial fulfillment of the
requirements for the Degree of
Doctor of Philosophy

Auburn, Alabama
August 4, 2012

Keywords: Molecular Photovoltaic Cell, Self-Assembly Technology,
Lipids Chemistry, Hybrid Bilayer Membrane

Approved by

Wei Zhan, Chair, Assistant Professor of Chemistry and Biochemistry
Vince Cammarata, Associate Professor of Chemistry and Biochemistry
Jeffrey Fergus, Professor of Materials Engineering
Curtis Shannon, Professor of Chemistry and Biochemistry

Abstract

Biological membranes offer an ideal place to assemble necessary components for plant photosynthesis in nature and suggest new strategies to build artificial photosynthetic systems by using lipid bilayers. In this dissertation, we develop a novel artificial photovoltaic system based on a hybrid bilayer membrane (HBM). The hybrid bilayer membrane is composed of a self-assembled monolayer (SAM) of alkanethiols on Au substrate and another monolayer of palmitoyloleoyl-phosphatidylcholine (POPC) phospholipids. The structure of the hybrid bilayer membrane is characterized by cyclic voltammetry (CV), quartz crystal microbalance (QCM) and impedance spectroscopy. We observe the photocurrent generation by incorporating either ruthenium tris(bipyridyl) complexes ($Ru(bpy)_3^{2+}$) or monomalonic fullerenes (C_{63}) as photoagents with the hybrid bilayer membrane. By modifying SAM with functionalized alkanthiols, we could modulate the photocurrent and photovoltage. The photocurrent generation and electron transfer mechanisms of this new system provide potential usefulness in the fundamental photoconversion study.

In an effort to present the thesis in as a clear manner as possible, this synopsis provides a brief summary of the chapters and contents.

Chapter 1 provides the motivation of the studies and contains an introduction of lipid bilayer membranes and their application towards artificial photosynthesis.

Chapter 2 describes the preparation of photoagents embedded liposomes and presents general analytical methods to characterize the HBM.

Chapter 3 studies photocurrent generation on unsubstituted alkanethiol SAMs based HBM systems.

Chapter 4 investigates photocurrent modulation by ferrocene terminated alkanethiols based HBM systems.

Chapter 5 explores the dipole effect of alkenthiols on different photoagents embedded HBM systems.

Chapter 6 is a conclusion of the thesis, presents existing issues, and provides an outline for possible future directions that would follow this work.

Acknowledgments

I would like to express my deepest appreciation to Dr. Wei Zhan for his continuous guidance, patience, support and providing me with an excellent atmosphere for doing research during the Ph.D period at Auburn University. I would like to thank all my committee members, Dr. Vince Cammarata, Dr. Jeffrey Fergus, and Dr. Curtis Shannon for their valuable suggestions in the course of my research. I would like to thank my outside reader Dr. Minseo Park for his participation in evaluating my work. I would also like to thank Dr. Anne Gorden for her permission to use UV-vis spectroscopy; Dr John Gorden for his suggestions for operating glovebox; Dr. Peter Livant for his help of $Ru(bpy)_3^{2+}$-DOPE NMR analysis; Dr. Yonnie Wu for his assistance in MS analysis. I am very thankful to my colleagues in Dr. Zhan's group: Dr. Kai Jiang, Dr. Chenguo Hu, Ms. Lixia Liu.

I would like to thank my parents, for their support and encouragement during my graduate studies. At Last, my greatest thanks to my husband Xuefeng Yu, for his encourage and support during my graduate study.

Table of Contents

List of Tables

List of Figures

List of Abbreviations

HBM	hybrid bilayer membrane
SAM	self-assembled monolayer
POPC	1-palmitoyl-2-oleoyl-sn-glycero-3-phophocholine
CV	cyclic voltammetry
QCM	quartz crystal microbalance
PC	L-α-phosphatidylcholine (Egg, Chicken)
BLM	black lipid membranes
$Ru(bpy)_3^{2+}$	ruthenium tris(bipyridyl) complexes
C_{63}	monomalonic fullerenes
ET	electron transfer
$C_{12}SH$	1-dodecanethiol
C_6SH	1-hexanethiol
$C_{18}SH$	1-octadecanethiol,
$Fc\text{-}C_{11}SH$	11-ferrocenyl undecanethiol
$C_{10}F_{17}SH$	1H,1H,2H,2H-perfluorodecanethiol

Chapter One

1.1 Introduction

Sunlight is our ultimate energy source. Solar energy can potentially cut our dependence on fossil fuels. Inspired by natural photosynthesis, artificial photosynthetic systems are proposed to convert and store solar energy[1]. A plausible artificial photosynthetic system should consist[2]: (1) antenna molecules to absorb photons; (2) a reaction center for charge separation (electron-hole pair); (3) an interface to physically separate the products. A number of organic molecules have been synthesized to work as antenna molecules and reaction centers[3]. For example, many porphyrin-fullerene moieties[4] are often synthesized as charge-separation devices with high efficient photo absorption and long-lived charge-separated states. However, an efficient artificial photosynthetic system must satisfy an important requirement – separate the oxidized and reduced products in order to avoid charge recombination. As occurs in natural systems, photosynthesis in plants takes place in chloroplasts which are surrounded by lipid bilayer membranes. Biological membranes offer an ideal place to assemble necessary components for plant photosynthesis and suggest new strategies to build artificial photosynthetic systems by using lipid bilayers. (Figure 1.1)

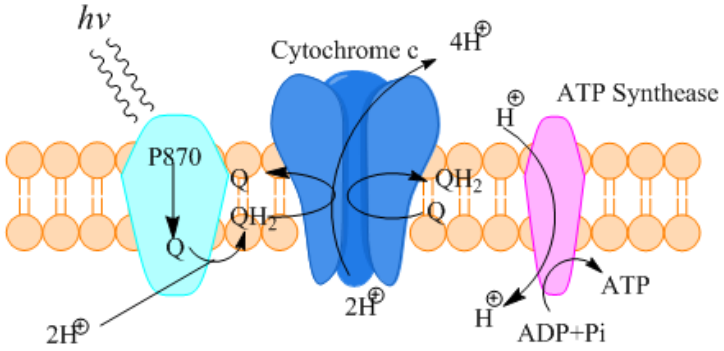

Figure 1.1 Illustration of lipid bilayer membrane for photosynthesis.

1.1.2 The Roles of Lipid Bilayer in Photosynthesis

There has been a lasting interest in better understanding the mechanisms of how photosynthetic organisms capture and store the solar energy[5]. All photosynthetic organisms contain antenna molecules and reaction centers embedded in a lipid bilayer process[6]. It is this assembled structure that help to keep ions, proteins and pigments where they are needed to be; in addition, it functions as a semi-permeable barrier and plays important roles in the signal tranduction in living organisms.

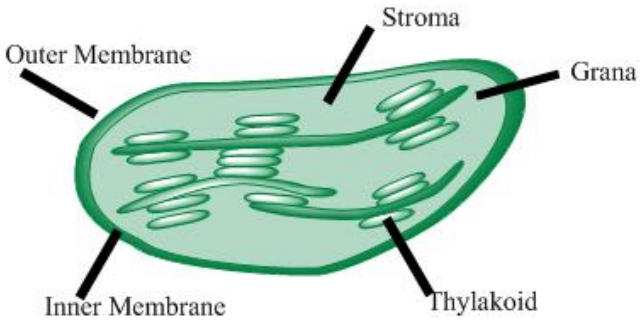

Figure 1.2 Illustration of thylakoids inside a chloroplast

Photosynthesis in green plants, the photosynthetic process takes place in thylakoids inside the chloroplasts[7] which are lipid membranes embedded with photosynthetic pigments (Figure 1.2). They are arranged in the forms of stacks of disks referred as grana. The thylakoid membrane as an alternating pattern regulates photosystem II and photosystem I in the photosynthetic process (Figure 1.3). In photosystem II, light absorption induces an electron transfer from the excited state of one pigment system through a number of steps to oxidize a water molecule near the inner surface of the thylakoid membrane. On the other hand, electron transfer in photosystem I eventually leads to reduction of a carbon dioxide molecule, near the outer surface of the thylakoid membrane. Those reactions are facilitated by thermodynamically downhill electron transfer pathways in the form of an electrochemical gradient across membrane, which helps the photosynthetic systems to achieve a high photoconversion efficiency.

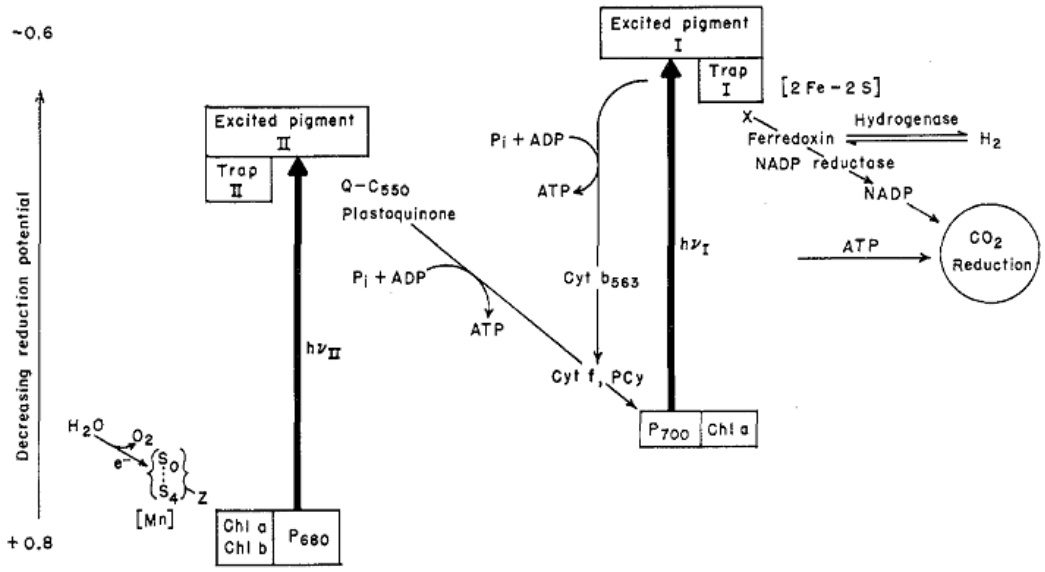

Figure 1.3 Illustration of photosynthetic electron transfer. Taken with permission from Ref.8[8].

Due to the structure of lipid bilayer, a defined spatial relationship of highly organized components can be created in the photosynthetic system, with a high photoconversion efficiency achieved. It is shown that it only requires one-millionth-millionth of a second to produce on molecule of oxygen from four photos of visible light[9].

1.1.3 Phospholipids and Lipid Bilayers

Phospholipids make up a major portion of many naturally occurring lipid structures. The most common phospholipid is phosphatidylcholine (PC) --- an amphiphilic molecule in which a glycerol bridge links a pair of hydrophobic alkyl hydrocarbon chains and a polar head group (Figure 1.4). Molecules of phospholipids normally are not soluble in water. Instead, they tend to align themselves closely to form planar bilayer sheets, or wrap up in the forms of vesicles in order to minimize the unfavorable interactions between water and alkyl hydrocarbon chains (Figure 1.3 a). Importantly, phospholipids are capable of organizing not only themselves but also associated other species either within the hydrophilic region or hydrophobic environment. Phospholipids can be obtained from natural sources (e.g. egg PC) as well as synthetic ways (e.g. POPC), but synthetic phospholipids are preferred due to their high purity.

One of the most import properties of a lipid bilayer is the fluidity, which refers to the mobility of individual phospholipid in the bilayer. For typical PC lipids, there exists a phase transition temperature, T_c, which is the critical temperature where the phospholipids undergo a phase change from a liquid crystalline (LC) phase to a gel phase. In the LC phase, the phospholipids can move laterally relatively freely through the planar sheet. In gel phase, however, the hydrophobic alkyl chains only occupy a relatively fixed position, exhibiting neither flip-flop nor lateral mobility. Just PC lipids, other types of phospholipids exhibit their own

transition temperatures. For example, for the most commonly phospholipid - 1-palmitoyl-2-oleoyl-*sn*-glycero-3-phophocholine (POPC), the transition tempreature is -2 ℃. For 1,2-dioleoyl-*sn*-glycero-3-phosphoethanolamine (DOPE), the transition temperature is -16 ℃. The influence of alkyl chain length and unsaturation level affect the transition temperature. The phase transitions and fluidity of phospholipids is important in the manufacture of liposomes, because the phase behavior of a lipid bilayer determines the permeability, fusion, and rapture of the vesicles, which can affect the interactions with biological systems. In order to keep the fluidity of the lipid bilayer, it is important to stay above all the transition tempreature of mixed phospholipids. In our case, we set the room tempreature (~20 ℃) for vesicle preparation.

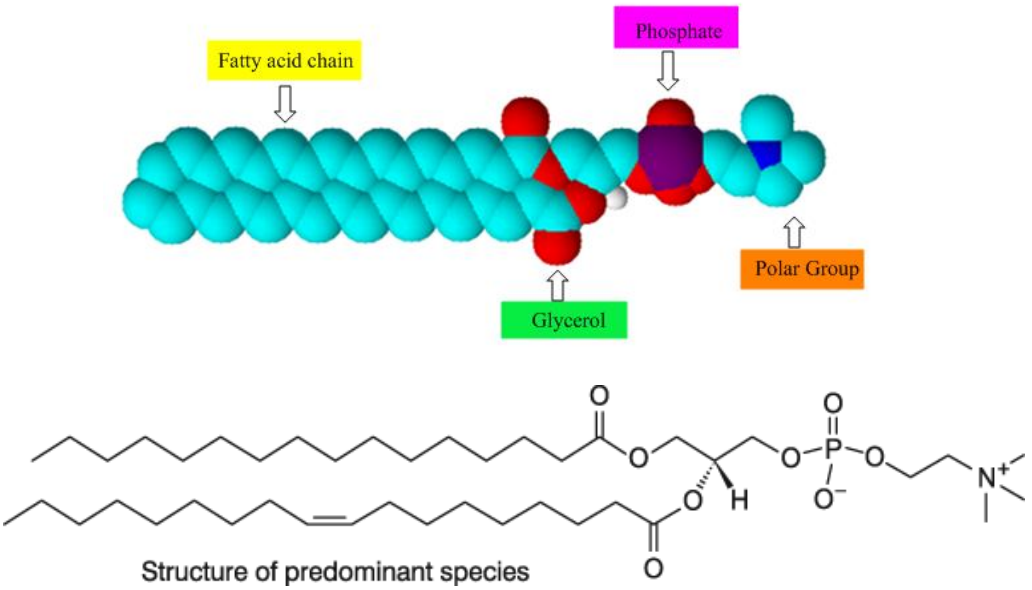

L-α-phosphatidylcholine (Egg, Chicken) (PC)

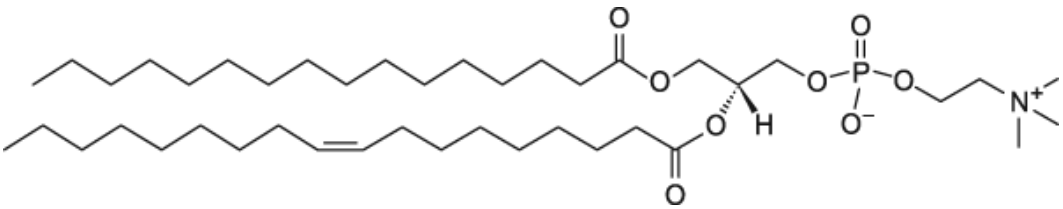

1-palmitoyl-2-oleoyl-*sn*-glycero-3-phophocholine (POPC)

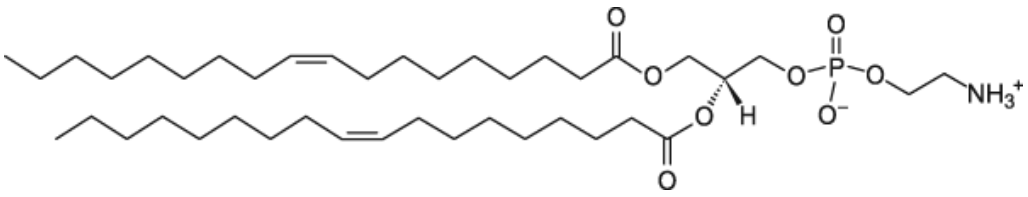

1,2-dioleoyl-*sn*-glycero-3-phosphoethanolamine (DOPE)

Figure 1.4 Illustration of the structure of phospholipids

Liposomes are simply spherical vesicles containing one or more bilayers of phospholipids. They can form spontaneously when dispersing phospholipids in aqueous media, producing vesicles with size ranging from tens of nanometers to tens of micrometers. Liposomes can form several types of vesicles: mulilamellar vesicles (MLVs), large unilamellar vesicles (LUVs) and small unilamellar vesicles (SUVs). The small unilamellar vesicles are referred as the lowest limit of size possible and with only a planar bilayer sheet surrounded phospholipid vesicles. The values of the unilamellar liposomes are that they can form lipid bilayers, which resembles cell membrane in some key aspects, such as fluidity, semi-permeability and bio-compatibility. Liposome and lipid bilayers have long been employed as general building blocks to mimic photosynthesis. Particularly, synthetic phospholipids such as POPC have been established as the primary elements for experimental models. In our lab, we have taken these advantages of the lipid bilayers and liposomes to organize different redox so a heterogeneous electrochemical distribution across the hydrophobic region and hydrophilic environment can be obtained.

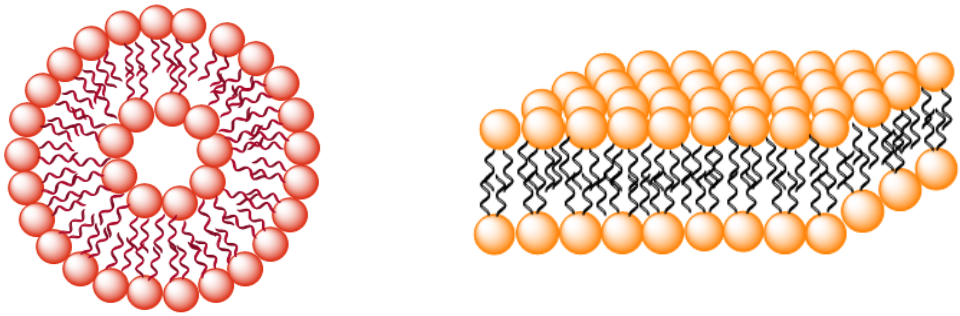

(a) **(b)**

Figure 1.5 Illustration of (a) the structure of a unilamellar liposome; (b) the structure of a lipid bilayer.

1.1.4 Building Artificial Photosynthetic System by Lipid Bilayers

By continuous exploration of natural photosynthesis[10], we can better understand the roles of lipid bilayers in the biological system. To this end, several types of artificial lipid bilayer systems have been developed in recent years.

1.1.4.1 Black Lipid Membranes

To investigate the electrical properties of a planar lipid bilayer, Mueller et al.[11] had developed the first black lipid membrane (BLM) system in the 1960s. In this system, there was a 1mm hole between two solution chambers, and the phospholipid molecules were painted across the hole. Mueller et al found out interference bands giving rise to color in the membrane during the formation of the lipid membranes. When the painted lipid mass became thinner, the interference effect disappeared. Under optical microscopy, this phenomenon was apparent and

indicated the formation of a single bilayer membrane. That was the reason why it was called black lipid membrane (BLM).

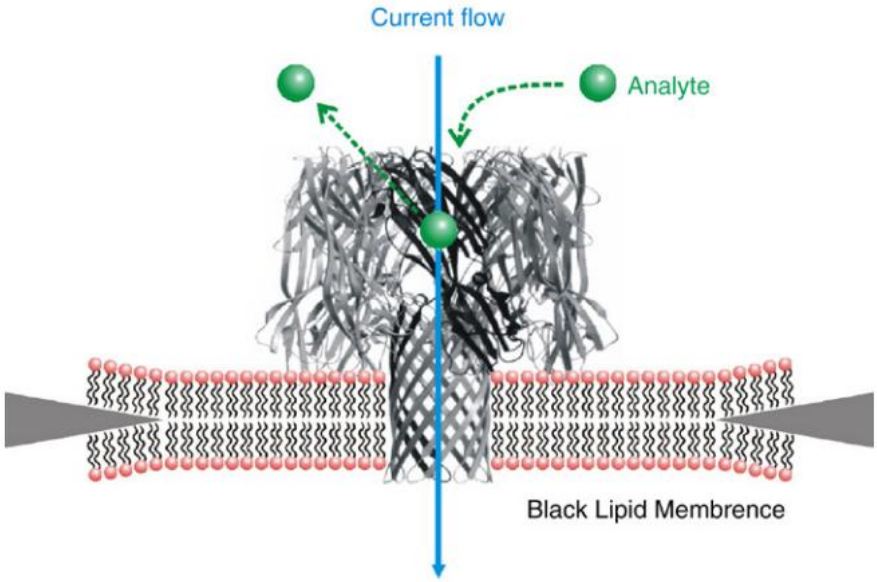

Figure 1.6 Illustration of a black lipid membrane. Taken with permission from Ref.12[12].

A planar black lipid membrane separates two aqueous solutions and has similar thickness to biological membranes. By measuring small changes in membrane capacitance, impedance and conductivity, the membranes and membrane phenomena can be precisely characterized[13]. By applying a single and varying electrical potential across the membrane, the charge character of ionic concentration gradients can be identified. By altering reactant concentrations, many membrane's parameters can be studied[14]. Anionic or cationic compounds can be used to transfer surface charge to BLM. A useful method to analyze BLM membrane is by spectroscopic methods. Several methods to produce black lipid membranes have been developed[15]. The

common part is to form a membrane over a small aperture and the typical aperture diameter is less than 1mm. There are two compartments filled with aqueous solutions, and each compartment has a reference electrode built inside. The wall separating two compartments is made of hydrophobic materials, such as polyethylene and Teflon, and that's the place where the hole is located. Among all the methods, the most popular one is by painting the lipid solution over the aperture and the other is forming a folded bilayer. The generated bilayer is suspended over the aperture and each side is an aqueous compartment.

Using black lipid membranes (BLMs), Fendler's group produced a series of biomimetic photosynthetic systems in the 1980-90s[16]. For example, a lipid bilayer is formed inside a small hole on a Teflon sheet partitioning two sample chambers. The sensitizer, $Ru(bpy)_3^{2+}$ was bouned either on the surface or in the interior of the lipid bilayers, because the lipid bilayer can act as an effective barrier to suppress the unwanted charge recombination. The acceptor methylviologen, MV^{2+} was localized at the outer surface in aqueous media. This system enables photocurrents and photovoltages to be measured via two reference electrodes. an efficient photoconversion following the initial photoinduced electron transfer has been observed[17].

However, there are some difficulties to model BLMs as a biological membrane[18]. During the preparation period, relatively large amount of solvents are left in the membrane, and it's hard to know their exact composition. Due to the small area of BLMs, measuring diffusion rate and chemical reaction rate is not practical. Also membranes with size of 3 mm or above ~~is~~ are not stable over long period. Finally, BLMs cannot be used to perform biological binding studies.

1.1.4.2 Lipid Vesicles

Lipid vesicles represent another model biomembrane system and exhibit some advantages over black lipid membrane. Lipid vesicle is kind of spherical bilayer lipid membrane and it contains a small volume aqueous solution in the center (Figure 1.5). Usually the combine surface area of lipid vesicle is 10 times larger than BLM and they are also very stable. These properties render them suitable for diffusion and spectrophotometric measurements[13]. The binding and gas evolution can also be studied. There are full spectrum tools to study their characters, including ultra-centrifugation, gel filtration, electrophoresis, calorimetry, fluorescence, nuclear magnetic resonance, electron spin resonance[19]. The lipid vesicle can mimic many biological membrances for their asymmetrical structure, electrostatic and other orientation factors. The best part of it is that they can be generated precisely with defined composition and there is no need of extraneous materials. However, to accurately estimate and measure the area and volume is difficult[19]. And the vesicle interior solution cannot be easily altered once they are been generated and electrical measurement cannot be performed across these bilayers.

Lipid vesicles have been investigated in the study of photo-induced transfer[20]. Calvin and coworkers were among the first people recognizing the utility of lipid vesicles in building artificial photosynthetic systems[8, 21]. They showed that efficient photosensitized electron transfer across a lipid bilayer could be established between membrane-bound ruthenium tris(bipyridyl) complexes and aqueous viologen and EDTA. More significantly, an artificial photosynthetic system mimicking natural photosynthesis based lipid vesicle has been built by Gust, Moore and Moore[22]. They built the system base liposomes that were prepared from a liquid mixture that contained the lipid-soluble 2,5-diphenylbenzoquinone, Qs, and pyraninetrisulfonate (PS), a quinone-porphyrin-carotene triad conjugate as a reaction center and a water-soluble dye whose fluorescence indicates the pH of the solution. A vectorial electron and proton transport were

achieved by inserting the lipophilic carotenoid into the oily part of the lipid and the negatively charged carboxylate group close to the quinone resides near the outside of the liposome surface. In this system, a photo gradient is produced between the outside and inside aqueous media of the liposme which drive ATP synthesis at the liposome hosts.

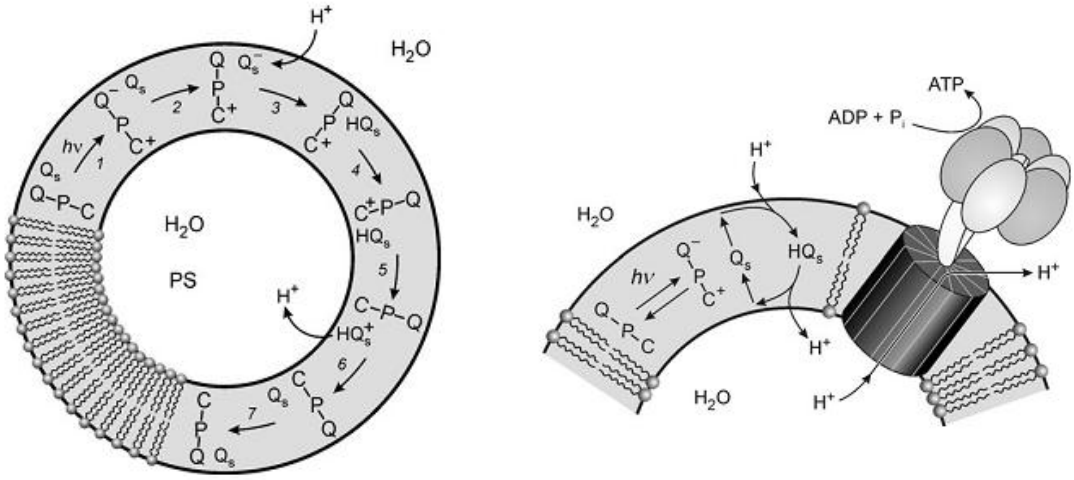

(a) **(b)**

Figure 1.7 Illustration of (a) a liposome-based proton pump powered by a photoinduced charge-separation process; (b) ATP synthase embedded in a lipid vesicle. Taken with permission from Ref.22 [22a].

Overall, combing the BLM and lipid vesicle can help us obtain deeper understanding of many biological events in complicated biological environments. Each of them has its shortcoming and cannot be used to faithfully model the nature phenomena. By applying both tools, valuable insights can be gained and which can be applied for variety of area, such as artificial devices and super molecule constructions.

1.1.4.3 Solid Supported Lipid Bilayers

Continuing research in membrane biophysics and biotechnology has brought forth new lipid-bilayer structures in recent years[23]. For example, the work of McConnell[24], Boxer[25], Sakmann[26] and others has established that well-defined lipid bilayers can be formed on hydrophilic substrates such as glass and oxidized silicon which is called solid supported lipid bilayers. Structurally, these bilayers are symmetrical, with controllable fluidity and stable over long period of time (i.e., hours or longer) when immersed in aqueous media, which warrants their use as a model of cellular membranes.

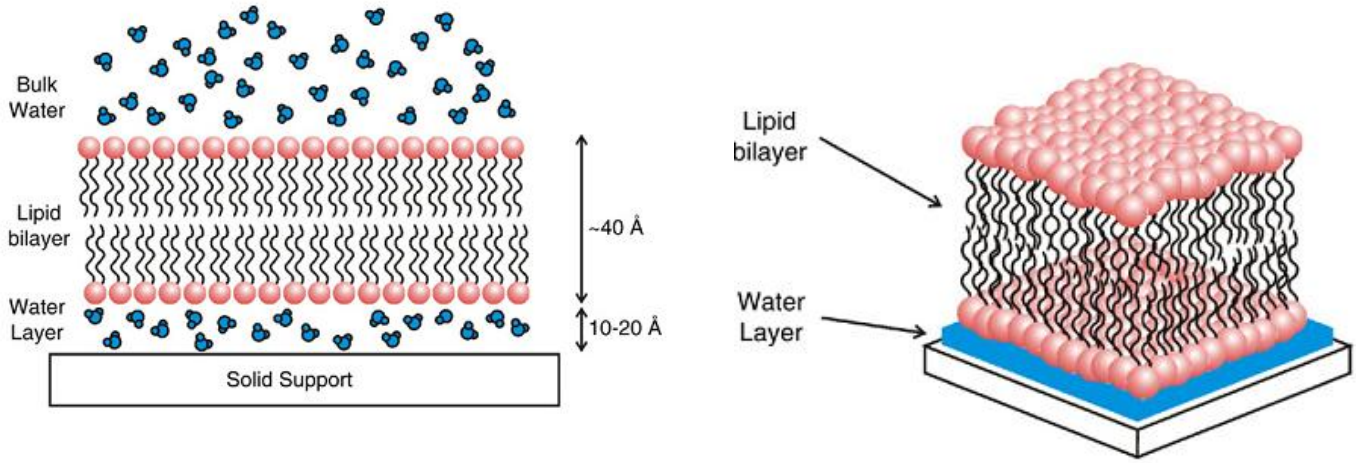

Figure 1.8 Illustration of a solid supported lipid bilayers. Taken with permission from Ref.12[12].

The solid supported lipid bilayers are much more stable than black lipid membranes. In this type of membrane, a 10–20 Å layer of water is trapped between the substrate and the bilayer, which provides the fluidity to the membrane[27]. To support a high quality membrane, the substrate surface must be clean, smooth and hydrophilic. In general, fused silica, borosilicate glass, mica and oxidized silicon are popular choices[28].

Phospholipid membranes are supported by the substrate with van der waals, electrostatic, hydration and steric forces. The water under lipid bilayer severs a lubrication, so lipid can more freely in lateral direction. The negatively charged vesicles cannot easily fuse to glass substrate at basic pH values and low ionic strengths. Uncharged vesicles made from zwitterionic lipids, can fuse more easily to Au substrates.

For biological applications, three methods can be used to form the phospholipid bilayers on planar supports. The first one is to transfer a lower leaflet of lipid from the air water interface using Langmuir–Blodgett method, then transfer a upper leaflet using Langmuir–Schaefer method by dipping the substrate horizontally. A second method includes adsorption and fusion of vesicles from an aqueous suspension to the substrate surface. A third method combines the above two methods, first transferring a monolayer via the Langmuir–Blodgett technique, then perform a vesicle fusion to form the upper layer.

In building molecular artificial photovoltaic systems, fullerenes have been frequently applied due to their unique electrical and photochemical properties[29], such as narrow HOMO-LUMO gap, long-lived photoinduced charge separation, and low reorganization energy associated with the electron\energy transfer. However, fullerens are extremely hydrophobic, which limits their handing and chemical modification on electrode surface. Fullerenes with functional groups can be synthesized to deposit as a self-assembled monolayer on surface electrode such as indium-tin oxide (ITO), and gold surface, but heavily functionalized fullerenes only display weakened photoconversion efficiency due to their perturbed electronic structure.

Taking advantage of solid supported lipid bilayers, Mauzerall and his co-workers systematically studied the photoconducting and photosensitizing behaviors of fullerenes embedded in planar lipid bilayers on conducting surface[30]. They can host fullerenes within the

hydrophobic region of the lipid bilayer structure. More recently, Tien and his colleagues extended this approach by forming fullerene-incorporated lipid bilayers on solid electrode surfaces[31]. In both cases, fullerenes are expected to exist in aggregates in lipid because of the use of pristine fullerene and organic solvent in the preparation. To maximize homogeneous dispersion of fullerenes in lipids, Zhan et al.[32] adopted an extrusion-based liposome formation methods, in which the fullerene/lipid mixture is repeatedly pushed through a series of pholycarbonate membranes of defined pore size. Less then 0.2% (mol % vs total lipids) C_{60} was incorporated into the lipid bilayer portion of the liposome this way, since the nanoporous membranes rejected most of the lipid/fullerene aggregates. It has been shown previously that high fulleren loading in liposomes could be achieved by using hydrophilic fullerene monoaddends[33].

1.1.5 Introduction to Hybrid Bilayer Membrane

The use of self-assembly monolayer (SAM) for the modification of electrode surfaces has been widely discussed and studied[34]. Recently, it has also been shown that a monolayer of phospholipids can be added on a pre-formed self-assembled monolayer (SAM), which can produce a hybrid bilayer membrane (HBM) on a solid support[35] (Figure 1.4). Nuzzo and Allara at Bell Laboratories in 1983 first developed this method. The hybrid bilayer membrane is composed of a metal supported alkanethiol SAM and a monolayer of phospholipid.

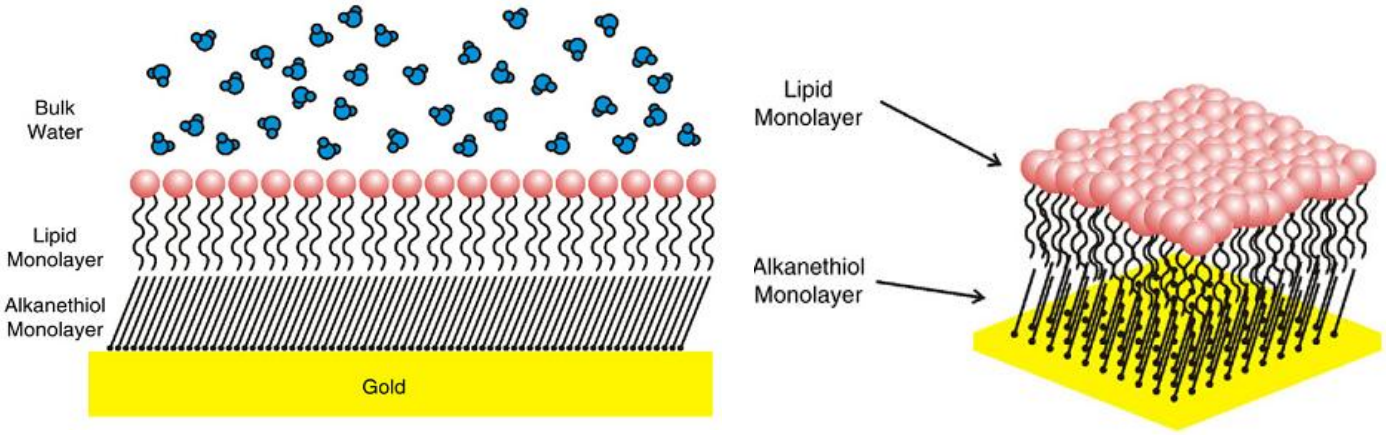

Figure 1.9 Illustration of a hybrid bilayer membrane. Taken with permission from Ref.12[12].

For biological applications, hybrid phospholipid platforms have their own merits. The direct coupling between a phospholipid monolayer directly to a metallic surface allows direct electrical measurement, surface plasmon resonance spectroscopy, and quartz crystal microbalance detection[36]. Due to the strong interactions between the alkanethiol SAM layer and the underlying substrate, hybrid phospholipid membranes are fairly robust. They can be dried and rehydrated and at same time keeping some of their physical and chemical properties. An alkanethiol SAM layer is typically more crystalline in structure comparing to a normal leaflet of a phospholipid bilayer. The packing density of the underlying SAM layer will affect the insertion of proteins and the proteins' function.

The advantage of hybrid bilayer membrane in study electron transfer in biological system is that it can keep the reactivity of natural components with the lipid layer, on the other hand, convert the biological reactions into electrochemical signal. More recently, Ma et al[37]. reported the reversible inter-conversion between NADH and NAD^+ at a low overpotential by ubiquinone

embedded hybrid bilayer membrane to mimic the initial stages of respiration in plants, which provided new insights into the mechanism of biological redox cycling. Hosseini et al[38] presented another hybrid bilayer sytem to study proton-coupled electron transfer (PCET) by controlling the proton flux . Within this system, oxygen reduction by an iron porphyrin was used as a model PCET reaction. By using this system, they observed a different catalytic behavior than obtained by simply changing the pH of the solution in the absence of an HBM.

1.2 My Work

We have been interested in building new artificial photosynthetic systems with the solid-supported lipid bilayers[32, 39]. The HBM provides us another new approach to study photoinduced electron transfer within lipid environment. In particular, because HBM are formed in two separate steps, it becomes possible to control the chemical components of each layer.

My works aim to better understand the photocurrent generation and modulation by using HBM as the basic model. By incorporating photoagent (either ruthenium tris(bipyridyl) complexes ($Ru(bpy)_3^{2+}$) or monomalonic fullerenes (C_{63})) within the HBM, we can quantitatively observe the photoconversion on the controlled conditions. Considering flexibility of lipid-based amphiphilic assembly, this HBM system should be found useful in study the photoinduced cross-membrane electron transfer (ET) processes, such as electron tunneling within lipid matrix, electrolyte/lipid interfacial properties, and distance between the photoactive species and the electrode.

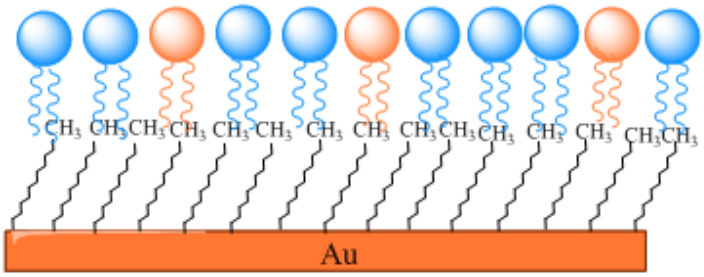

(a)

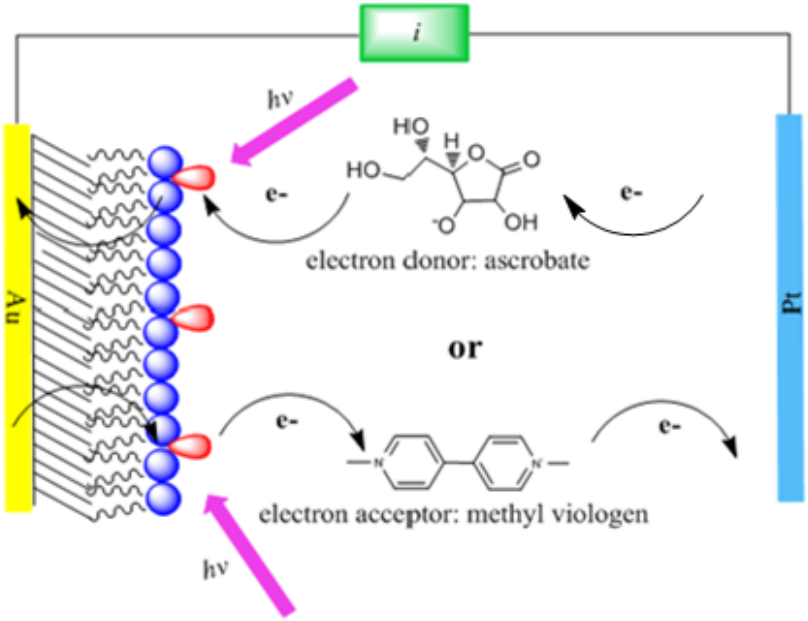

(b)

Figure 1.10 Illustration of (2) photoagent embedded hybrid bilayer membrane; (b) the photocurrent generating system based on a hybrid bilayer membrane. Photosensitizer is incorporated into phopholipid monolayer. Electron donor (ascrobate) and electron acceptor (methyl viologen) are provided separately in aqueous media to support electron transfer.

Reference

1. Solar Energy: Chemical Conversion and Storage (R. Hautala, R. B. K., C. Kutal), Humana Press, Clifton, **1979**.

2. Balzani, V.; Credi, A.; Venturi, M., Photochemical Conversion of Solar Energy. *Chemsuschem* **2008,** *1* (1-2), 26-58.

3. (a) Fukuzumi, S., Development of Bioinspired Artificial Photosynthetic Systems. *Physical Chemistry Chemical Physics* **2008,** *10* (17), 2283-2297; (b) Alstrum-Acevedo, J. H.; Brennaman, M. K.; Meyer, T. J., Chemical Approaches to Artificial Photosynthesis 2. *Inorganic Chemistry* **2005,** *44* (20), 6802-6827; (c) Imahori, H.; Mori, Y.; Matano, Y., Nanostructured Artificial Photosynthesis. *Journal of Photochemistry and Photobiology C: Photochemistry Reviews* **2003,** *4* (1), 51-83.

4. (a) Watanabe, N.; Kihara, N.; Furusho, Y.; Takata, T.; Araki, Y.; Ito, O., Photoinduced Intrarotaxane Electron Transfer between Zinc Porphyrin and [60] Fullerene in Benzonitrile. *Angewandte Chemie* **2003,** *115* (6), 705-707; (b) Ohkubo, K.; Kotani, H.; Shao, J.; Ou, Z.; Kadish, K. M.; Li, G.; Pandey, R. K.; Fujitsuka, M.; Ito, O.; Imahori, H., Production of An Ultra-Long-Lived Charge-Separated State in a Zinc Chlorin–C60 Dyad by One-Step Photoinduced Electron Transfer. *Angewandte Chemie* **2004,** *116* (7), 871-874.

5. (a) Barter, L.; Durrant, J. R.; Klug, D. R., A Quantitative Structure–Function Relationship for the Photosystem II Reaction Center: Supermolecular Behavior in Natural Photosynthesis. *Proceedings of the National Academy of Sciences* **2003,** *100* (3), 946; (b) Gust, D.; Moore, T. A., A Synthetic System Mimicking the Energy Transfer and Charge Separation of Natural Photosynthesis. *Journal of Photochemistry* **1985,** *29* (1-2), 173-184; (c) Scarascia-Mugnozza, G.; Angelis, P. D.; Matteucci, G.; Valentini, R., Long-Term Exposure to

Elevated [CO2] in A Natural Quercus ilex L. Community: Net Photosynthesis and Photochemical Efficiency of PSII at Different Levels of Water Stress. *Plant, Cell & Environment* **1996,** *19* (6), 643-654.

6. Robinson, J. N.; Cole hamilton, D. J., Electron-Transfer across Vesicle Bilayers. *Chemical Society Reviews* **1991,** *20* (1), 49-94.

7. (a) Dekker, J. P.; Plijter, J. J.; Ouwehand, L.; Van Gorkom, H. J., Kinetics of Manganese Redox Transitions in the Oxygen-Evolving Apparatus of Photosynthesis. *Biochimica et Biophysica Acta (BBA)-Bioenergetics* **1984,** *767* (1), 176-179; (b) Anderson, J. M., The Molecular Organization of Chloroplast Thylakoids. *Biochimica et Biophysica Acta* **1975,** *416* (2), 191.

8. Calvin, M., Simulating Photosynthetic Quantum Coversion *Accounts of Chemical Research* **1978,** *11* (10), 369-374.

9. L. Milgrom, New Scientist, 2nd February **1984,** p. 26.

10. Natr, L., Mineral Nutrients - A Ubiquitous Stress Factor for Photosynthesis (Review). *Photosynthetica* **1992,** *27*, 271-294.

11. (a) Mueller, P.; Rudin, D. O.; Ti Tien, H.; Wescott, W. C., Reconstitution of Cell Membrane Structure in vitro and Its Transformation into An Excitable System. *Nature* **1962,** *194*, 979-980; (b) Mueller, P.; Rudin, D. O., Induced Excitability in Reconstituted Cell Membrane Structure. *Journal of Ttheoretical Biology* **1963,** *4* (3), 268-280.

12. Castellana, E. T.; Cremer, P. S., Solid Supported Lipid Bilayers: From Biophysical Studies to Sensor Design. *Surface Science Reports* **2006,** *61* (10), 429-444.

13. Berns, D. S.; MacColl, R., Phycocyanin in Physical Chemical Studies. *Chemical Reviews* **1989,** *89* (4), 807-825.

14. Pagano, R.; Ruysschaert, J.; Miller, I., The Molecular Composition of Some Lipid Bilayer Membranes in Aqueous Solution. *Journal of Membrane Biology* **1972,** *10* (1), 11-30.

15. Tien, H. T., BilayerLlipid Membranes (BLM): Theory and Practice. M. Dekker: **1974.**

16. Fendler, J. H., Photochemical Solar-Energy Conversion - An Assessment of Scientific Accomplishements. *Journal of Physical Chemistry* **1985,** *89* (13), 2730-2740.

17. (a) Fendler, K.; Grell, E.; Haubs, M.; Bamberg, E., Pump Currents Generated by the Purified Na+ K+-ATPase from Kidney on Black Lipid Membranes. *The EMBO Journal* **1985,** *4* (12), 3079; (b) Nagel, G.; Fendler, K.; Grell, E.; Bamberg, E., Na+ Currents Generated by the Purified (Na++ K+)-ATPase on Planar Lipid Membranes. *Biochimica et Biophysica Acta (BBA)-Biomembranes* **1987,** *901* (2), 239-249.

18. Berns, D. S., Photosensitive Bilayer Membranes as Model Systems for Photobiological Processes. *Photochemistry and Photobiology* **1976,** *24* (2), 117-139.

19. Ti Tien, H., Membrane Photobiophysics and Photochemistry. *Progress in Surface Science* **1989,** *30* (1-2), 1-199.

20. Ford, W. E.; Otvos, J. W.; Calvin, M., Photosensitized Electron Transport across Lipid Vesicle Walls: Quantum Yield dependence on Sensitizer Concentration. *Proceedings of the National Academy of Sciences* **1979,** *76* (8), 3590.

21. Calvin, M., Artificial Photosynthesis: Quantum Capture and Energy Storage. *Photochemistry and Photobiology* **1983,** *37* (3), 349-360.

22. (a) Steinberg-Yfrach, G.; Rigaud, J. L.; Durantini, E. N.; Moore, A. L.; Gust, D.; Moore, T. A., Light-Driven Production of ATP Catalysed by F0F1-ATP Synthase in An Artificial Photosynthetic Membrane. *Nature* **1998,** *392* (6675), 479-482; (b) Gust, D.; Moore, T. A.;

Moore, A. L., Mimicking Photosynthetic Solar Energy Transduction. *Accounts of Chemical Research* **2001,** *34* (1), 40-48.

23. Brian, A. A.; McConnell, H. M., Allogeneic Stimulation of Cytotoxic T cells by Supported Planar Membranes. *Proceedings of the National Academy of Sciences* **1984,** *81* (19), 6159.

24. Tamm, L. K.; McConnell, H. M., Supported Phospholipid Bilayers. *Biophysical journal* **1985,** *47* (1), 105-113.

25. Groves, J. T.; Boxer, S. G., Micropattern Formation in Supported Lipid Membranes. *Accounts of chemical research* **2002,** *35* (3), 149-157.

26. Sackmann, E., Supported Membranes: Scientific and Practical Applications. *Science* **1996,** *271* (5245), 43-48.

27. Johnson, S.; Bayerl, T.; McDermott, D.; Adam, G.; Rennie, A.; Thomas, R.; Sackmann, E., Structure of An Adsorbed Dimyristoylphosphatidylcholine Bilayer Measured with Specular Reflection of Neutrons. *Biophysical Journal* **1991,** *59* (2), 289-294.

28. Sackmann, E.; Tanaka, M., Supported Membranes on Soft Polymer Cushions: Fabrication, Characterization and Applications. *Trends in Biotechnology* **2000,** *18* (2), 58-64.

29. (a) Fukuzumi, S.; Ohkubo, K.; Imahori, H.; Guldi, D. M., Driving Force Dependence of Intermolecular Electron-Transfer Reactions of Fullerenes. *Chemistry-A European Journal* **2003,** *9* (7), 1585-1593; (b) Ikemoto, J.; Takimiya, K.; Aso, Y.; Otsubo, T.; Fujitsuka, M.; Ito, O., Porphyrin-Oligothiophene-Fullerene Triads as An Efficient Intramolecular Electron-Transfer System. *Organic Letters* **2002,** *4* (3), 309-311; (c) Imahori, H.; Sakata, Y., Donor-Linked Fullerenes: Photoinduced Electron Transfer and Its Potential Application. *Advanced Materials*

1997, *9* (7), 537-546; (d) Guldi, D. M.; Prato, M., Excited-State Properties of C60 Fullerene Derivatives. *Accounts of Chemical Research* **2000,** *33* (10), 695-703.

30. (a) Hwang, K. C.; Mauzerall, D., Photoinduced Electron Transport across A Lipid Bilayer Mediated by C70. *Nature* **1993,** 361, 138-140; (b) Hwang, K. C.; Mauzerall, D., Vectorial Electron Transfer from An Interfacial Photoexcited Porphyrin to Ground-State Fullerene C60 and C70 and from Ascorbate to Triplet C60 and C70 in A Lipid Bilayer. *Journal of the American Chemical Society* **1992,** *114* (24), 9705-9706.

31. Ti Tien, H.; Wang, L. G.; Wang, X.; Ottova, A. L., Electronic Processes in Supported Bilayer Lipid Membranes (s-BLMs) containing A Geodesic form of Carbon (Fullerene C60). *Bioelectrochemistry and Bioenergetics* **1997,** *42* (2), 161-167.

32. Zhan, W.; Jiang, K., A Modular Photocurrent Generation System Based on Phospholipid-Assembled Fullerenes. *Langmuir* **2008,** *24* (23), 13258-13261.

33. Janot, J. M.; Bienvenüe, E.; Seta, P.; Bensasson, R. V.; Tomé, A. C.; Enes, R. F.; Cavaleiro, J. A. S.; Leach, S.; Camps, X.; Hirsch, A., [60] Fullerene and Three [60] Fullerene Derivatives in Membrane Model Environments. *J. Chem. Soc., Perkin Trans. 2* **2000,** (2), 301-306.

34. (a) Whitesides, G. M.; Boncheva, M., Beyond Molecules: Self-Assembly of Mesoscopic and Macroscopic Components. *Proceedings of the National Academy of Sciences* **2002,** *99* (8), 4769; (b) Porter, M. D.; Bright, T. B.; Allara, D. L.; Chidsey, C. E. D., Spontaneously Organized Molecular Assemblies. 4. Structural Characterization of n-Alkyl Thiol Monolayers on Gold by Optical Ellipsometry, Infrared Spectroscopy, and Electrochemistry. *Journal of the American Chemical Society* **1987,** *109* (12), 3559-3568.

35. (a) Meuse, C. W.; Niaura, G.; Lewis, M. L.; Plant, A. L., Assessing the Molecular Structure of Alkanethiol Monolayers in Hybrid Bilayer Membranes with Vibrational Spectroscopies. *Langmuir* **1998,** *14* (7), 1604-1611; (b) Plant, A. L., Self-Assembled Phospholipid Alkanethiol Biommetic Bilayers on Gold. *Langmuir* **1993,** *9* (11), 2764-2767.

36. Hubbard, J.; Silin, V.; Plant, A., Self Assembly Driven by Hydrophobic Interactions at Alkanethiol Monolayers: Mechanism of Formation of Hybrid Bilayer Membranes. *Biophysical Chemistry* **1998,** *75* (3), 163-176.

37. Ma, W.; Li, D. W.; Sutherland, T. C.; Li, Y.; Long, Y. T.; Chen, H. Y., Reversible Redox of NADH and NAD+ at a Hybrid Lipid Bilayer Membrane Using Ubiquinone. *Journal of the American Chemical Society* **2011**, 133, 12366-12369

38. Hosseini, A.; Barile, C. J.; Devadoss, A.; Eberspacher, T. A.; Decreau, R. A.; Collman, J. P., Hybrid Bilayer Membrane: A Platform to Study the Role of Proton Flux on the Efficiency of Oxygen Reduction by a Molecular Electrocatalyst. *Journal of the American Chemical Society* **2011**, 133, 11100-11102

39. (a) Zhan, W.; Jiang, K.; Smith, M. D.; Bostic, H. E.; Best, M. D.; Auad, M. L.; Ruppel, J. V.; Kim, C.; Zhang, P., Photocurrent Generation from Porphyrin/Fullerene Complexes Assembled in a Tethered Lipid Bilayer. *Langmuir* **2010,** *26* (19), 15671-15679; (b) Liu, L.; Zhan, W., Molecular Photovoltaic System Based on Fullerenes and Carotenoids Co-assembled in Lipid/Alkanethiol Hybrid Bilayers. *Langmuir* **2012**, 28, 4877-4882

Chapter Two

Hybrid Bilayer Membrane: Preparation and Characterization

2.1 Introduction to Hybrid Bilayer Membrane

The original concept of hybrid bilayer membrane (HBM) was first developed by Nuzzo and Allara[1] at Bell Laboratories in 1983. Then, Kalb et al.[2] proposed a mechanism to suggest that a stable vesicles might delaminate on a hydrophobic surface. Particularly, Plant and coworkers [3] have investigated extensively studies on the HBM formation. Their work demonstrated that the interaction of small phospholipid vesicles with well-characterized surfaces has been determined by the effect of the surface free energy of the underlying monolayer on the formation of phospholipid/alkanethiol hybrid bilayer membrane.

HBMs usually contain an alkanethiol self-assembled monolayer (SAM) on gold substrate which provides a well-defined hydrophobic surface, and another monolayer of phospholipids added to the top due to van der Waals force. The SAM of alkanethiol on Au has the benefits of easy surface modification and stability in aqueous and biological conditions[4]. Also, thiolate affinity for Au is very strong and the conductive properties of Au make it properly suited for conduction electrochemical studies. SAM can be formed by incubating a clean gold substrate with an alkanethiol solution in ethanol solution typically for a minimum of 12 hours through self-assembly. A certain amount of liposome solution was added on the SAM to allow self-

assembling. The formation of lipid monolayer is based on liposome adsorption, vesicle fusion and rupture at SAM. It is found that the lipid monolayer formation is controlled by the concentration, size, and viscosity of liposome solution[5]. Therefore, to prepare the controlled liposome solution is the key to lipid monolayer formation.

2.2 Methods to Prepare Unilamellar Liposomes

Apart from chemical composition, liposomes can be either characterized by their size or bounded by their layers of membrane sheets. Mutlilamellar liposomes are composed of multiple layers stacked one on top of the other like onions. Unilamellar liposomes are composed of a single bilayer membrane and they are currently the most popular model membrane systems to mimic biomembranes. There are four basic stages involved in making unilammellar liposomes: (1) dissolve lipids needed in organic solution; (2) dry the lipids from organic solvents; (3) dispersion of the lipids in aqueous media; (4) extrusion of liposomes into controllable size.

An organic solution is the starting point for all liposome preparation. It ensures completely homogeneous mixing of different phospholipids. During this step, photoagents such as $Ru(bpy)_3^{2+}$ complex or fullerenes can be added in organic solvent. The process of drying organic solution is carried out in a rotary evaporator by gentle warming (20 – 40 ℃) under reduced pressure (400- 700 mm Hg). The dried lipid films are dispersed by addition of the buffer solution (pH ~ 7.7), followed by hand-shaking which enables lipids suspended off the sides of a glass vessel into the aqueous medium. Then, sonication is used for reducing the size of liposomes by providing high energy to breakdown the large multiple layer vesicles. Ultrasonic irradiation can largely reduce the vesicle size, but it may not be possible to reach the minimum size requirement. Therefore, another method called extrusion method is applied. Liposome

extrusion is the process that multilamellar liposomes are forced through filters with defined pores sizes to obtain a liposome population with a mean diameter that reflects the diameter of the filter pore. The most common used filters are standard polycarbonate filters that has prove to be reliable inert, durable and easy to apply without damage. It is currently one of the most commonly encountered procedures for reducing liposome size and producing unilamellar liposomes on a research scale. Figure 2.2 illustrates the formation of unilamellar liposomes.

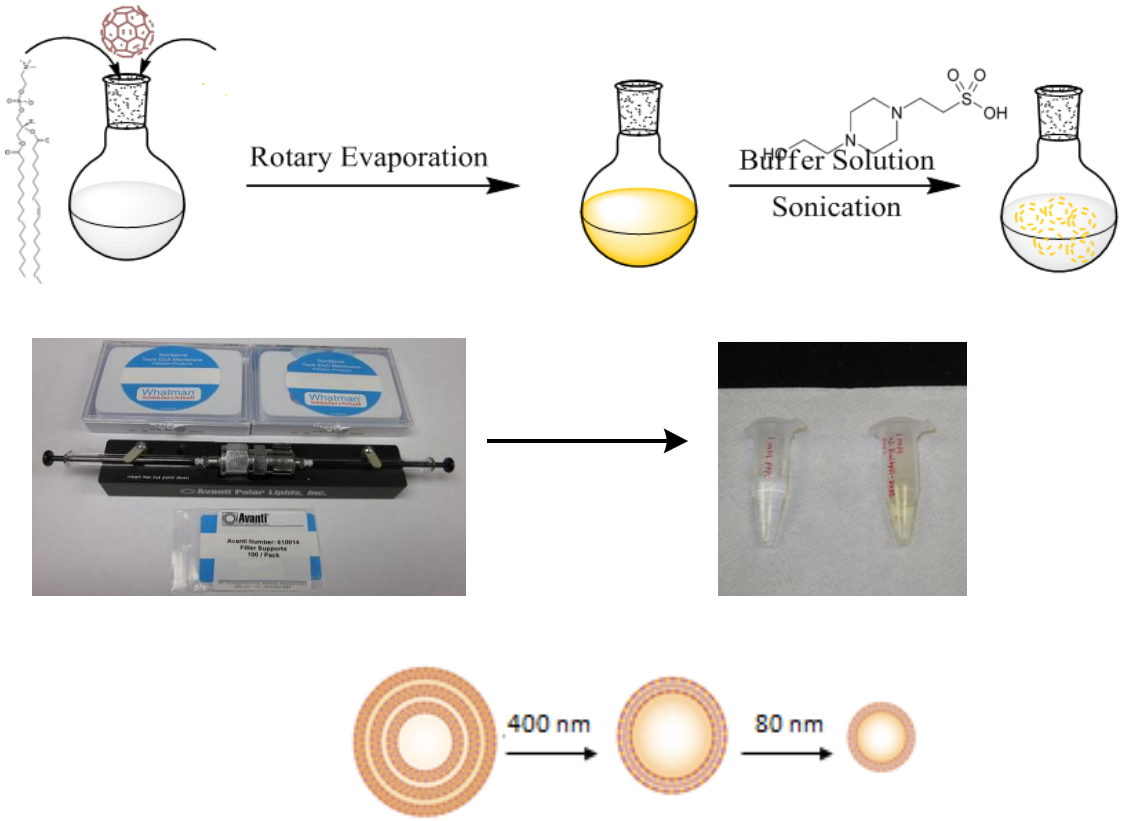

Figure 2.1 Illustration of the formation of unilamellar liposomes.

2.3 Characterization of Hybrid Bilayer Membrane

Although it is technically challenging to precisely monitoring the interaction of liposomes on the SAM, many techniques have been investigated to study the process such as surface

plasmon resonance (SPR), quartz crystal microbalance (QCM), and impedance spectroscopy[3c]. Here, several analytical methods are introduced to study the structure of HBM.

2.3.1 Contact Angle

The wettability is the basic characteristic of a solid surface determined by a force balance between adhesive and cohesive forces. Adhesive forces between a liquid and solid cause a liquid drop to spread across the surface, while cohesive forces with the liquid cause the drop to avoid contact with the surface. The contact angle is determined by the result between adhesive and cohesive forces, and is one of the easiest qualities to measure the wettability of a solid surface. According to study by Silin, et al[3c], the hydrophobicity of surface plays a key role in liposome rapture and lipid monolayer formation. To study the hydrophobicity of alkanethiol SAMs on gold (Au) electrode, the static contact angle of a water drop lying on the substrate was measured (Figure 2.3). Ideally, a contact angle less than 90 ºindicates that the surface is hydrophilic, while a contact angle greater than 90 º generally means the surface is hydrophobic. However, the hydrophobicity of the surface is also affected by the surface roughness and experimental conditions[6].

Figure 2.2 Schematic illustration of (a) a water drop on a more hydrophilic surface; (b) a water drop on a more hydrophobic surface.

2.3.2 Cyclic Voltammetry

Cyclic voltammetry (CV) is an electrochemical technique in which the faradic current responding to applied potential vs. scan rate is investigated (Figure 2.4). Typically, CV is used to probe the reactivity of redox active species in electrolyte or bound to the electrode. It has been widely applied to study the insulating ability of alkanthiol SAM on the Au electrode[7]. Here, we applied this technique to qualitatively study the insulating ability of both SAMs and HBMs.

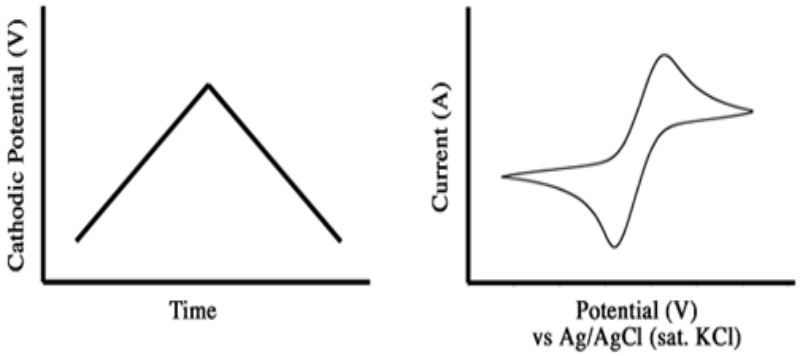

(a) **(b)**

Figure 2.3 Schematic diagram of (a) applied potential scan vs. time; (b) current response vs. potential

2.3.3 Quartz Crystal Microbalance

The quartz crystal microbalance (QCM) has been used to study mass changes at the electrode surface. QCM was initially used in ex situ experiments to measure mass change at electrode surfaces[8]. Later, it was used as an in situ mass sensor for monitoring thin films formation on electrode surfaces in real time. The QCM comprises a thin quartz crystal sandwiched between two metal electrodes which can establish an alternating electric field across the crystal, providing vibrational motion of the crystal at its resonant frequency. Therefore, the resonant frequency is sensitive to mass changes (Figure 2.4).

Ideally, if the particle displacement and shear stress are continuous across the interface between the quartz and the thin layer, which is referred to as the "no-slip" conditions. Sauerbrey equation is given to describe [8]: $\Delta f = -C_f \cdot \Delta m$, where Δf is the observed frequency shift (Hz), Δm the change in mass per unit area (g/cm^2) and C_f the sensitivity factor for the crystal. Sauerbrey equation has been investigated in many studies to calculate the monolayer formation by assuming an ideal rigid layer behavior[9]. However, several factors can lead to a non-ideal behavior, such as the interfacial liquid properties, the electrode morphology, the stiffness of the film on the electrode, and the longitudinal coupling with the liquid phase[8]. In this case, Sauerbrey equation cannot be applied.

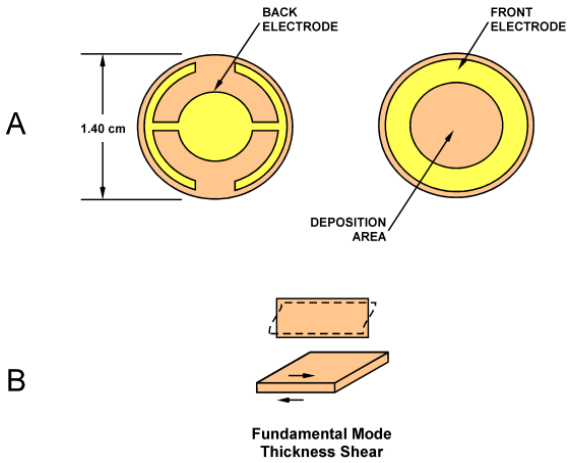

Figure 2.4 A schematic of quartz crystal sandwiched between two Au electrodes. Taken from Ref. 10 with permission[10].

2.3.4 Impedance Spectroscopy

Impedance is the form of current-voltage relationship in an alternating current (AC) circuit, which is measured as a function of the frequency of AC potentials in an electrochemical cell.

Because of its high precision, it is frequently used to study double layer structure and evaluate heterogeneous charge-transfer parameters. In the study of HBM formation, impedance measurement is used to follow changes in the surface coverage when liposomes are added to the SAM[3a] . The thickness, *d*, of the dielectric layer is related to the specific capacitance: $1/C = d/\varepsilon\varepsilon_0$, where is *d* is the thickness of the dielectric medium that separates the two conducting plates (i.e., the gold electrode and the electrolyte solution), ε is the dielectric constant of the separating medium, and ε_0 is the permittivity of free space. For the hybrid bilayers, the capacitance of the lipid layer alone (C_{lipid}) can be calculated from the capacitance of the bilayer (C_{BL}) and the alkanethiol SAM (C_{SAM}) layer by the following relation: $C_{lipid}^{-1} = C_{BL}^{-1} - C_{SAM}^{-1}$. The calculated dielectric thickness can help us to quantitatively compare the lipid monolayer formation on different alkanethiol SAMs.

Reference

1. Nuzzo, R. G.; Allara, D. L., Adsorption of Bifunctional Organic Disulfides on Gold Surfaces. *Journal of the American Chemical Society* **1983,** *105* (13), 4481-4483.

2. Kalb, E.; Frey, S.; Tamm, L. K., Formation of Supported Planar Bilayers by Fusion of Vesicles to Supported Phospholipid Monolayers. *Biochimica et Biophysica Acta (BBA)-Biomembranes* **1992,** *1103* (2), 307-316.

3. (a) Plant, A. L., Self-assembled Phospholipid Alkanethiol Biommetic Bilayers on Gold. *Langmuir* **1993,** *9* (11), 2764-2767; (b) Plant, A. L.; Brighamburke, M.; Petrella, E. C.; Oshannessy, D. J., Phospholipid/Alkanethiol Bilayers for Cell-Surface Receptor Studies by Surface Plasmon Resonance. *Analytical Biochemistry* **1995,** *226* (2), 342-348; (c) Silin, V. I.; Wieder, H.; Woodward, J. T.; Valincius, G.; Offenhausser, A.; Plant, A. L., The Role of Surface

Free Energy on the Formation of Hybrid Bilayer Membranes. *Journal of the American Chemical Society* **2002,** *124* (49), 14676-14683.

4. Whitesides, G. M.; Boncheva, M., Beyond Molecules: Self-assembly of Mesoscopic and Macroscopic Components. *Proceedings of the National Academy of Sciences* **2002,** *99* (8), 4769.

5. Hubbard, J.; Silin, V.; Plant, A., Self Assembly Driven by Hydrophobic Interactions at Alkanethiol Monolayers: Mechanism of Formation of Hybrid Bilayer Membranes. *Biophysical Chemistry* **1998,** *75* (3), 163-176.

6. Bain, C. D.; Whitesides, G. M., A Study by Cntact Angle of the Acid-Base Behavior of Monolayers Containing Oega.-Mercaptocarboxylic Acids Adsorbed on Gold: An Example of Reactive Spreading. *Langmuir* **1989,** *5* (6), 1370-1378.

7. (a) Allara, D. L.; Nuzzo, R. G., Spontaneously Organized Molecular Assemblies. 1. Formation, Dynamics, and Physical Properties of n-Alkanoic Acids Adsorbed from Solution on An Oxidized Aluminum Surface. *Langmuir* **1985,** *1* (1), 45-52; (b) Allara, D. L.; Nuzzo, R. G., Spontaneously Organized Molecular Assemblies. 2. Quantitative Infrared Spectroscopic Determination of Equilibrium Structures of Solution-Adsorbed n-Alkanoic Acids on An Oxidized Aluminum Surface. *Langmuir* **1985,** *1* (1), 52-66.

8. Buttry, D. A.; Ward, M. D., Measurement of Interfacial Processes at Electrode Surfaces with the Electrochemical Quartz Crystal Microbalance. *Chemical Reviews* **1992,** *92* (6), 1355-1379.

9. (a) Bruckenstein, S.; Shay, M., An in situ Weighing Study of the Mechanism for the Formation of the Adsorbed Oxygen Monolayer at A Gold Electrode. *Journal of Electroanalytical Chemistry and Interfacial Electrochemistry* **1985,** *188* (1-2), 131-136; (b) Schneider, T. W.; Buttry, D. A., Electrochemical Quartz Crystal Microbalance Studies of

Adsorption and Desorption of Self-assembled Monolayers of Alkyl Thiols on Gold. *Journal of the American Chemical Society* **1993,** *115* (26), 12391-12397.

10. (a) Mecea, V.; Bucur, R., The Mechanism of the Interaction of Thin Films with Resonating Quartz Crystal Substrates: the Energy Transfer Model. *Thin Solid Films* **1979,** *60* (1), 73-84.

Chapter Three

Photocurrent Generation based on $Ru(bpy)_3^{2+}$ tethered Phospholipid/Alkanethiol Hybrid Bilayer Membranes

3.1 Introduction

Conventional monolayer-based photoconversion systems[1] typically rely on the covalent linkage of thiol- or silane-functionalized photoactive conjugates on electrodes, which often require nontrivial synthesis in organic media. By contrast, we herein report a new photocurrent generation system based on $Ru(bpy)_3^{2+}$ (bpy = 2,2'-bipyridine) tethered on phospholipid/alkanethiol hybrid bilayer membrane (HBM) in aqueous media (Figure 3.1). The construction of such a system is described as in Chapter 2: first, a self-assembled monolayer (SAM) of alkanethiol is formed on gold and then, liposome solution containing $Ru(bpy)_3^{2+}$-conjugated dioleoylphosphoethanolamine (DOPE) and POPC are spreaded to the preformed SAM to form another monolayer of phospholipids. Either anodic or cathodic photocurrent generation can be obtained in the presence of suitable sacrificial electron donor(acceptor). The method described here takes advantage of the versatile assembly[2] of phospholipids in water and potentially provides a new approach to modular photoelectrochemical cell design.

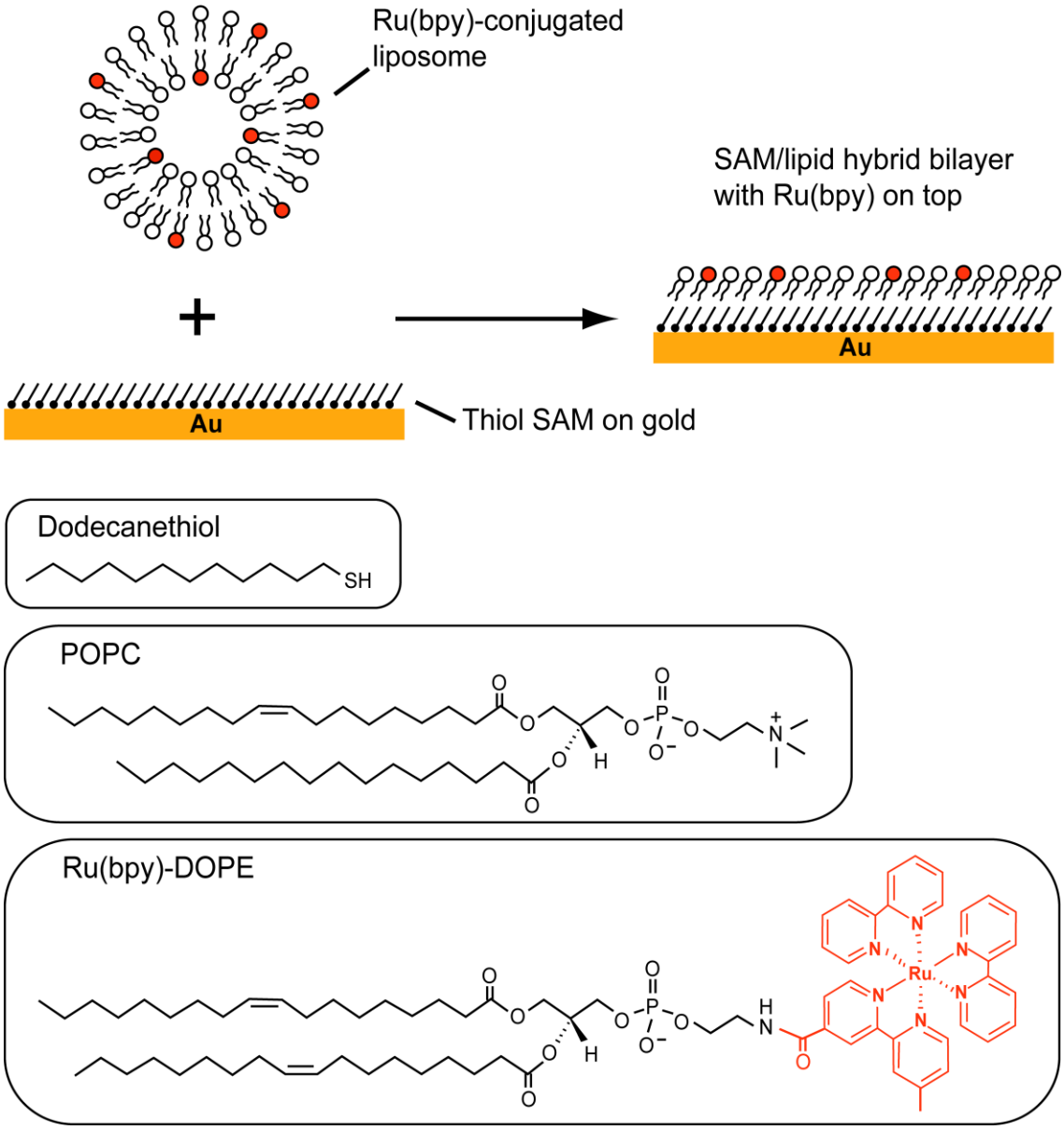

Figure 3.1 Schematic diagram of the formation of $Ru(bpy)_3^{2+}$ tethered Phospholipid/Alkanethiol Hybrid Bilayer Membrane. Taken with permission from Ref.3[3].

3.2 Experimental

3.2.1 Chemicals and reagents

Phospholipids such as 1-palmitoyl-2-oleoyl-sn-glycero-3-phosphocholine (POPC) and 1,2-dioleoyl-sn-glycero-3-phosphoethanolamine (DOPE) were obtained from Avanti Polar Lipids. Potassium hexacyanoferrate(III) ($K_3Fe(CN)_6$) was from Riedel-de Haën. Other chemicals, including Bis(2,2′-bipyridine)-4′-methyl-4-carboxybipyridine-ruthenium *N*-succinimidyl ester-bis(hexafluorophosphate) (($Ru(bpy)_3^{2+}$-NHS), *N*,*N*-dimethylformamide (DMF), triethylamine, 1-hexanethiol, 1-dodecanethiol, 1-octadecanethiol, 4-(2-hydroxyethyl)piperazine-1-ethanesulfonic acid (HEPES), methyl viologen dichloride hydrate (MV^{2+}), L(+)-ascorbic acid sodium salt (sodium ascorbate), D-(+)-glucose, glucose oxidase (type X-S, from *Aspergillus niger*) and catalase from bovine liver are purchased from Sigma-Aldrich. All solutions employed in these experiments were prepared using 18.2 MΩ•cm deionized water (Millipore).

3.2.2 Synthesis of $Ru(bpy)_3^{2+}$-DOPE

$Ru(bpy)_3^{2+}$-DOPE was made in one step by reacting $Ru(bpy)_3^{2+}$-NHS with DOPE. To start, 2.5 μmol of DOPE in chloroform was added into a flask and dried by an argon stream, to which 0.8 mL DMF and 25 μmol of triethylamine were added and stirred for 30 min. Next, 5 μmol of $Ru(bpy)_3^{2+}$-NHS in DMF was injected into the flask and thoroughly mixed. The final reaction volume was close to 1 mL. The reaction proceeded overnight at room temperature in dark. The resulting products were dried and separated on silica gel column (200-400 mesh) using chloroform and chloroform/methanol/water (90:10:0.5 and then 65:25:4, v/v). The production of $Ru(bpy)_3^{2+}$-DOPE was confirmed by TLC, ^1H NMR (in $CDCl_3$) and EIS-MS (calculated molecular weight: 1352.6; found: $[M+H]^+$: 1353.6; $[M+H]^{2+}$: 676.8).

3.2.3 Assembly of Hybrid Bilayer Membrane

Gold-coated substrates were fabricated by sputtering gold on the chromium-coated silicon wafers. The thickness of gold layer was about 1000 nm. Prior to the self-assembling of alkanethiol monolayers, the gold-coated substrates were cleaned in piranha solution[4] (3:1, concentrated H_2SO_4 to 30% H_2O_2 solution, v/v) for 15 min, and thoroughly rinsed by water and ethanol and dried by an argon stream. Then, cleaned gold electrodes were immersed in 1mM of alkanethiol in ethanol solution at room temperature for at least 12h. After that, the SAM-modified gold substrates were rinsed by copious ethanol and DI water, dried under argon, and then assembled in the Teflon cell for further use.

Liposomes of various compositions are prepared by an extrusion method as previously described in chapter 2. Briefly, appropriate quantities of lipids in chloroform were thoroughly mixed and dried to a film by rotary evaporation. This mixture was then sonicated (Bransonic, model: 3510-DTH) in HEPES buffer (10 mM HEPES, 100 mM NaCl, pH 7.7) at room temperature for 2h. The resulting solution was then extruded consecutively through polycarbonate membranes (Nuclepore, Whatman) of 400 and 80 nm-diameter pore at room temperature. The total lipids concentration of the final product was approximately 2 mM. The exact compositions of lipids used in the preparation are specified in the main text.

To form the SAM/lipid hybrid bilayers, typically a 300 μL of liposome solution with a total lipid concentration of 1 mM was added onto the SAM fixed in a Teflon cell and incubated at room temperature for 2h. The unbound liposome solution was then removed from the cell by exchanging with HEPES buffer solution at least 20 times.

3.2.4 Contact angle

Water contact angle measurements are obtained by the sessile drop method on a Ram ́e-Hart20 model 200 automated goniometer (Ram ́e-Hart, Inc. Mountain Lakes, NJ) using DRO Pimage Standard software. Measurement error for this technique is ±2.0◦

3.2.5 Impedance Analysis

Impedance of the alkanethiol monolayer and lipid/alkanethiol hybrid bilayer was measured by an SI 1260 Impedance/Gain-Phase Analyzer (Solartron). The measurements were carried out on a two-electrode setup (Au working and Pt counter electrodes) in 10 mM KCl. A sinusoidal *ac* amplitude of 10 mV vs. the open circuit potential was applied throughout the measurements. An impedance analysis software package, ZView, was employed to fit the impedance data, which is based on an equivalent circuit consisting of a resistor (the electrolyte solution) and a capacitor (the surface-bound layers) connected in series.

3.2.6 QCM Measurements

QCM measurements were carried out using a QCM analyzer with a 5 MHz crystal oscillator (Model: QCM25, Stanford Research Systems) at 23 ℃. Prior to the SAM formation, the gold coated quartz crystals were cleaned in piranha solution for 3 min, then rinsed with copious water, ethanol and dried under argon. The crystals were mounted onto the QCM oscillator equipped with a flow cell. To monitor the SAM formation using QCM, ethanol was first flowed through the cell until a steady baseline of frequency was obtained. Following that, a proper amount of 100 mM dodecanethiol in ethanol was injected into the flow cell so that a final thiol concentration of 1 mM was obtained. For the hybrid bilayer formation, the cleaned crystal was first immersed in 1 mM C_{12}-thiol in ethanol overnight, thoroughly rinsed by ethanol and

water, and finally dried under argon. To introduce POPC liposome solution into the cell, liposome solutions were injected into the QCM chamber pre-equilibrated with HEPES buffer. The final lipid concentration was about 0.1 mM.

3.2.7 Fluorescence Spectroscopy

The fluorescence emission spectra of $Ru(bpy)_3^{2+}$-containing hybrid bilayer on semi-transparent gold-coated glass slides were acquired using a PI Acton spectrometer (SpectraPro SP 2356, Acton, NJ) that is connected to the side port of an epifluorescence microscope (Nikon TE-2000U, Japan). The emission signal was recorded by a back-illuminated digital CCD camera (PI Acton PIXIS:400B, Acton, NJ) operated by a PC. The excitation was generated by a mercury lamp (X-Cite 120, EXFO, Ontario, Canada) filtered by a band-pass filter at 470±20 nm. The emission signal was filtered by a long-pass filter with a cutoff wavelength of 515 nm.

3.2.8 Electrochemical and Photoelectrochemical Measurements

The electrochemical and photoelectrochemical measurements were carried out in a three-electrode Teflon cell. The three-electrode setup contains the gold substrate (with/without SAM or lipid/SAM bilayer) as the working electrode, Pt and Ag/AgCl (KCl saturated) as counter and reference electrodes. The effective area of gold electrode is 1.13 cm^2. The cyclic voltammetry experiments were conducted by a potentiostat (CHI 910B, CH Instruments) in 1mM potassium hexacyanoferrate (III) ($K_3Fe(CN)_6$) in 1 M KCl and the scan rate was 100 mV/s.

In the photoelectrochemical measurements, the electrolytes contain either 50 mM ascorbate (cathodic) or methyl viologen (anodic) in HEPES buffer. The cell was irradiated with light from a Hg lamp (X-Cite, Series 120 PC, EXFO) filtered at 470±20 nm (average intensity:

26.8 mW/cm^2). In the case of anodic current generation, oxygen in the cell was removed by an enzymatic method[5]. The resulting photocurrent was recorded by a potentiostat (CHI 910B, CH Instruments). The photoconversion efficiency was calculated according to equation, $\Phi = (i/e)/[(W\lambda/hc)(1-10^{-A})]$, where i is the measured photocurrent, e is the elementary charge, W is the light power at wavelength λ, h is the Planck's constant, c is the light speed, A is the absorbance of $Ru(bpy)_3^{2+}$-DOPE in hybrid bilayer at 470 nm. The absorbance (A) of $Ru(bpy)_3^{2+}$-DOPE in bilayer at 470 nm, $1.5x10^{-4}$, was estimated by averaging the total absorbance from multiple layers formed on glass slides. The gold surface reflectance[6] of 0.34 was used to correct the light reflection by gold and its subsequent re-absorption by the photoactive layers.

3.3 Results and Discussion

3.3.1 Characterization of Hybrid Bilayers

Cyclic voltammetry(CV), quartz crystal microbalance (QCM) and impedance analysis were employed to characterize the formation and structure of the phospholipid/alkanethiol hybrid bilayer membrane on gold substrates.

Because alkanethiol and lipid thin films can effectively block electron transfer, their formation on a conducting surface can be followed electrochemically[7]. Figure 3.2 shows cyclic voltammograms of $Fe(CN)_6^{3-}$ probed by gold electrodes covered with a C_{12} SAM or a POPC/SAM bilayer in 1 M KCl solution. Clearly, the presence of a C_{12} SAM significantly diminishes the reduction/oxidation of $Fe(CN)_6^{3-}/Fe(CN)_6^{4-}$ on gold electrode and further addition of a POPC monolayer almost completely blocks the flow of a faradaic current within this potential window. These results thus indicate the formation of well-packed C_{12} SAM and POPC/SAM hybrid bilayer on gold surfaces.

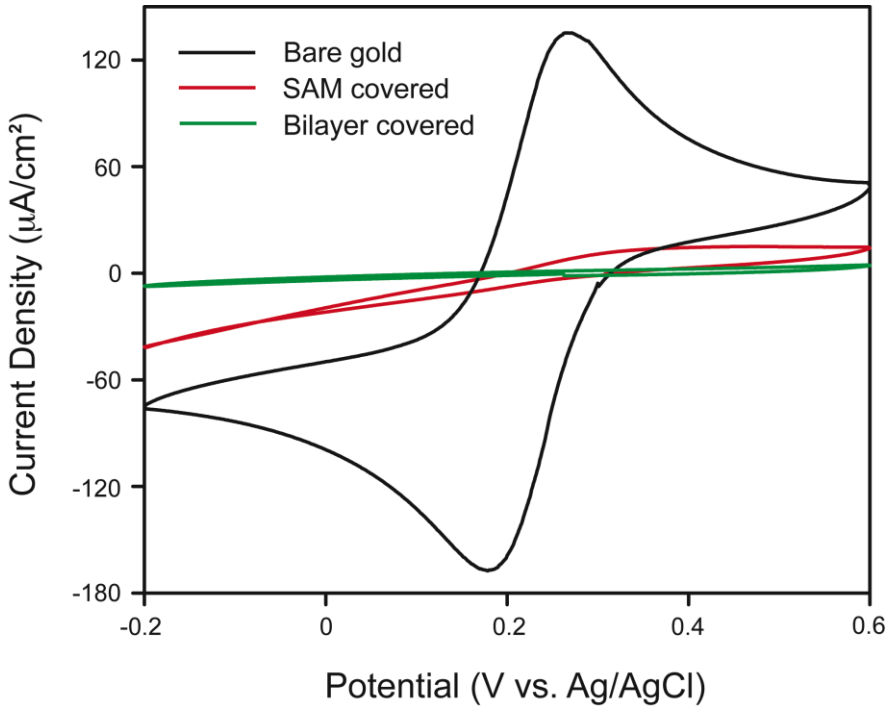

Figure 3.2 Electrochemical diagnosis of the formation of a C_{12}SAM and a POPC/C_{12} SAM hybrid bilayer membrane on the gold substrate. A three-electrode setup with a Ag/AgCl reference electrode and a Pt counter electrode was used. Scan rate: 100 mV/s. Taken with permission from Ref. 3[3].

The adsorption of phospholipid monolayer on SAM modified gold was monitored by QCM. Here, if we assume that the it is in a "non-slip" condition[8], the associated mass change of the quartz crystal corresponds to its oscillation frequency change according to the Sauerbrey equation[8] is obtained: $\Delta f = -C_f$, where Δm is obtained, where Δf is the observed frequency shift (Hz), Δm the change in mass per unit area ($\mu g/cm^2$) and C_f the sensitivity factor for the crystal (i.e., 56.6 Hz $\mu g^{-1} cm^2$ for a 5-MHz AT-cut quartz crystal at room temperature). As shown in Figure 3.3, a 6.2-Hz frequency decrease was observed immediately after the C_{12}SH was injected into the QCM chamber. This frequency shift corresponds to a thiol coverage of 3.2×10^{14}

molecules/cm^2, which is lower than an ideal SAM coverage on gold (i.e., 4.16x10^{14} molecules/cm^2)[9]. When the same calculation was performed for the formation of a POPC monolayer on top of the C_{12} SAM, a coverage of 3.65x10^{14} molecules/cm^2 was obtained. This value was significantly higher than the ideal lipid monolayer of 1.43x10^{14} molecules/cm^2 by assuming that the unit area per POPC[10] molecule is 70 Å^2. However, several factors might contribute to these apparent mismatches. For example, the Sauerbrey equation is known to be applied in "non-slip" condition, in which case viscoelastic effects arising from the solution is not considered[11]. Also, water molecules entrapped within the polar portion of the lipid layer[11] may also contribute to the observed frequency shift.

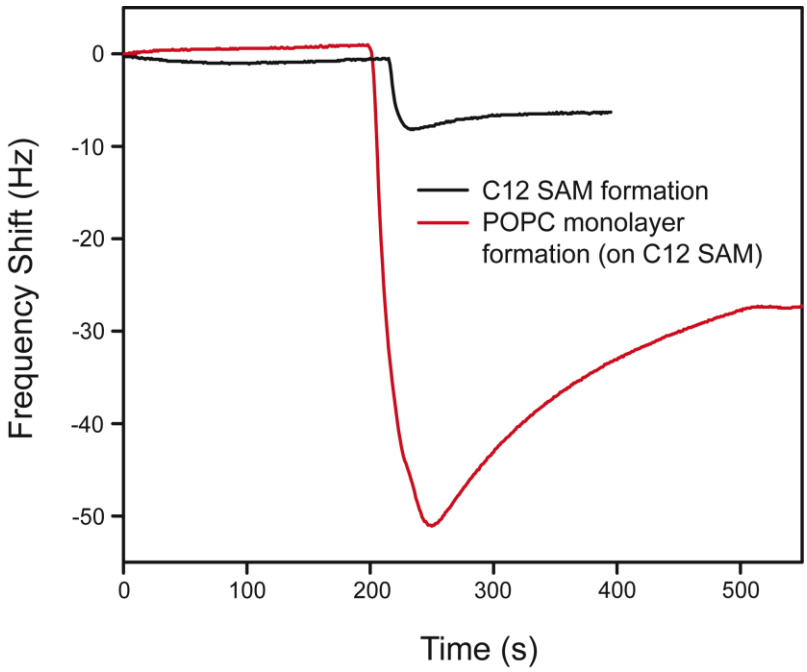

Figure 3.3 QCM monitor of the formation of a C_{12} thiol SAM and sequentially a POPC/C_{12} SAM hybrid bilayer on gold. To form the top phospholipid layer, liposomes of POPC in 10 mM HEPES buffer saline (0.1MNaCl, pH 7.7) solution were injected into the QCM flow cell. The

estimated final concentrations of $C_{12}SH$ and POPC were 1 and 0.1 mM, respectively. Taken with permission from Ref. 3[3].

Impedance spectroscopy results reveal the capacitance change associated with the formation of thiol monolayer (C_6, C_{12} and C_{18}) and lipid/alkanethiol bilayer on gold substrates (Figure 3.4). A series RC circuit model is used to fit the resultant impedance in all measurements[12]. As shown in Table 1, C_6 SAM displays the highest capacitance in this series, which can be attributed to the existence of packing defects in the film. The capacitance data is consistent with contact angle (each sample was measured 3times) in which C_6 SAM is 73.9 ± 2.1 º, C_{12} SAM is 103.1 ± 1.2 º and C_{18} SAM is 110.3 ± 0.5 º. When a POPC liposome solution was used to form hybrid bilayers with these SAMs, the same trend was obtained. The capacitance of the lipid monolayer alone (C_{lipid}) can be calculated by the equation: $1/C_{lipid} = 1/C_{bilayer} - 1/C_{SAM}$. Thus, the POPC layer exhibits the highest capacitance when a C_{12} SAM serves as the underlying layer, followed by that of C_{18} and C_6. These results are in good agreement with that reported in a previous study[12]. Similar measurements were carried out for C_{12} SAM based hybrid bilayers containing different amount of $Ru(bpy)_3^{2+}$-DOPE in the POPC top layer (Table 2). Here, the presence of increasing amount of cationic lipids led to a gradual increase of capacitance in the lipid layers. As will be discussed in the following sections, this increase in capacitance can strongly influence the observed photocurrents.

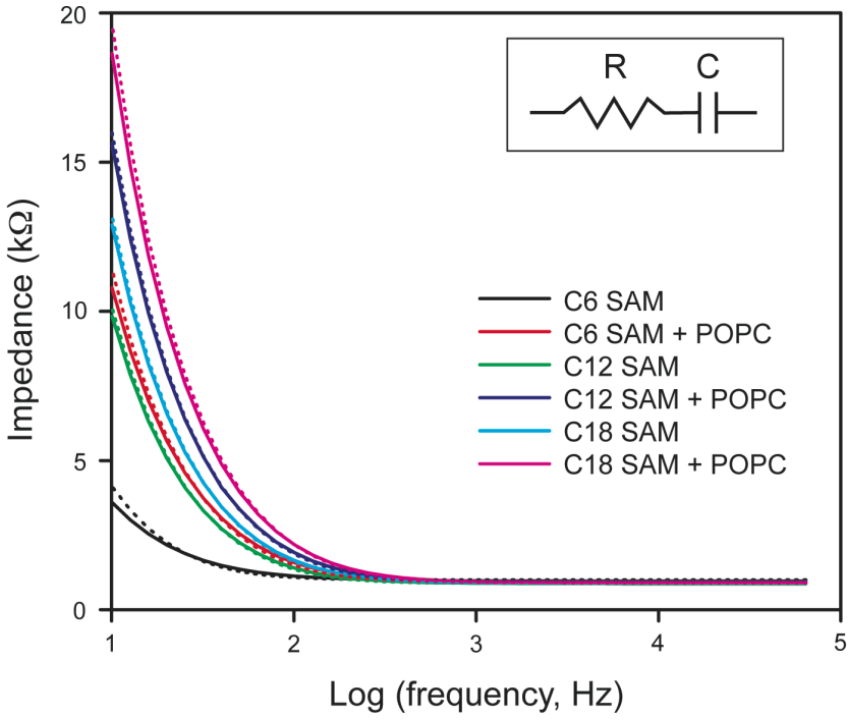

Figure 3.4 Impedance analysis of SAMs (of C_6-, C_{12}-, and C_{18}-thiol) and hybrid bilayers as a function of the applied ac frequency. Taken with permission from Ref. 3[3].

Table 1. Effect of different alkanethiol SAMs on the capacitance of the resulting POPC/alkanethiol bilayer membranes

	Capacitance of SAM layer (C_{SAM}: μF/cm^2)[a]	Capacitance of bilayer ($C_{bilayer}$: μF/cm^2)[a]	Capacitance of lipid layer (C_{lipid}: μF/cm^2)[b]
C_6	3.53	1.19	1.81
C_{12}	1.35 ± 0.02[c]	0.85 ± 0.03[c]	2.31 ± 0.09[d]
C_{18}	1.03	0.69	2.11

[a]Values are obtained by fitting the impedance data with a series-*RC* circuit model. [b]Calculated values. See text for more detail. [c]n = 3. [d]Calculated values.

Table 2. Effect of different amount of $Ru(bpy)_3^{2+}$-DOPE on the capacitance of the resulting POPC/C12 SAM bilayer membrane

	Capacitance of bilayer ($C_{bilayer}$: μF/cm^2)[a]	Capacitance of lipid layer(C_{lipid}: μF/cm^2)[b]
1%[c]	0.81 ± 0.04[d]	2.06
2%[c]	0.86 ± 0.02[d]	2.37
3%[c]	0.89	2.66

[a]Values are obtained by fitting the impedance data with a series-*RC* circuit model. [b]Calculated values. [c]Amounts of $Ru(bpy)_3^{2+}$-DOPE included in the POPC layer. [d]n = 3.

3.3.2 Photocurrent Generation

A series of experiments were carried out to understand the general behavior of the present photoconversion system based on $Ru(bpy)_3^{2+}$-tethered hybrid bilayer, which include 1) the dependence of photocurrents on light of different intensity and wavelength, 2) the dependence of photocurrents on the light exposure time, 3) the dependence of photocurrents on the potential bias applied and 4) the energetics associated with the anodic/cathodic photocurrent generation.

Figure 3.5 shows a preliminary photocurrent action spectrum in the range of 350-550 nm, which covers the metal-to-ligand charge transfer (MLCT) region of $Ru(bpy)_3^{2+}$-based complexes[13]. The MLCT state corresponds to an excited electronic state in which electron transfer from the metal to a ligand has occurred. In $Ru(bpy)_3^{2+}$, MLCT describes an electron is promoted from a metal-based dπ orbital to a low-lying π* level on the polypyridyl ligand (equation 1)[13a]:

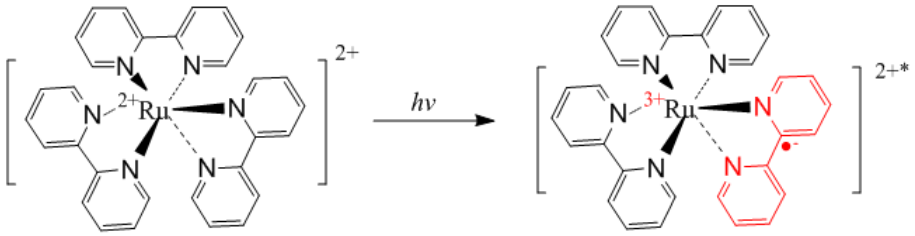

$$Ru^{II}(bpy)_3^{2+} \xrightarrow{h\nu} (bpy)_2Ru^{III}(bpy^{\bullet-})^{2+*}$$

The MLCT of $Ru(bpy)_3^{2+*}$ offers several desirable features: (1) excitation of $Ru(bpy)_3^{2+}$ to $Ru(bpy)_3^{2+*}$ is throughout the near UV and visible region, giving a maximum absorption at ~ 450nm; (2) $Ru(bpy)_3^{2+*}$ are quite stable; (3) they have long enough lifetime to undergo a chemical reaction; (4) they can easily to be oxidized or reduced, which facilitate electron transfer.

The spectrum generally correlates with the UV-vis spectrum taken directly from $Ru(bpy)_3^{2+}$-containing lipid bilayer formed on glass, indicating that the excited-state $Ru(bpy)_3^{2+}$* is responsible for the observed photocurrent generation.

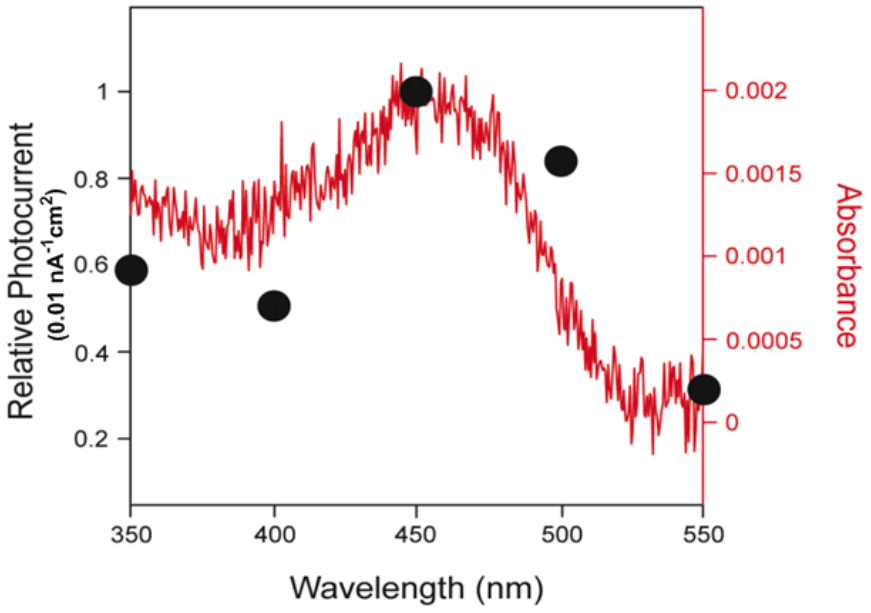

Figure 3.5 Photocurrent action spectrum obtained from POPC/C_{12} SAM hybrid bilayer membrane containing 3% $Ru(bpy)_3^{2+}$-DOPE. Ascorbate (50 mM) was used as the sacrificial

electron donor, in which the oxygen was depleted by adding 50mM glucose, 50 units/ mL glucose oxidase, and 200 units/mL catalase[5]. All photocurrents were measured against the cell open-circuit potentials (vs Ag/AgCl). The trace in red is the corresponding UV-vis absorption spectrum obtained from POPC lipid bilayers containing 3% $Ru(bpy)_3^{2+}$-DOPE formed on a clean glass substrate. Taken with permission from Ref. 3[3].

A linear relationship between the incident light intensity and the resulting photocurrent was observed when the light intensity was varied from 3.1 to 31.1 mW/cm^2 (Figure 3.6 a). Moreover, the photocurrents were also found to increase linearly with the increase of the electron mediator concentration up to ~100 mM (Figure 3.6 b). At still higher ascorbate concentrations, the photocurrents follow the same trend but at a somewhat slower rate. These results indicate that the photocurrent generation is limited by the diffusion of the mediator molecules to the $Ru(bpy)_3^{2+}$-bound lipid surface.

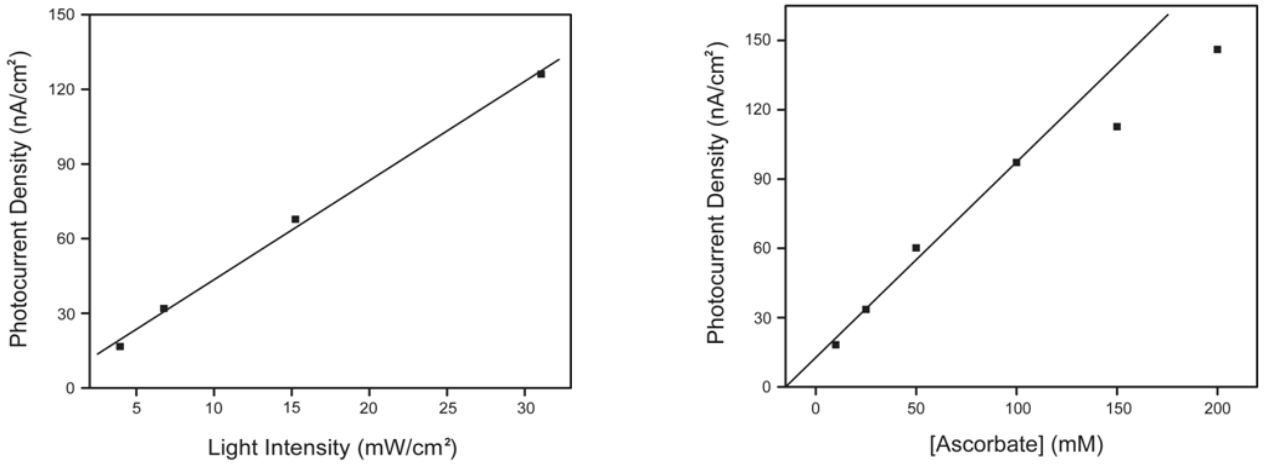

(a) **(b)**

Figure 3.6 Photocurrent vs. (a) the incident light intensity and (b) the sacrificial donor concentration. (a) The photocurrents were generated on a gold substrate covered with a

POPC/C_{12} SAM hybrid bilayer containing 3% $Ru(bpy)_3^{2+}$-DOPE. (b) Photocurrents were generated on a gold substrate covered with a POPC/C12SAM hybrid bilayer of 3% $Ru(bpy)_3^{2+}$-DOPE with various ascorbate concentrations. Light: 470 $\pm$ 20 nm. Other conditions are the same as in figure 3.5. Taken with permission from Ref. 3[3].

Figure 3.7 shows that either anodic or cathodic photocurrent generation can be realized in this system, when ascorbate (anodic) or methyl viologen/oxygen (cathodic) is used as sacrificial electron donor and acceptor, respectively. Moreover, for the cells based on 1% $Ru(bpy)_3^{2+}$-DOPE in POPC/C_{12} SAM hybrid bilayer membrane, a light conversion quantum efficiency (%) of 0.84(0.21) could be determined in the anodic (cathodic) photocurrent generation. Both processes are initiated by the photoexcitation of $Ru(bpy)_3^{2+}$, which produces a highly reactive electron/hole pair that can facilitate both reduction and oxidation at electrode depending on the energy level of the redox species present in solution. Noticeably, the cathodic photocurrent generated measures only 25% of the anodic current, which might be due to several reasons. First, the apparent thermodynamic driving force, i.e., the potential difference associated with anodic electron transfer processes, is about 560 mV higher than that of the cathodic case, (Figure 3.7 b), which eventually leads to a higher anodic photocurrent. Furthermore, compared to the reversible reduction of MV^{2+}/O_2 involved in the cathodic route, the oxidation of ascorbate in the anodic current generation directly leads to its decomposition. This irreversible process, therefore, greatly favors the forward electron transfer between ascorbate and $Ru(bpy)_3^{2+}$* by eliminating the competing charge recombination[14] between the two. Different redox intermediates are likely involved in the two photocurrent generation pathways (Figure 3.7 b). In the cathodic process, the excited $Ru(bpy)_3^{2+}$* species reduces MV^{2+} and O_2 and becomes $Ru(bpy)_3^{3+}$, which is then

reduced back to $Ru(bpy)_3^{2+}$ heterogeneously by the gold electrode[1b, 15]. In the anodic route, however, the excited $Ru(bpy)_3^{2+}$* is first reduced by ascorbate to $Ru(bpy)_3^{+}$, which then injects an electron into the electrode[16].

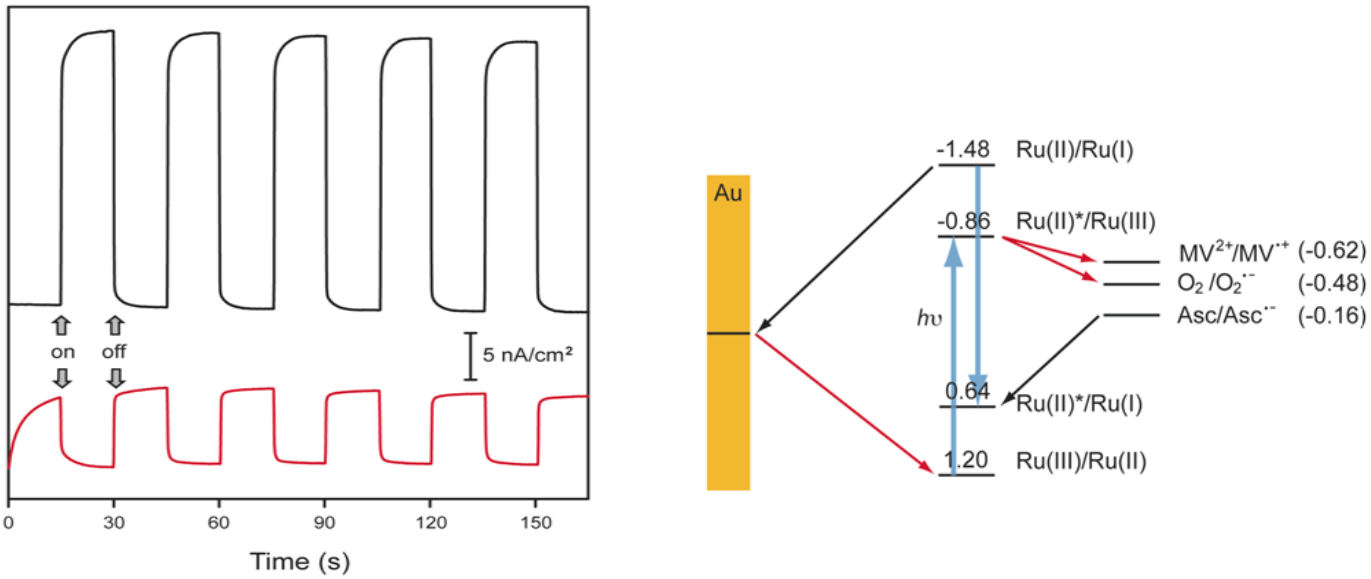

(a) **(b)**

Figure 3.7 Photocurrent (a) Anodic (curve in black) vs. cathodic (curve in red) photocurrents (taken after the initial decay, see Figure 3.8) from POPC/C_{12} SAM hybrid bilayers containing 1% $Ru(bpy)_3^{2+}$-DOPE. (b) Electrochemical potentials of species involved in the photocurrent generation. Taken with permission from Ref. 3[3].

Based on the electrochemical potential and electron transfer pathways involved in the anodic photocurrent generation, it can be derived that a positive bias applied on the gold electrode will induce a higher photocurrent, whereas a negative bias will do the opposite. This trend is confirmed by the result shown in Figure 3.8.

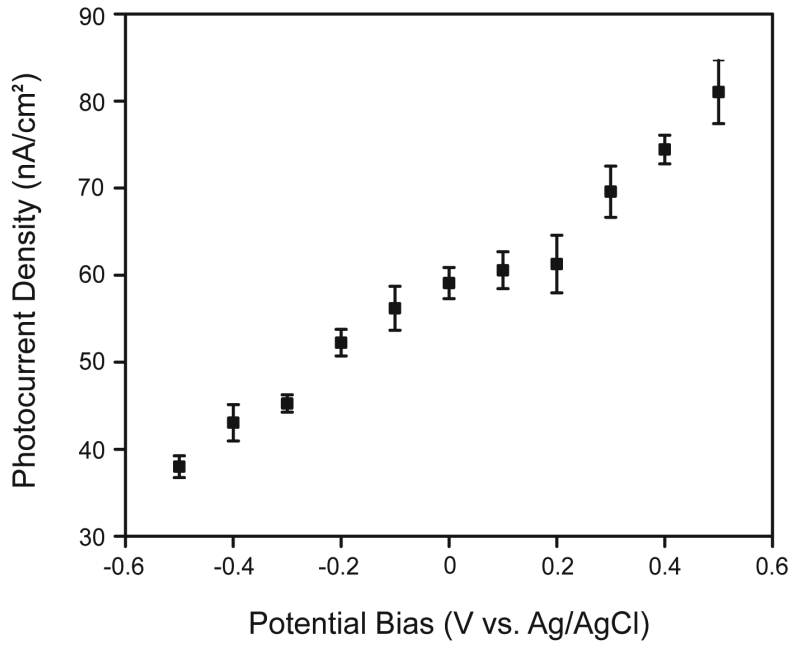

Figure 3.8 Effect of potential bias on the measured photocurrents.The lipid top layer contains 3% $Ru(bpy)_3^{2+}$-DOPE. Taken with permission from Ref. 3[3].

A decay of photocurrents was generally observed in the present photocurrent generation system. As shown in Figure 3.9, the sharpest decay occurred immediately after the initial light excitation, which was followed by a slower decay upon further exposure. Over a period of 20-min irradiation of the film with 15-s light pulses, a 43% decrease of photocurrent was resulted. This decay, however, can be greatly reduced by increasing the ascorbate concentration in the solution (red trace, Figure 3.9). Presumably, the photogenerated $Ru(bpy)_3^{2+}$* can react with some unidentified lipid moieties, which then leads to the degradation of the photoactive layer and thus the photocurrent decay. When a higher level of ascorbate is present, more $Ru(bpy)_3^{2+}$* become directly scavenged, leaving only less $Ru(bpy)_3^{2+}$* available for the photo-destructive reaction path. This result, therefore, indicates it is $Ru(bpy)_3^{2+}$*, rather than $Ru(bpy)_3^{+}$, that causes the photocurrent decay in the present system. It should be also mentioned that photocurrent decays

have also been observed previously in lipid-based systems, e.g., a photoelectrochemical cell based on fullerenes embedded in a black lipid membrane[17].

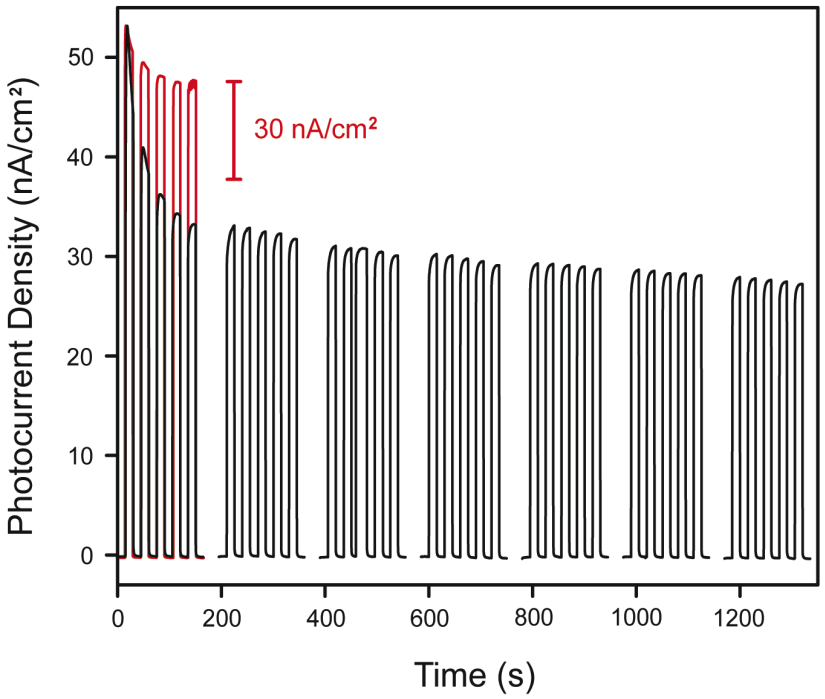

Figure 3.9 Photocurrent output as a function of photoexcitation time from POPC/C_{12} SAM hybrid bilayers containing 1% $Ru(bpy)_3^{2+}$-DOPE. The superimposed trace in red records the initial photocurrent decay when 200 mM ascorbate is used. Taken with permission from Ref. 3[3].

3.3.3 Photoinduced Electron Transfer across Hybrid Bilayer Membrane

It is important to understand how the photo induced electron transfer processes are initiated and sustained on a solid-supported phospholipid/alkanethiol hybrid bilayer membrane. Although discussions directly applicable to our system are not found in literature, general observations obtained from previous lipid-based photoconversion studies[18] can serve as a good starting point.

Depending on the chemical composition and structural arrangement of the system, photo induced electron transfer across lipid bilayers can follow either direct or mediated transfer pathways. In the absence of an electron mediator, moreover, the direct electron transfer pathway can proceed via either diffusion or electron-exchange based mechanisms, or to some extent, their combination. A mixed scenario has often been suggested, since the fluidic and dynamic lipids allow translocation and conformational change of photoactive species to occur within the matrix. On the other hand, a transfer process based on electron tunneling is more favored for systems in which the lipid matrix is rigid (i.e., polymerized or liquid-crystalline lipids) or the photosensitizer is too bulky to move freely. In these cases, a distance-dependent photocurrent generation is normally observed and an effective tunneling distance up to 40 Å has been proposed[18].

The overall performance of this new photoelectrochemical cell depends on the distance between the photoactive species and the electrode, and therefore, the thickness of the constituent SAM and phospholipid layers. To study this distance dependence, three alkanethiols (C_6-, C_{12}- and C_{18}-thiol) were used to form the hybrid bilayers with a POPC top layer and the resulting photocurrents taken after the initial decay were compared. As shown in Figure 3.10, relatively stable photocurrents were observed in all three cases. Moreover, a ~15% higher response was obtained when C_{12} SAM was the underlying layer, whereas photocurrents generated from hybrid bilayers with C_6 and C_{18} SAMs were roughly comparable. Compared to alkanethiols with relatively long alkane chains, C_6-thiol is too short to form a well-packed SAM on gold[7], which, in turn, prohibits the formation of a well-packed phospholipid monolayer. This explains why the hybrid bilayer based on the C_{12} SAM displays a higher photocurrent than that based on the C_6 SAM – even though the $Ru(bpy)_3^{2+}$ to electrode distance is likely smaller in the latter case, its

relatively lower $Ru(bpy)_3^{2+}$ surface coverage affords only a smaller photocurrent. On the other hand, while a similarly well-packed lipid monolayer is expected to form on both C_{12} and C_{18} SAMs, $Ru(bpy)_3^{2+}$ complexes are placed further away from the electrode when the C_{18} SAM serves as the base layer. This results in a weakened electron tunneling process and thus a smaller photocurrent.

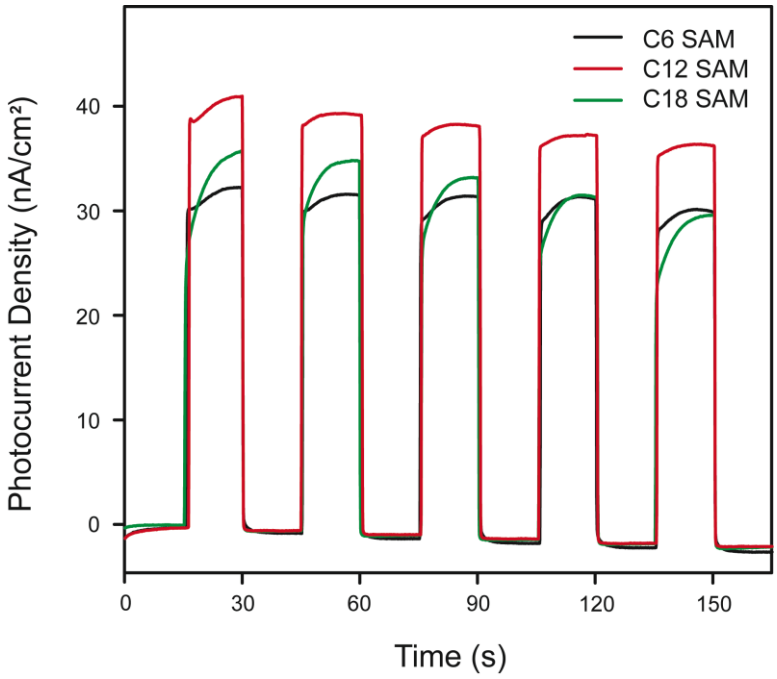

Figure 3.10 Effect of different alkanethiols on the obtained photocurrents. A POPC monolayer containing 1% $Ru(bpy)_3^{2+}$-DOPE was formed on top of different SAMs. Taken with permission from Ref. 3[3]

It is possible to estimate the apparent electrical thickness (d) of the POPC top layer from the calculated capacitance values using the following relationship: $1/C = d/\varepsilon\varepsilon_0$. As shown in Table 3, the thickness of POPC layers tends to vary depending on the underlying SAMs. The thinnest POPC layer is obtained when a C_{12} SAM is employed as the base, which again agrees with what observed by Silin and coworkers.[18] Noticeably, a significantly larger lipid layer

thickness, i.e., 1.32 nm, was obtained in the case of C_6 SAM, which is likely due to the poor packing and low ordering of the lipid/C_6 SAM bilayer that can lower the accuracy of the estimation. Additionally, when $Ru(bpy)_3^{2+}$-DOPE was added into POPC to form a mixed lipid top layer, the measured capacitance increased with the amount of $Ru(bpy)_3^{2+}$-DOPE included (Table 2). Assuming that the presence of $Ru(bpy)_3^{2+}$-DOPE does not affect the dielectric constant of the resulting lipid layers[19], it can be concluded that $Ru(bpy)_3^{2+}$-DOPE can reduce the electrical thickness of the lipid layer on the C_{12} SAM (Table 3). For example, a thickness of 0.90 nm was obtained for POPC layer containing 3% $Ru(bpy)_3^{2+}$-DOPE, as compared to 1.03 nm from the lipid layer of POPC alone. This thickness decrease can be understood as following: (1) the unsaturated dioleoyl chain in DOPE (T_m = −16 °C) further increases the degree of disorder of the POPC (T_m = −9 °C) layer and therefore, lowers the apparent thickness of the mixed lipid layer; (2) the hydrophilic, bulky $Ru(bpy)_3^{2+}$ moieties in the head group region of the lipid layer enlarges the penetration depth of water and ionic molecules into the lipid matrix, again resulting in a decrease in the apparent thickness of the mixed lipid layer.

Table 3. Calculated thickness of alkanethiol SAM and lipid layers[a]

	Thickness of SAM layer (nm)	Thickness of POPC lipid layer (nm)
C_6	0.58	1.32
C_{12}	1.51	1.03
		1.16 (1%)[b]
		1.01 (2%)[b]
		0.90 (3%)[b]
C_{18}	1.98	1.13

[a] ε values of 2.3 and 2.7 were used for alkanethiol and POPC monolayer in the calculation.[18] [b] Amounts of $Ru(bpy)_3^{2+}$-DOPE included in the POPC layer.

The above results obtained from impedance analysis enable us to correlate the measured photocurrents with the thickness of the hybrid bilayers and thus the electron tunneling distance. While higher loadings of $Ru(bpy)_3^{2+}$ in the lipid layer generally lead to higher photocurrents, a disproportionally larger current is obtained for the cell containing 3% $Ru(bpy)_3^{2+}$ (Figure 3.10a). Clearly, this extra increase of photocurrent arrives from the electrically thinner lipid layer induced by the presence of 3% $Ru(bpy)_3^{2+}$-DOPE, which allows electron transfer to occur more efficiently. Notice that this increase is not due to a proportionally higher loading of photoactive species in the film containing 3% $Ru(bpy)_3^{2+}$-DOPE. As shown in Figure 3.10b, the absorption/fluorescence spectroscopy data indicate that the amount of surface-immobilized $Ru(bpy)_3^{2+}$ varies almost linearly with its starting concentration in liposomes.

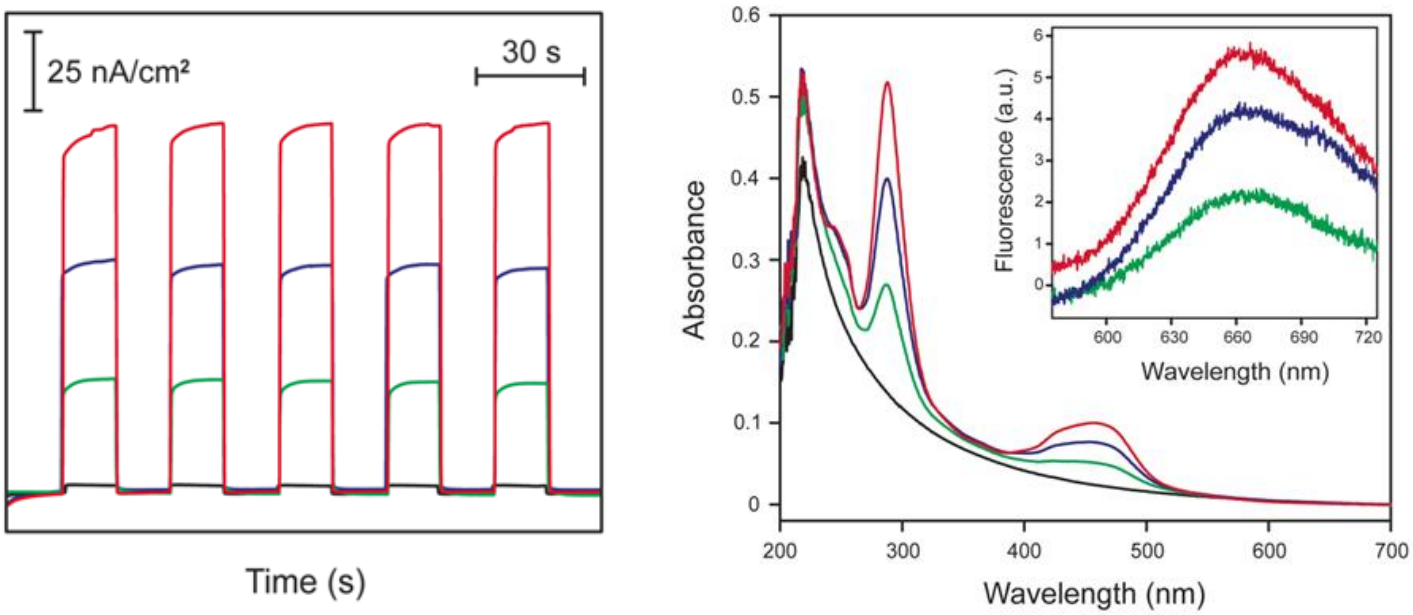

Figure 3.11 (a) Photocurrent vs. $Ru(bpy)_3^{2+}$-DOPE loading in the POPC phospholipid layer. (b) UV spectra (from bottom to top) are obtained from 0.25 mM POPC liposome solutions containing 0, 1, 2, and 3% $Ru(bpy)_3^{2+}$-DOPE in 10mMHEPES buffer solution. The inset records the corresponding fluorescence emission spectra obtained from $Ru(bpy)_3^{2+}$-DOPE lipid monolayers (1-3%, from bottom to top) formed on gold substrates. Taken with permission from Ref. 3[3].

A combined mechanism including both diffusion and electron tunneling processes can be proposed to account for the $Ru(bpy)_3^{2+}$-to-electrode electron transfer in the present system. Here, the hybrid bilayer yields a total electrical thickness of < 3 nm, which should allow electrons to tunnel directly from the top of the bilayer. In addition, $Ru(bpy)_3^{2+}$-DOPE lipids may also undergo some conformational change, through the bending of the DOPE head group within the lipid layer. These lipid-associated $Ru(bpy)_3^{2+}$ complexes can still bridge the electron transfer

path in the bilayer by taking electrons from those surface-oriented $Ru(bpy)_3^{2+}$ via the electron-tunneling based exchange mechanism[19]. This conformational change is considered possible here because (1) the mixed POPC/DOPE layer is highly disordered and fluidic, (2) $Ru(bpy)_3^{2+}$ exhibits a high solubility in both organic and aqueous media[20], and (3) upon photoexcitation, $Ru(bpy)_3^{2+}$ is reduced by ascorbate to $Ru(bpy)_3^{+}$, which should experience a lowered barrier moving towards the hydrophobic region of the lipids. Further research is needed to determine if this is indeed the case.

3.4 Conclusions

We have demonstrated here a new photocurrent generation system constructed on phospholipid/alkanethiol hybrid bilayers. This system exhibits important technical advantages over that based on symmetrical lipid bilayers, in that the two monolayers are added onto the electrode surface sequentially and the chemical/electrical properties of each layer can be separately tailored to achieve a higher performance. A number of strategies can be added into the present system to enhance the photoconversion efficiency. For example, multi-component systems containing multiple photosensitizing and antenna species, and, further improvements of the electron transfer paths across the bilayer using electrically conducting SAMs. Investigations along these lines are currently underway in this laboratory.

Supporting Information

(1) ^{1}H NMR spectra of $Ru(bpy)_3^{2+}$-DOPE in $CDCl_3$

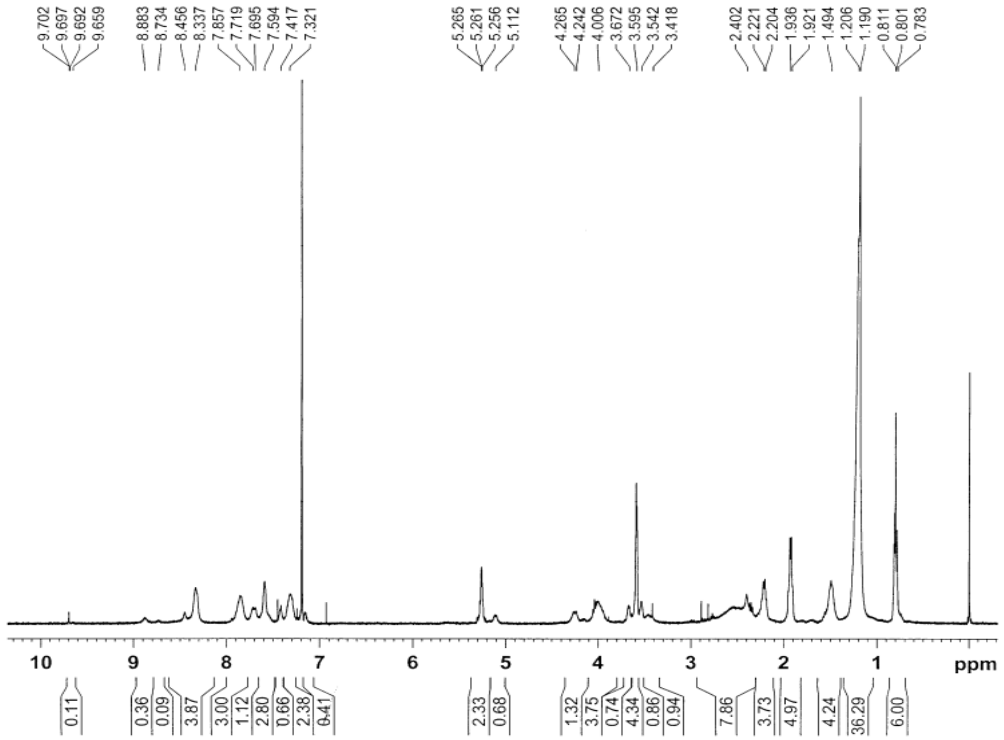

(2) Mass Spectrum of $Ru(bpy)_3^{2+}$-DOPE (Calculated M: 1352.6; $[M+H]^+$: 1353.6; $[M+H]^{2+}$: 676.8)

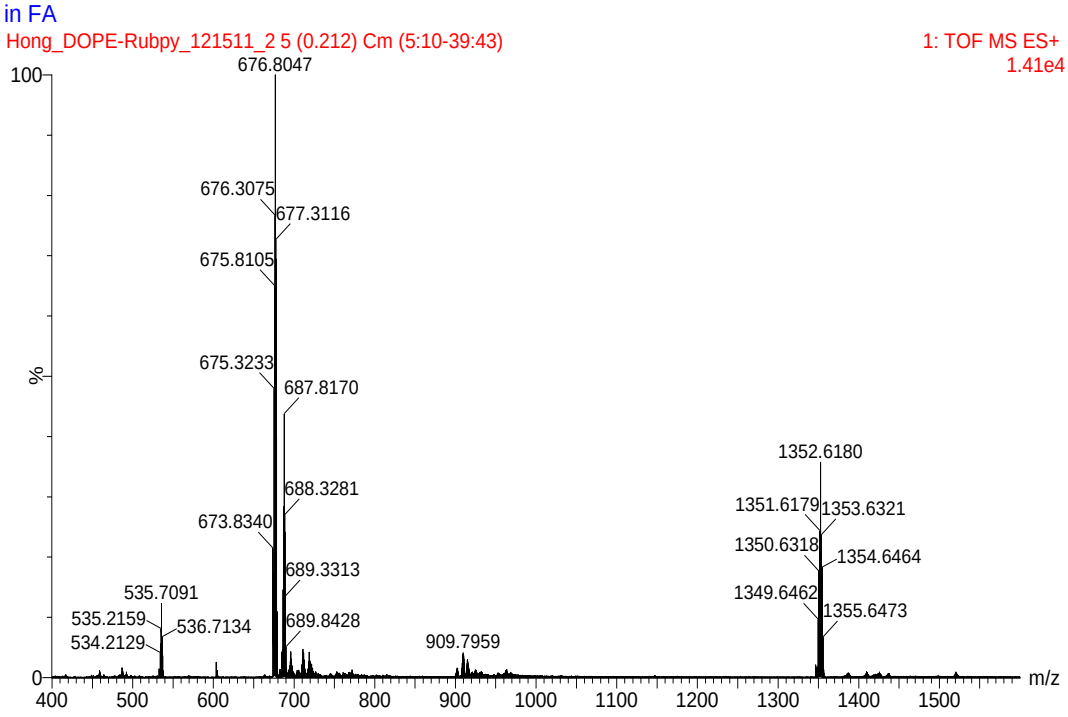

Reference

1. (a) Vuorinen, T.; Kaunisto, K.; Tkachenko, N. V.; Efimov, A.; Lemmetyinen, H., Photoinduced Interlayer Electron Transfer in Alternating Porphyrin–Fullerene Dyad and Regioregular Poly (3-hexylthiophene) Langmuir–Blodgett Films. *Journal of Photochemistry and Photobiology A: Chemistry* **2006,** *178* (2), 185-191; (b) Terasaki, N.; Akiyama, T.; Yamada, S., Structural Characterization and Photoelectrochemical Properties of the Self-Assembled Monolayers of Tris (2, 2'-bipyridine) ruthenium (II)-Viologen Linked Compounds Formed on the Gold Surface. *Langmuir* **2002,** *18* (22), 8666-8671; (c) Matsuo, Y.; Kanaizuka, K.; Matsuo, K.; Zhong, Y. W.; Nakae, T.; Nakamura, E., Photocurrent-generating Properties of Organometallic Fullerene Molecules on An Electrode. *Journal of the American Chemical Society* **2008,** *130* (15), 5016-5017.

2. (a) Sackmann, E., Supported Membranes: Scientific and Practical Applications. *Science* **1996,** *271* (5245), 43-48; (b) Lasic, D. D., Novel Applications of Liposomes. *Trends in biotechnology* **1998,** *16* (7), 307-321.

3. Jiang, K.; Xie, H.; Zhan, W., Photocurrent Generation from Ru(bpy)(3)(2+) Immobilized on Phospholipid/Alkanethiol Hybrid Bilayers. *Langmuir* **2009,** *25* (18), 11129-11136.

4. Love, J. C.; Estroff, L. A.; Kriebel, J. K.; Nuzzo, R. G.; Whitesides, G. M., Self-assembled Monolayers of Thiolates on Metals as A Form of Nanotechnology. *Chemical Reviews-Columbus* **2005,** *105* (4), 1103-1170.

5. Aitken, C. E.; Marshall, R. A.; Puglisi, J. D., An Oxygen Scavenging System for Improvement of Dye Stability in Single-Molecule Fluorescence Experiments. *Biophysical Journal* **2008,** *94* (5), 1826-1835.

6. Zhan, W.; Bard, A. J., Electrogenerated Chemiluminescence. 83. Immunoassay of Human C-reactive Protein by Using Ru (bpy) 32+-Encapsulated Liposomes as Labels. *Analytical Chemistry* **2007,** *79* (2), 459-463.

7. Porter, M. D.; Bright, T. B.; Allara, D. L.; Chidsey, C. E. D., Spontaneously Organized Molecular Assemblies. 4. Structural Characterization of n-alkyl Thiol Monolayers on Gold by Optical Ellipsometry, Infrared Spectroscopy, and Electrochemistry. *Journal of the American Chemical Society* **1987,** *109* (12), 3559-3568.

8. Buttry, D. A.; Ward, M. D., Measurement of Interfacial Processes at Electrode Surfaces with the Electrochemical Quartz Crystal Microbalance. *Chemical Reviews* **1992,** *92* (6), 1355-1379.

9. Dubois, L. H.; Nuzzo, R. G., Synthesis, Structure, and Properties of Model Organic Surfaces. *Annual Review of Physical Chemistry* **1992,** *43* (1), 437-463.

10. Silin, V. I.; Wieder, H.; Woodward, J. T.; Valincius, G.; Offenhausser, A.; Plant, A. L., The Role of Surface Free Energy on the Formation of Hybrid Bilayer Membranes. *Journal of the American Chemical Society* **2002,** *124* (49), 14676-14683.

11. Griffith, O.; Dehlinger, P.; Van, S., Shape of the Hydrophobic Barrier of Phospholipid Bilayers (Evidence for Water Penetration in Biological Membranes). *Journal of Membrane Biology* **1974,** *15* (1), 159-192.

12. Plant, A. L., Self-assembled Phospholipid Alkanethiol Biommetic Bilayers on Gold. *Langmuir* **1993,** *9* (11), 2764-2767.

13. (a) Meyer, T. J., Chemical Approaches to Artificial Photosynthesis. *Accounts of Chemical Research* **1989,** *22* (5), 163-170; (b) Alstrum-Acevedo, J. H.; Brennaman, M. K.;

Meyer, T. J., Chemical Approaches to Artificial Photosynthesis II. *Inorganic chemistry* **2005,** *44* (20), 6802-6827.

14. Wasielewski, M. R., Photoinduced Electron Transfer in Supramolecular Systems for Artificial Photosynthesis. *Chemical Reviews* **1992,** *92* (3), 435-461.

15. Nitahara, S.; Akiyama, T.; Inoue, S.; Yamada, S., A Photoelectronic Switching Device using A Mixed Self-assembled Monolayer. *The Journal of Physical Chemistry B* **2005,** *109* (9), 3944-3948.

16. Jukes, R. T. F.; Adamo, V.; Hartl, F.; Belser, P.; De Cola, L., Electronic Energy Transfer in A Dinuclear Ru/Os Complex Containing A Photoresponsive Dithienylethene Derivative as Bridging Ligand. *Coordination Chemistry Reviews* **2005,** *249* (13), 1327-1335.

17. Hwang, K. C.; Mauzerall, D., Photoinduced Electron Transport across A Lipid Bilayer Mediated by C70. *Nature* **1993**, 361, 138-140.

18. Lymar, S.; Parmon, V.; Zamaraev, K., Photoinduced Electron Transfer across Membranes. *Photoinduced Electron Transfer III* **1991**, 1-65.

19. Benz, R.; Frohlich, O.; Lauger, P.; Montal, M., Electrical Capacity of Black Lipid Films and of Lipid Bilayers made from Monolayers. *Biochimica et Biophysica Acta (BBA)-Biomembranes* **1975,** *394* (3), 323-334.

20. Latorre, R.; Oberhauser, A.; Labarca, P.; Alvarez, O., Varieties of Calcium-activated Potassium channels. *Annual Review of Physiology* **1989,** *51* (1), 385-399.

Chapter Four

Photocurrent Modulation by Ferrocene Terminated Alkanethiol based Hybrid Bilayer Membranes

4.1 Introduction

Alkanethiol SAMs can be engineered to exhibit a variety of chemical functionality, such as hydrophobicity[1], biocompatibility[2], and electroactivity[3] by varying the end group "X". In electrochemical applications, SAMs allow control of various physical and chemical properties at the electrode/electrolyte interface, therefore, they are used to study electron transfer processes[3c]. Since the electrochemistry of the ferrocene group (Fc = (η^5-C_5H_5) Fe (η^5-C_5H_5)) is known to be easy[3b, c, 4], it as the terminate group linked on alkanethiols has been widely used to study electron transfer on gold electrode[4a, 5]. However, a few examples of adding ferrocene groups within the hybrid bilayer membrane (HBM) have been studied [6]. For example, Nuzzo and co-workers [6a] formed a ferrocene groups embedded HBM by using ferrocene terminated alkanethiols and DMPC vesicles. Their analysis demonstrated that the hydrophobic environment of the HBM perturbs the electroactivity of the ferrocene group. Hosseini and co-workers [7] reported the ferrocene groups embedded HBM system by studying the effect of variations in lipids composition and counter ions in electrolyte. They found that although the midpoint potential and

electron transfer rate of the embedded ferrocene were affected by the hydrophobic nature of lipids, the redox ability of the lipid-embedded ferrocenium ions to was evaluated and found to be dependent on the nature of the counter ions.

Based on the previous study, it is shown that ferrocene terminated alkanthiol SAM can work as potential electron mediator to modulate electron transfer within HBM. With those results in mind, Chapter 4 investigated the possibility of using the ferreocene groups embedded HBM with photoactive species (either fullerenes or ruthenium tris(bipyridyl) complex) to modulate photocurrent generation, by comparing with the unsubstituted alkanethiol ($C_{12}SH$) based HBM. In both cases, it is found that the presence of a ferrocene layer in between the photoactive layer and the gold electrode can significantly modulate the observed photocurrents, leading to an enhanced cathodic current and an attenuated anodic current. This work presents an alternative strategy of organizing multiple photo-/redox-active agents on electrodes for photocurrent generation and may also provide a modular model system for studying photoinduced electron transfer across lipid membranes[8] (Figure 4.1).

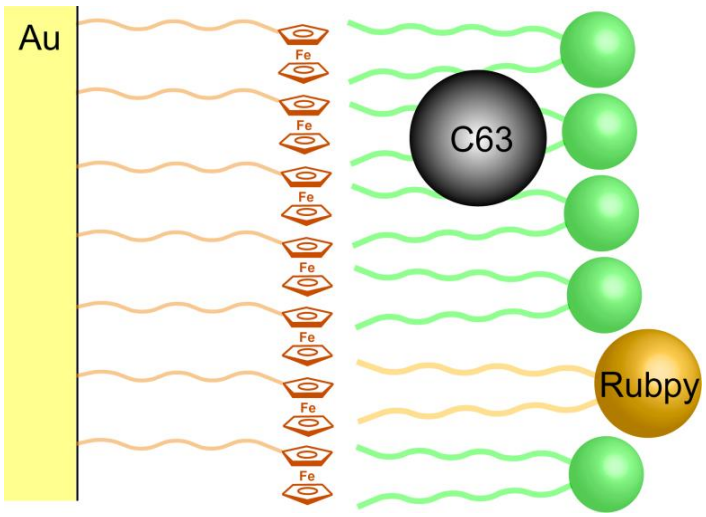

Figure 4.1 Schematic illustration of the multicomponent photocurrent-generating system constructed on hybrid bilayers The hybrid bilayers comprise a ferrocenyl-terminated SAM and

an upper lipid monolayer assembled with either fullerene or $Ru(bpy)_3^{2+}$. Taken with permission from Ref. 8[8].

4.2 Experimental

4.2.1 Reagents

Phospholipids such as 1-palmitoyl-2-oleoyl-*sn*-glycero-3-phosphocholine (POPC) and 1,2-dipalmitoyl-*sn*-glycero-3-phosphoethanolamine (DOPE) were obtained from Avanti Polar Lipids. Synthesis of monomalonic fullerene (C_{63})[9] and $Ru(bpy)_3^{2+}$-conjugated DOPE[10] was reported previously. 11-ferrocenyl undecanethiol (Fc-C_{11}SH) was received from Dojindo Co. and used without further purification. Sodium sulfate and sodium perchlorate were obtained from Fisher Scientific. Other reagents, including dodecanethiol (C_{12}SH), chlorophyll *a* (from spinach), 4-(2-hydroxyethyl)piperazine-1-ethanesulfonic acid (HEPES), methyl viologen dichloride hydrate (MV^{2+}), ruthenium (III) hexamine chloride, tetrabutylammonium tetrafluoroborate (Bu_4NBF_4, 99%), L(+)-ascorbic acid sodium salt (sodium ascorbate), D-(+)-glucose, glucose oxidase (type X-S, from *Aspergillus niger*) and catalase (from bovine liver) were obtained from Sigma-Aldrich. Tetrahydrofuran (THF, Reagent ACS grade) is from J. T. Baker, Inc. All aqueous solutions employed in these experiments were prepared using 18.2 M•Ω cm deionized water (Millipore).

4.2.2 Monolayer and Hybrid Bilayer Preparation

Gold-coated substrates were fabricated by sputtering gold (thickness: 100 nm) onto chromium-coated (thickness: 100 nm) silicon wafers. Prior to the self-assembly of alkanethiol monolayers, the gold-coated substrates were cleaned in piranha solution (3:1 v/v concentrated

H_2SO_4/30% H_2O_2 solution) for 15 min and then thoroughly rinsed with water and ethanol and dried in an argon stream. The cleaned gold electrodes were incubated in the ethanol solutions of 1 mM thiols ($C_{12}SH$, Fc-$C_{11}SH$ or their 1:1 mol mixture) at room temperature typically for >15h. After that, the SAM-modified gold substrates were carefully rinsed with ethanol and DI water, dried in argon, and then assembled in the Teflon cell for further use.

Liposomes of various compositions are prepared by an extrusion method as previously described in chapter 2. To form the SAM/lipid hybrid bilayers, typically a 300 μL of liposome solution with a total lipid concentration of 1 mM was added onto the SAM fixed in a Teflon cell and incubated at room temperature for 2h. The unbound liposome solution was then removed from the cell by exchanging with HEPES buffer solution (10 mM HEPES, 100 mM Na_2SO_4, pH 7.7) at least 20 times.

4.2.3 Quartz Crystal Microbalance (QCM)

QCM measurements were performed on a QCM analyzer equipped with a 5 MHz crystal oscillator (Model QCM25, Stanford Research Systems) at room temperature. The gold-coated quartz crystals were cleaned in piranha solution for 3 min and then rinsed with copious amount of water and ethanol and dried under argon. Thus cleaned crystals were incubated in the ethanol solutions of 1 mM thiols ($C_{12}SH$ or Fc-$C_{11}SH$) at room temperature for at least 15 h and then rinsed with ethanol and DI water, dried in argon. These SAM-covered gold crystals were then mounted onto the QCM oscillator connected to a flow cell. HEPES buffer (10 mM HEPES, 100 mM Na_2SO_4, pH 7.7) was first flowed through the cell until a steady frequency baseline was obtained (i.e., $\Delta f < 1.0$ Hz over 10 min). To initiate the lipid deposition on the SAMs, POPC liposome solutions of approximately 0.15 mM total lipids were flowed into the cell. Switching of

solutions delivered to the gold-coated QCM crystals was realized by the flow cell controlled by a peristaltic pump.

4.2.4 UV-vis Absorption Spectroscopy

UV-vis spectra were acquired with a UV-visible spectrophotometer (Cary 50 Bio, Varian). To obtain absorption spectra of chlorophyll *a* in hybrid bilayers, a home-machined Teflon cell was fitted to the sample holder of the same spectrometer and so optically aligned. The cell is configured to have an all-through liquid reservoir that can be sandwiched between two planar substrates, one of which is a semi-transparent gold substrates (10 nm Au coated on glass slides, Sigma-Aldrich) and the other microscope cover slides (VWR).

4.2.5 Impedance Analysis

The impedance of the alkanethiol monolayer and lipid/alkanethiol hybrid bilayer was measured with an SI 1260 impedance/gain-phase analyzer (Solartron). The measurements were carried out on a two-electrode setup, which comprises a gold film electrode covered with a monolayer (or a bilayer) and a Ag/AgCl (saturated KCl) electrode in 10 mM $NaClO_4$ aqueous solution. Throughout the measurements, the gold electrodes were poised at 0.0 V vs. Ag/AgCl, on which a sinusoidal ac wave of 10 mV is superimposed. The obtained data were fitted to an equivalent circuit consisting of a resistor (the electrolyte solution) and a capacitor (the surface bound layers) connected in series using the included analysis software package (ZView).

4.2.6 Fluorescence Spectroscopy

The fluorescence emission spectra of $Ru(bpy)_3^{2+}$-containing hybrid bilayers on 10-nm

gold-coated glass slides (Sigma-Aldrich) were acquired using a PI Acton spectrometer (SpectraPro SP 2356, Acton, NJ) that is connected to the side port of an epifluorescence microscope (Nikon TE-2000U, Japan). The emission signal was recorded by a back-illuminated digital CCD camera (PI Acton PIXIS: 400B, Acton, NJ) operated by a PC. The excitation was generated by a mercury lamp (X-Cite 120, EXFO, Ontario, Canada) filtered by a band-pass filter at 470±20 nm. The emission signal was filtered by a long-pass filter with a cutoff wavelength of 515 nm.

4.2.7 Electrochemistry and Photoelectrochemistry

The electrochemical and photoelectrochemical measurements were carried out in a three-electrode Teflon cell containing SAM-covered gold substrates (with/without lipid bilayer) as the working electrode, Pt wire as the counter electrode and Ag/AgCl (in saturated KCl) as the reference electrode. Cyclic voltammetry experiments were carried out in 1 mM hexaamine ruthenium (III) chloride ($Ru(NH_3)_6^{3+}$) in 100 mM $NaClO_4$ with a potentiostat (CHI 910B, CH Instruments). The scan rate was 100 mV/s.

Different solutions were employed in the anodic and cathodic photocurrent generation. For the anodic process, a 50 mM ascorbate in a buffer (10 mM HEPES, 100 mM Na_2SO_4, pH 7.7) was used; whereas a 50 mM methyl viologen in 100 mM Na_2SO_4 electrolyte solution was used in the cathodic process. The cell was irradiated with light from a Hg lamp (X-Cite, series 120 PC, EXFO) filtered at 470 ± 20 nm for $Ru(bpy)_3^{2+}$-based devices (average intensity: 20 mW/cm^2) and at 417 ± 30 nm for fullerene-based systems (average intensity: 40.0 mW/cm^2). In the case of anodic current generation, oxygen in the cell was removed by adding 50 mM glucose, 50 units/mL glucose oxidase, and 200 units/mL catalase in the solutions. To obtain the photocurrent

action spectra, the bilayer samples were irradiated with monochromated light from a Xe lamp (100 W) and the resulting photocurrents were recorded on a potentiostat (CHI 910B, CH Instruments). The variation of excitation light intensity at different wavelengths was corrected with a photometer (Thorlabs).

4.3 Results and Discussion

4.3.1 Characterization of Ferrocene-SAM/Lipid Hybrid Bilayers

Four techniques were employed to characterize the deposition of lipids on pre-formed $C_{12}SH$ and Fc-$C_{11}SH$ SAMs: quartz crystal microbalance (QCM), UV-vis absorption spectroscopy, cyclic voltammetry, and impedance analysis. Figure 1 shows the result of the QCM measurement, where the $C_{12}SH$ and Fc-$C_{11}SH$ SAMs were formed on gold-coated quartz crystals and the oscillation frequency shifts of these crystals were then used to monitor the deposition of lipids on corresponding SAMs. While a similar deposition profile was observed for the two SAMs when exposed to a POPC liposome solution, the frequency decrease associated with lipid deposition on the $C_{12}SH$ SAM was found to be slight larger: ~320 Hz vs. ~300 Hz for the Fc-$C_{11}SH$ SAM. According to the Sauerbrey equation[11], $\Delta f = -C_f \cdot \Delta m$, this result indicates that a slightly larger amount of POPC is deposited on the $C_{12}SH$ SAM than the Fc-$C_{11}SH$ SAM. For both SAMs, however, the magnitude of the frequency shifts would also suggest the formation of lipid multilayers, rather than a monolayer. Deviations from the ideal Sauerbrey behavior have been observed experimentally, which can be attributed to several factors[12], such as viscoelastic effect, surface roughness, interfacial liquid properties, and the stiffness of the film on the electrode. In a revealing study, Ha and Kim [13] evaluated the relative significance of these factors using a modified four-layer QCM model. In their case, frequency shifts as large as 1000-

2000 Hz were recorded when lipid vesicles were deposited on a $C_{18}SH$ SAM, whereas the accompanying ellipsometry measurement indicated exclusively monolayer formation. This large decrease in frequency was primarily attributed to a substantial increase in the viscosity of the liquid layer adjacent to the QCM electrode. When a monolayer of lipids was formed on top of the SAM, it alters the hydrophobicity of the surface and thus modifies the organization of the water layer near the electrode. To a less extent, the change of interfacial slippage conditions during lipid deposition can also cause the oscillation frequency to decrease.

On the other hand, the formation of alkanethiol-SAM/phospholipid hybrid bilayers, under conditions similar to ours, has been well established and characterized[14]. Since the deposition profiles obtained on $C_{12}SH$ SAM and Fc-$C_{11}SH$ SAM are rather similar, it is tentatively concluded that a monolayer, or close-to-monolayer, amount of POPC can be deposited on the Fc-$C_{11}SH$ SAM. As shown below, this conclusion is generally supported by other characterization results.

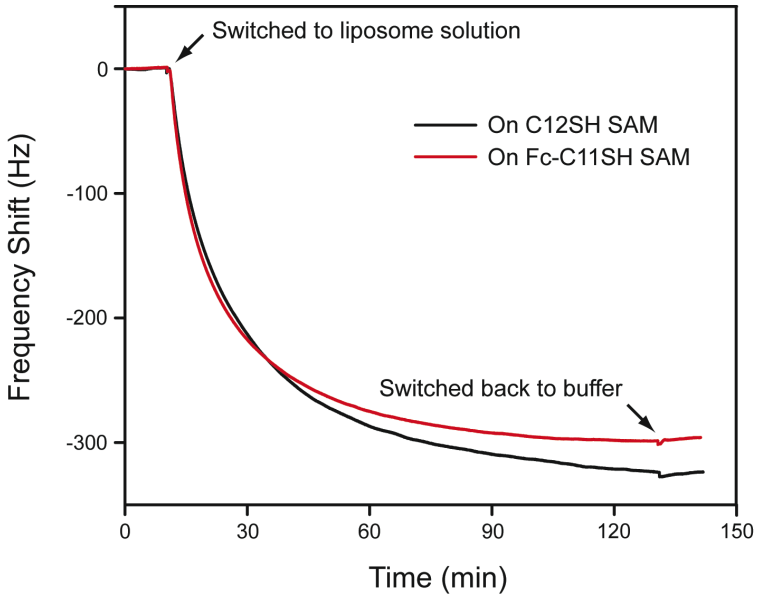

Figure 4.2 QCM monitoring of lipid deposition on either $C_{12}SH$ SAM (trace in black) or Fc-$C_{11}SH$ SAM (in red). Arrows indicate the times at which the solutions were switched from buffer

(10 mM HEPES, 100 mM Na_2SO_4, pH 7.7) to a POPC liposome solution (0.15 mM POPC in the same buffer) and then back. Taken with permission from Ref. 8[8].

4.3.2 UV-vis Absorption Spectroscopy

Taking advantage of the exceedingly high absorptivity of chlorophyll *a* (ε_{430}, ε_{660}: 1.1×10^5, 8.6×10^4 $M^{-1}cm^{-1}$ in diethyl ether)[15] and its high dispersity in lipid-based matrices[16], we formed bilayers containing chlorophyll *a* at the top lipid layer, whose absorption response was then used to quantify the amount of deposited lipids on $C_{12}SH$ and Fc-$C_{11}SH$ SAMs. In order for this quantification method to be valid, it is necessary to assume that the deposition of chlorophyll *a* on SAMs proceeds quantitatively, that is, proportional to its loading level in liposomes. As shown in Figure 4.3, for lipid layers deposited on both SAMs, the absorbance of associated chlorophyll *a* appears closely comparable. This result thus suggests that a lipid monolayer can be formed on a pure Fc-C_{11} SAM similar to C_{12} SAMs. This observation is consistent with the formation mechanism[17] of SAM/lipid hybrid bilayers, which is largely driven by the hydrophobic/hydrophobic interaction between the hydrocarbon portions of the two materials. The fact that a lipid monolayer can be formed on the two SAMs indicates that such a bilayer formation may take place as long as the terminal group of the underlying SAM is hydrophobic.

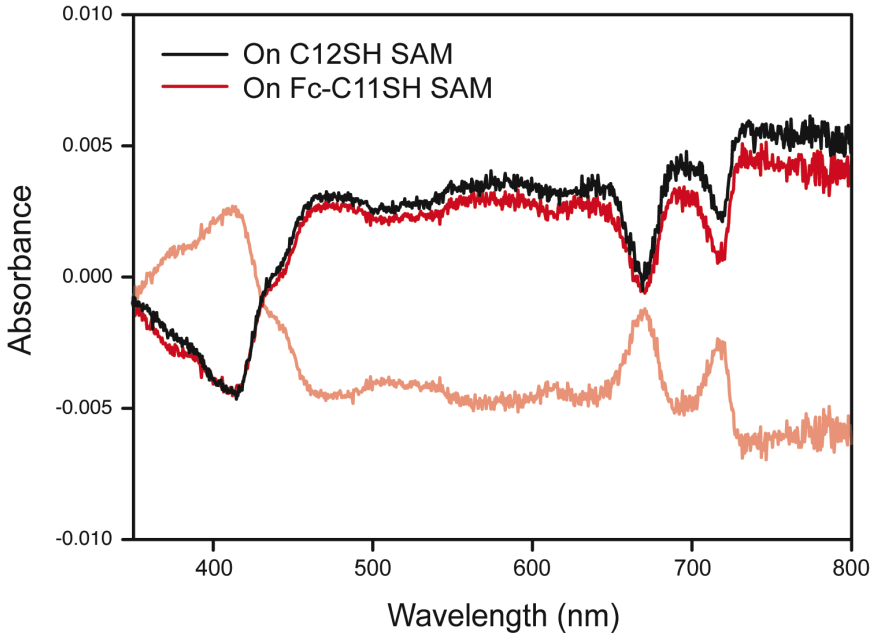

Figure 4.3 UV-vis spectra of 5% (mol) chlorophyll a in the POPC layer formed on either C_{12}SH SAM (in black) or Fc-C_{11}SH SAM (in red). For clarity, the spectrum in red was also inverted and offset in the Fig. (as shown in light red). To form such bilayers, POPC liposomes (~1 mM in HEPES buffer saline) incorporated with 5% chlorophyll a were incubated with the SAMs for 2h. Taken with permission from Ref. 8[8].

4.3.3 Electrochemistry

Cyclic voltammetry (CV) was used to monitor the formation of C_{12}SH and Fc-C_{11}SH SAMs on gold substrates. As shown in Figure 4.4, a quasi-reversible voltammogram was obtained on a bare gold surface using ruthenium hexamine ($Ru(NH_3)_6^{3+}$) as a probe. $Ru(NH_3)_6^{3+}$ was chose instead of $Fe(CN)_6^{3-}$, due to its redox potential will not affect that of ferrocene group on the alkanthiols. It is shown that SAM films on gold block the access of probe molecules to the electrode surface, thus resulting in decreased voltammetric responses. Noticeably, a higher level of blocking was observed on Fc-C_{11}SH SAM as compared to the C_{12}SH SAM. This phenomena can be explained in two aspects: first, it may be caused by the relatively bulky

ferrocene moiety in Fc-C_{11}SH that can separate the probe molecules in electrolyte farther away from the gold electrode as compared to C_{12}SH; second, $Ru(NH3)_6^{3+}$ may insert into SAM due to its smaller size and flexible orientation[18]. Compared with $Fe(CN)_6^{3-}$ we used previously[10], the level of blocking by C_{12}SH SAM is noticeably less when $Ru(NH3)_6^{3+}$ is used. According to study by Krysinski et. al[19], this phenomena may caused by the differences in their heterogeneous electron transfer rate constants and their hydrophobic/hydrophilic character.

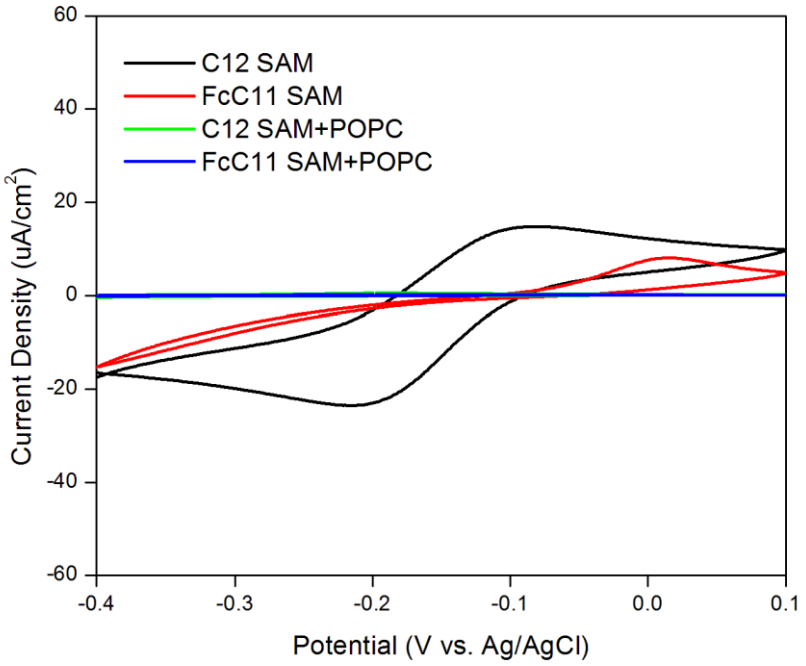

Figure 4.4 Voltammetric characterization of formation of C_{12}SH and Fc- C_{11}SH SAMs on gold electrodes. A deaerated solution containing 1 mM $Ru(NH3)_6^{3+}$ in 0.1 M NaClO4 was probed with gold film electrodes covered with different SAMs. A three-electrode setup with a Ag/AgCl reference electrode and a Pt counter electrode was used; scan rate: 100 mV/s.

Cyclic voltammetry was also performed on the Fc-C_{11}SH SAMs before and after lipid adsorption (Figure 4.5) in solution as well as in THF. For the pure ferrocene-covered SAM, a broad, nearly symmetrical oxidation/reduction wave was apparent, i.e., E_{pa}(E_{pc}) = 0.39(0.38) V

vs. Ag/AgCl. Integration of the charges associated with the voltammogram gives a ferrocene coverage of 2.1 x 10^{14} molecules/cm^2 (Figure 4.6 & table 1), consistent with a monolayer formation on gold[20]. Forming another lipid monolayer produces a drastic change on the resulting CV. In particular, the onset of the oxidation wave is shifted positively by more than 100 mV and once the onset is reached, additional increase of the applied potential gives rise to a sharp oxidation wave. Despite this significant difference, the integrated charges from the two CVs appear reasonably close, i.e., 1.9 x 10^{14} molecules/cm^2 for the lipid-covered SAM. The cathodic wave is similarly modified. While the E_{pa} almost stays unchanged, there is a ~−40 mV shift in E_{pc}. Additional measurements were also conducted on 1:1 C_{12} SH/Fc-C_{11}SH mixed SAM with/without the POPC top layer. Similar to the pure ferrocene SAM, the CV of the mixed SAM is broad and nearly symmetrical. Once it is covered with POPC, however, the CV response becomes narrowed and the oxidation peak is further shifted to more positive potential, i.e., 0.48 V. In THF, the CV of the pure Fc-C_{11} SH SAM features a positively shifted onset of the oxidation potential (as compared to that of POPC-covered Fc-C11SH SAM in water) and a large ΔE_p of nearly 200 mV , which indicates significant reorganization of ferrocene moieties in this solvent during reduction/oxidation. For the 1:1 C_{12} SH/Fc-C_{11} SH mixed SAM, the positive potential shift (as compared to that of the Fc-C_{11}SH SAM) is still observed but appears less pronounced than the case of lipid-covered SAMs probed in water, especially in the oxidation scan.

The difference in shape and onset potentials of these CVs confirms that a lipid film can be successfully deposited on ferrocene-terminated SAMs. For the Fc-C_{11} SH SAM directly exposed to the supporting electrolyte in water, the main redox wave at 0.39 V is broad and before it, there exists a small but still noticeable shoulder wave. Such kind of peak broadening

can be generally attributed to the heterogeneous orientation and organization of ferrocenyl moieties in the monolayer[21] and accompanying these changes, a modified interfacial potential distribution[22]. One explanation of the existence of two apparent redox waves in ferrocene SAMs is based on the argument of electrostatics. When the SAM is directly immersed in aqueous media, these ferrocenyl moieties would either form clusters with their immediate neighbors in the SAM, or remain isolated. Compared to the isolated ferrocenyl groups, the oxidation of clustered ferrocenes demands higher electrochemical potential, because, electrostatically, the presence of positively charged ferrocenium ions nearby disfavors further removal of electrons from the remaining ferrocenes within the cluster[23]. In turn, the presence of two populations of ferrocenes in the SAM produces two apparent redox waves in the voltammogram. Such electrostatic constrain is comparatively less significant in the 1:1 C_{12} SH/Fc-C_{11} SH mixed SAM, as the dilution lowers the chance of interaction among Fc-C_{11}SH thiol molecules and thus the fraction of clustered ferrocenes. As a result, its main redox wave appears less positive to that of the pure Fc-C_{11} SH SAM.

When these ferrocene-containing SAMs are further covered with a layer of lipids, the local dielectric environment surrounding these ferrocenyl groups is switched from water (high ε) to hydrocarbon chains of lipids (low ε), which modifies the interfacial potential distribution among different layers and thus the apparent redox potentials[22]. The fact that the potential shift and peak sharpening is also observed in THF points to the importance of local media immediately surrounding the electroactive layer in shaping the voltammetric response of the ferrocene moieties. Once in place, moreover, the top lipid layer would also impose a mass-transfer barrier for supporting electrolyte ions to reach the ferrocenyl sites for charge compensation. The transport of ions through the lipid layer appears to be strongly lipid

dependent, producing almost no potential shift when egg PC was used[20]; whereas for another bilayer formed with DMPC of two saturated C_{14} chains, a shift of >300 mV was observed[6a]. Our result shows that POPC top layer behaves closer to egg PC than DMPC in ferrocene-containing hybrid bilayers, which is likely related to the fluidity of these lipids at room temperature. In addition, it is evident from our result that the loading of ferrocenes in the mixed SAMs can also influence the level of potential shift.

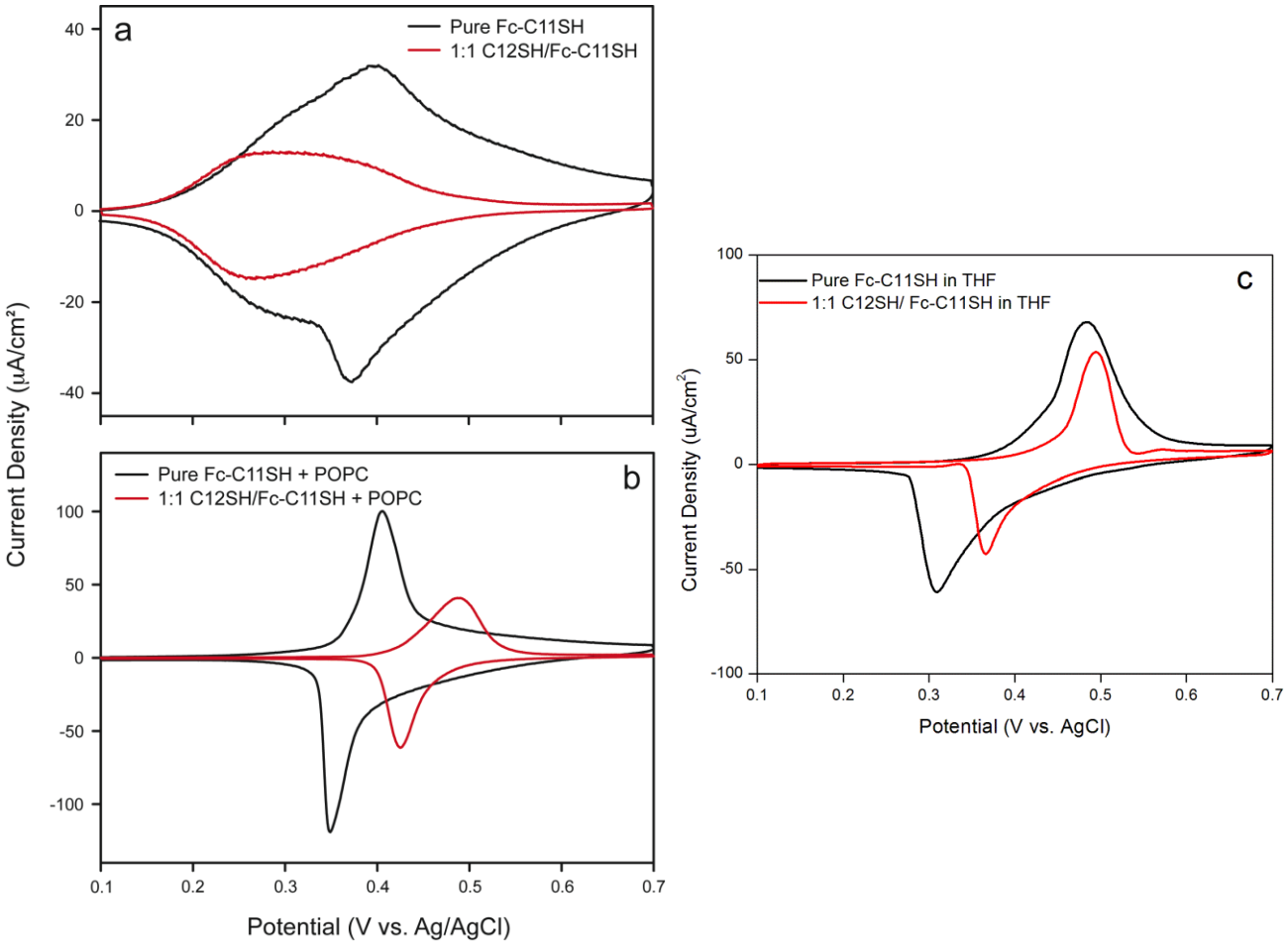

Figure 4.5 Cyclic voltammograms of ferrocenyl-terminated SAMs with/without coverage of a POPC top layer. Reduction/oxidation waves of ferrocene are obtained: (a) SAMs alone in 0.1 M

$NaClO_4$; (b) SAMs covered with POPC lipid monolayer in 0.1 M $NaClO_4$; (c) SAMs in THF. The SAMs are formed from either pure Fc-C_{11} SH thiols or a 1:1 (mol) mixture of C_{12} SH and Fc-C_{11} SH thiols. A three-electrode setup with a Ag/AgCl reference electrode and a Pt counter electrode was used. Scan rate: 100 mV/s.

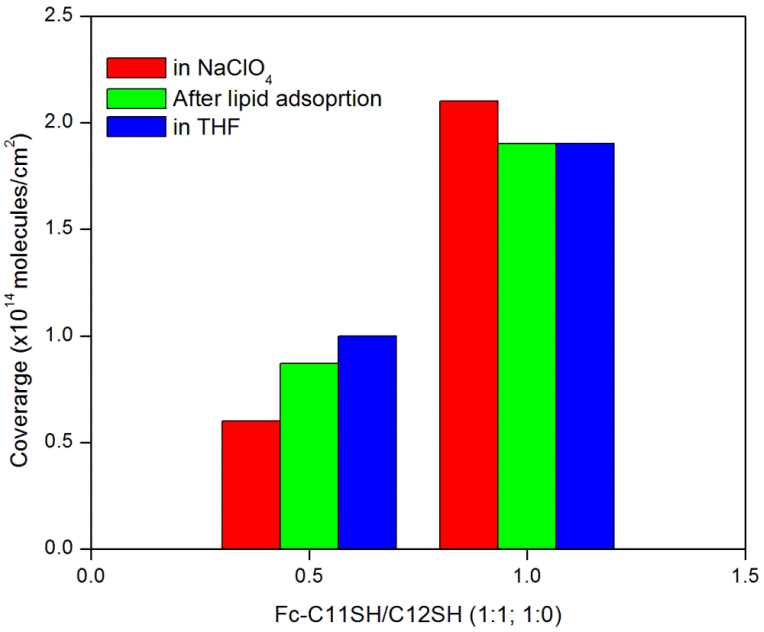

Figure 4.6 A schematic diagram of ferrocene surface coverage of ferrocenyl-terminated SAMs with/without a POPC top layer. Fc-C_{11} SH/ C_{12} SH (1:1 or 1:0) in $NaClO_4$ (red); after lipid adsorption (green); in THF (blue).

Table 4 Ferrocene surface coverage

Ferrocene surface coverage ($\times 10^{14}$ molecules/cm^{-2})	0.1 M NaClO4	Lipid adsorption	0.1 M THF
1:1 Fc-C_{11}/C_{12} SAM	0.60	0.87	1.0
Pure Fc-C_{11} SAM	2.1	1.9	1.9

4.3.4 Impedance Spectroscopy

Impedance analysis was performed on C_{12} SH and Fc-C_{11} SH SAMs as well as SAM/POPC bilayers similar to previous studies[10]. As shown in Figure 4.7, an increase in the circuit impedance is generally observed when the SAMs are further covered by a POPC layer. Fitting these data to a series *RC* circuit model, the capacitance associated with each SAM/bilayer can then be extracted (Table 5). The capacitance of the C_{12} SH self-assembled monolayer was found to be 1.51 μF/cm^2, in good agreement with 1.50 μF/cm^2 reported by Silin et al[24]. Furthermore, the thickness of the monolayer can be calculated from the following relationship: $1/C = d/\varepsilon\varepsilon_0$, where d is the thickness of the dielectric medium that separates the two conducting plates (i.e., the gold electrode and the electrolyte solution), ε is the dielectric constant of the separating medium (i.e., 2.3 for SAMs), and ε_0 is the permittivity of free space ($\varepsilon_0 \approx 8.854\times10^{-12}$ F m^{-1}). The capacitive thickness of the C_{12} SH SAM layer was thus calculated to be 13.5 Å. By contrast, the capacitance of Fc-C_{11} SH SAM was measured to be 1.66 μF/cm^2, which corresponds to a thickness of 12.3 Å and hence is close to the C_{12} SH SAM.

For the hybrid bilayers, the capacitance of the lipid layer alone (C_{lipid}) can be calculated from the capacitance of the bilayer (C_{BL}) and the alkanethiol SAM (C_{SAM}) layer by the following relation: $C_{\text{lipid}}^{-1} = C_{\text{BL}}^{-1} - C_{\text{SAM}}^{-1}$. The capacitance of POPC lipid monolayer formed on the C_{12} SH SAM is determined to be 2.78 μF/cm^2, whereas on the Fc-C_{11} SH SAM it is 2.86 μF/cm^2. In turn, these capacitance values allow the dielectric thickness of the POPC layer to be calculated: 8.6 Å (on C_{12} SH SAM) vs. 8.4 Å (on Fc-C_{11} SH SAM), using ε = 2.7 for POPC. These results again suggest that monolayer quantity of POPC is formed on the ferrocene-terminated SAM as compared to its methyl-terminated counterpart.

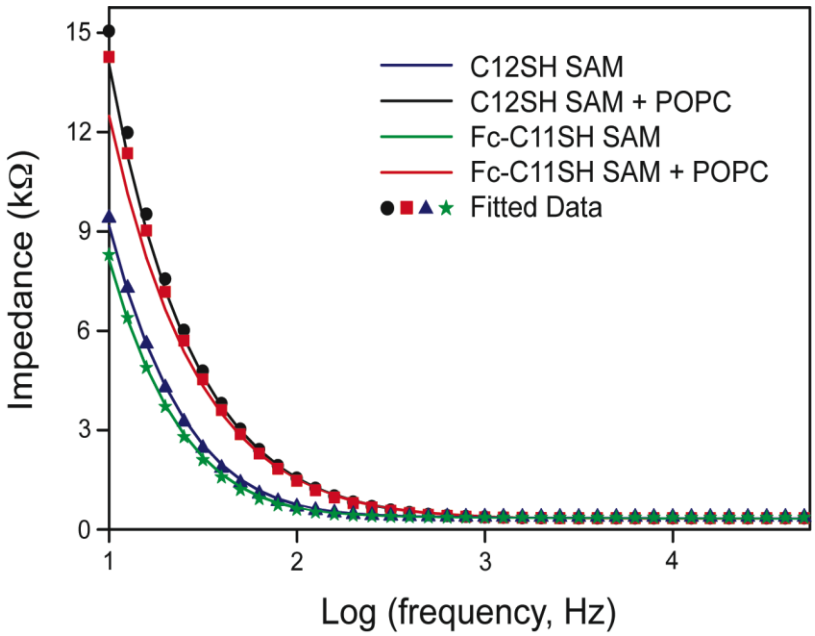

Figure 4.7 Impedance spectra (curves in solid lines) of C_{12}SH and Fc-C_{11}SH SAMs and the corresponding hybrid bilayers. Here, impedance of the films was monitored as a function of the applied ac frequency. A series-*RC* circuit model is used to fit the resultant cell impedance in all measurements. The fitted data are presented by four different symbols colored according to their corresponding impedance spectrum. Taken with permission from Ref. 8[8].

Table 5 Effect of C_{12}SH SAM and Fc-C_{11}SH SAM on the Capacitance of the POPC/Thiol Bilayers

	Capacitance of SAM layer[a] (C_{SAM}: μF/cm^2)	Capacitance of the bilayer[a] (C_{BL}: μF/cm^2)	Capacitance of the lipid layer[b] (C_{lipid}: μF/cm^2)
C_{12}SH SAM	1.51 ± 0.01	0.98 ± 0.02	2.78
Fc-C_{11}SH SAM	1.66 ± 0.01	1.05 ± 0.02	2.86

[a]Measured values of same samples (n = 3). [b]Calculated values.

Table 6 Calculated Dielectric Thicknesses of SAMs and Lipid Layers[a]

	Thickness of the SAM layer (Å)	Thickness of the POPC lipid layer (Å)
C_{12} SH SAM	13.5	8.6
Fc-C_{11} SH SAM	12.3	8.4

[a] ε values of 2.3 and 2.7 were used for alkanethiol and POPC monolayer, respectively, in the calculation.

4.3.5 Photocurrent Generation/Modulation on Hybrid Bilayers.

Two photoactive species, monomalonic fullerene (C_{63}) and $Ru(bpy)_3^{2+}$, are separately studied in the photocurrent generation. While fullerenes are directly embedded in the POPC top layer of the hybrid bilayer by fusing C_{63}-incorporated liposomes onto preformed SAMs, $Ru(bpy)_3^{2+}$ species are tethered on the head group of lipid layer (Figure 4.1). Consequently, when the Fc-C_{11}SH SAM is employed as the underlying layer, the hybrid bilayers contain the photoactive component (either C_{63} or $Ru(bpy)_3^{2+}$) at the top and the redox active ferrocenes roughly at the center of the hybrid bilayer.

Figure 4.8 records the photoelectrochemical action spectra of hybrid bilayers containing either $Ru(bpy)_3^{2+}$ or fullerene C_{63}. For the $Ru(bpy)_3^{2+}$-containing bilayer the maximal current was observed at ~450 nm, which matches the metal-to-ligand charge transfer electronic transitions of $Ru(bpy)_3^{2+}$-DOPE in the liposome sample; and for the C_{63}-containing bilayer, the broad photocurrent profile again follows the absorption of the fullerene-based liposome sample. The general agreement between the action spectra and the corresponding UV-vis absorption

spectra thus establishes that these lipid-assembled photoactive species are responsible for the generated

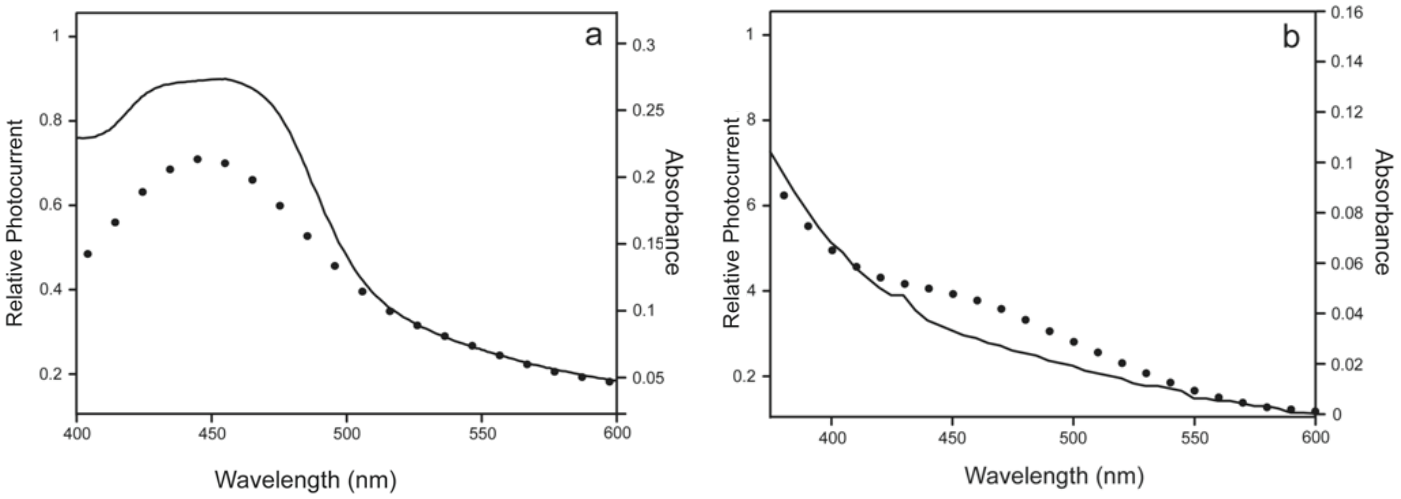

Figure 4.8 Photoelectrochemical action spectra (dotted responses) of hybrid bilayers comprised of either 2% $Ru(bpy)_3^{2+}$ (a) or 2% fullerene C_{63} (b) in the POPC top layer with a Fc-C_{11} SH SAM underlayer. The photocurrents were generated in a three-electrode cell containing 50 mM methyl viologen in HEPES buffer. The excitation light of different wavelengths was corrected with a photometer. The corresponding absorption spectra (solid lines) were obtained from 0.25 mM POPC liposome samples containing either 2% $Ru(bpy)_3^{2+}$-DOPE (a) or 2% C_{63} (b).

Figure 4.9a compares anodic/cathodic photocurrents generated from 2% $Ru(bpy)_3^{2+}$ deposited on C_{12} SAM and Fc-C_{11} SAM. Under anodic conditions, a ~30% less current was consistently generated from the bilayer containing Fc-C_{11} SH SAM compared to that with C_{12} SH SAM. This difference in the obtained photocurrents should not be caused by a higher loading of $Ru(bpy)_3^{2+}$-DOPE on the C_{12} SH SAM[10]: when the same films were subjected to the cathodic photocurrent generation, an approximately 40% higher current was obtained from the Fc-C_{11} SH

SAM based bilayer. Thus, the insertion of an electroactive ferrocene layer in between the layer of photoagents and the electrode can modulate the photocurrent generation in the bilayer-based system.

A similar trend was also observed on bilayers comprising fullerene C_{63} as the photoactive agent (Figure 4.9b). Here, a ~80% decrease of anodic photocurrent was seen for fullerenes immobilized on Fc-C_{11} SH SAM as compared to that formed on the C_{12} SH SAM; whereas a ~4-fold enhancement in cathodic current was observed for the ferrocene-containing bilayer. Thus, a significantly stronger modulation can be achieved on fullerene-based devices compared to those based on $Ru(bpy)_3^{2+}$.

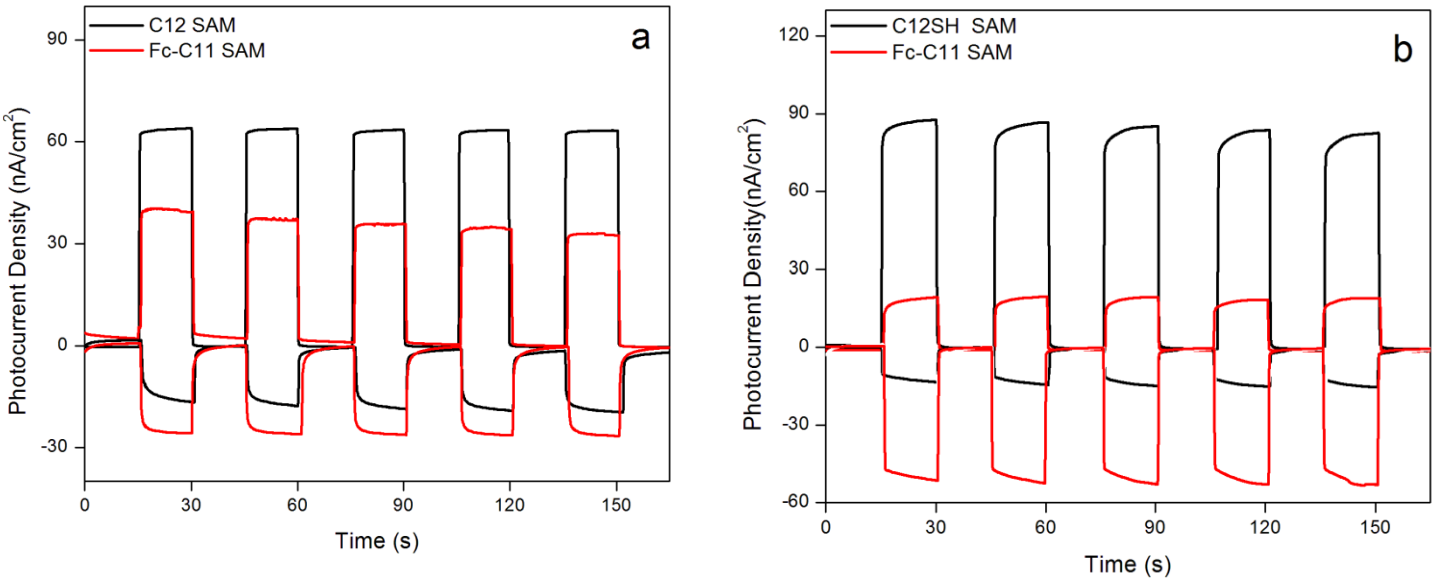

Figure 4.9 (a) Photocurrents generated from 2% $Ru(bpy)_3^{2+}$-DOPE in POPC lipid monolayer formed on Fc-C_{11} SH SAM/C_{12} SH SAM (0:1(black);1:0 (red)). (b) Photocurrents generated from 2% fullerene C_{63} embedded in POPC monolayer formed on Fc-C_{11} SH SAM/C_{12} SH SAM (0:1(black);1:0 (red)). The anodic photocurrents (traces in the top panel) were generated in 50 mM ascorbate dissolved in HEPES buffer (10 mM HEPES, 100 mM NaCl, pH 7.7), in which

oxygen was depleted by adding 50 mM glucose, 50 units/mL glucose oxidase, and 200 units/mL catalase. (Bottom) Cathodic photocurrents were obtained from 50 mM methyl viologen dissolved in the same buffer.

The generation and modulation of photocurrents in the present system can be understood by evaluating the energy levels and relative position of the involved species in the bilayer (Figure 4.10). In the anodic process and for fullerene C_{63} immobilized on the C_{12} SH SAM, the highly oxidizing excited-state fullerene takes one electron from ascorbate in the solution and thus formed anion radical then passes an electron to the gold electrode. By contrast, when the underlying layer is a Fc-C_{11} SH SAM instead, the presence of ferrocenes in the bilayer inserts a set of new energy states along the ET pathway that photogenerated electrons may temporarily occupy. Importantly, when the gold electrode is poised at 0 V vs. Ag/AgCl, further transfer of electrons from these intermediate states (centered at 0.38 V) becomes a thermodynamically uphill process and thus is expected to be hindered, leading to a decrease in the anodic photocurrents. A very different scenario exists in the cathodic photocurrent generation (bottom panel, Figure 4.10). Here, electrons flow out from gold first to ferrocenes and then to fullerenes. Together, these three energy levels form an overall downhill redox gradient that can facilitate cross-membrane ET processes. As theoretically analyzed by Warshel and coworkers,[49] one way to achieve efficient light-induced ET across low dielectric matrices such as a lipid bilayer is to form a cross-membrane electrochemical gradient; in this case, the forward ET steps can effectively compete with the backward processes because of the significantly lower activation barriers associated with the forward processes.

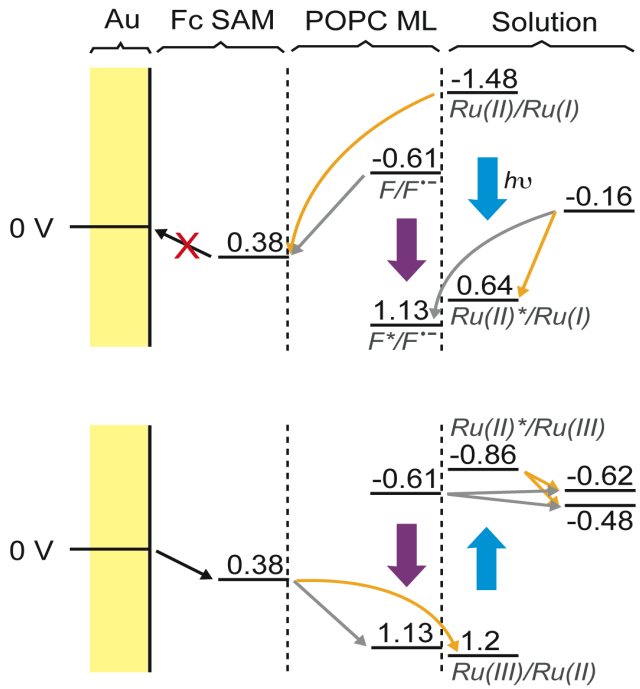

Figure 4.10 Energy diagrams of electro- and photo-active species involved in the anodic (top panel) and cathodic (bottom) photocurrent generation processes. Different mediators were employed in the anodic (ascorbate at −0.16 V vs. Ag/AgCl) and cathodic (O_2 at −0.48 V and methyl viologen at −0.62 V) processes. The redox potential of ferrocene is obtained from Figure 4.5 of this work, whereas the potentials associated with $Ru(bpy)_3^{2+}$ and fullerene are taken from Refs.10[10] and 25[25], respectively. The electron-flow pathways for $Ru(bpy)_3^{2+}$ (in orange) and fullerene (in gray) are indicated by arrows. Thick arrows indicate photoexcitation of the photoagents: 417 ±30 nm for fullerene (in purple) and 470 ±20 nm for $Ru(bpy)_3^{2+}$ (in blue).

A similar analysis can be raised for the $Ru(bpy)_3^{2+}$-based system. Here, the photoexcited $Ru(bpy)_3^{2+}$ first reacts with either ascorbate (in the anodic process) or oxygen/methyl viologen (cathodic) in the solution to give either $Ru(bpy)_3^{+}$ or $Ru(bpy)_3^{3+}$. Further electron exchange between these photogenerated species and the gold electrode is again modulated by the ferrocenes situated in between, resulting in either a deceased anodic current or an enhanced

cathodic current (Figure 4.9 a). Mechanistically, there exists a possibility that the ferrocenes in the bilayer may compete with the redox species in the solution for reacting with $Ru(bpy)_3^{2+*}$ via electron transfer. These processes, even present, are expected to be relatively small, considering that the lipid-conjugated $Ru(bpy)_3^{2+}$ molecules are directly exposed to the solution redox molecules, while on the other side separated from the underlying ferrocenes by the low dielectric hydrocarbon chains of POPC. This analysis is further supported by the fluorescence spectroscopy results of $Ru(bpy)_3^{2+}$-containing bilayers. As shown in Figure 4.11, $Ru(bpy)_3^{2+}$ immobilized on Fc-C_{11} SH SAM displayed ~25% higher fluorescence intensity as compared to that formed on the C_{12} SH SAM (spectrum 1 and 2). Besides ferrocene and ascorbate, it is important to realize that the gold film underneath can also quench fluorescence via energy transfer.[50-52] For fluorophores located close to a planar metal surface, the fluorescence lifetime decays inversely to the fourth power of the fluorophore-to-metal distance.[26,27] Thus, the less fluorescence observed from $Ru(bpy)_3^{2+}$ deposited on Fc-C_{11} SH SAM may be attributed to the slightly larger displacement of fluorophores from the gold surface in the ferrocene-containing bilayer. From these data, it is hard to directly gauge the contribution of ferrocenes in the resulted fluorescence quenching. Nevertheless, if this contribution is dominant, it should leave no further room for other quenchers to significantly quench the fluorescence. Yet, with the addition of ascorbate into the solution, the fluorescence emission was seen to decrease by ~55% on Fc-C_{11} SH SAM and ~65% on C_{12} SH SAM (spectrum 3 and 4, Figure 4.11), as a result of reductive quenching. These results thus indicate the electron exchange between photoexcited $Ru(bpy)_3^{2+}$ and electron donor species in solution is more likely the initial step of the ET cascade that eventually leads to the anodic photocurrent generation (Figure 4.9). A similar trend was also observed in the cathodic photocurrent generation where methyl viologen and oxygen were used

as electron acceptors. To gain a more quantitative understanding of the relative contribution of each quencher, we plan to perform time-resolved fluorescence analysis in the follow-up study.

On the other hand, the consistently lower degree of photocurrent modulation seen in the $Ru(bpy)_3^{2+}$-based systems reflects the importance of size and relative position of photoagents in the bilayer in determining such a modulation effect. As we discussed previously,[30,32] the hydrophobic bulk of the amphiphilic fullerene C_{63} is believed to be buried in the hydrocarbon region of the lipid layer, whereas the DOPE-conjugated $Ru(bpy)_3^{2+}$ moieties are relatively hydrophilic and thus should stick up from the lipid/water interface and directly face the initial layers of the aqueous phase. Consequently, the differences in location and size of the two agents render the fullerenes to be positioned closer to the underlying ferrocenes, which gives rise to a stronger electronic coupling between the two and thus a larger change in photocurrents as compared to the case of $Ru(bpy)_3^{2+}$.

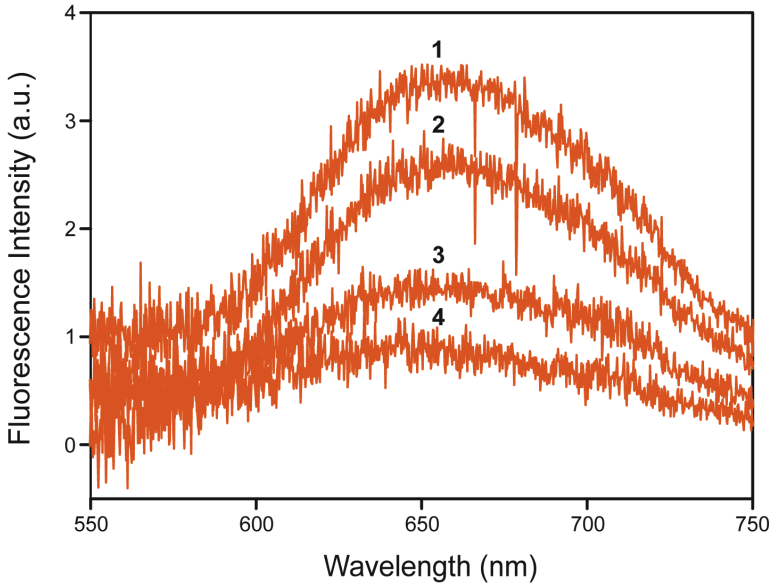

Figure 4.11 Fluorescence emission spectra of 2% $Ru(bpy)_3^{2+}$-DOPE assembled in either POPC/Fc-C_{11} SH SAM (spectrum 1 and 3) or POPC/C_{12} SH SAM (spectrum 2 and 4) bilayers. In

all samples, the oxygen was removed from the solution using an enzymatic oxygen scavenging system containing glucose oxidase, catalase and glucose (see the Experimental Section). Of these, samples used to acquire spectrum 2 and 4 in addition contained 50 mM ascorbate. Excitation was made at 470 ±20 nm.

Previous studies have detailed several other approaches of using ferrocene derivatives to modulate photocurrents in layered architectures. For example, by using Langmuir-Blodgett deposition technique to organize amphiphilic polymers containing either $Ru(bpy)_3^{2+}$ or ferrocene moieties on electrodes, Miyashita and coworkers[28] found the direction of photocurrents depends on the deposition order of the redox polymers on electrodes. By further connecting the anodic and cathodic films in series and altering the deposition order of the two components, logic operations such as 'OR' and 'XOR' could also be achieved. In another self-assembly based study, Matsuo and colleagues[29] synthesized penta(carboxylic) ferrocene-fullerene complexes that could be directionally immobilized on indium tin oxide electrodes. The close distance between the ferrocene and fullerene in the complex afforded a complete rectification of the obtained photocurrents. In comparison, a complete rectification of anodic photocurrent is not seen in the present system, even for just 2% fullerene C_{63} immobilized on the pure Fc-C_{11}SH SAM, which may be caused by the following factors. First of all, compared to the system studied by Matsuo et al.,[29] the distance between fullerene and ferrocene in our system is still not ideal for maximal electronic coupling. Further, the low dielectric matrix formed by the SAMs and lipids can pose additional barriers to the photoinduced ET processes across the bilayer. Finally, it is also conceivable that gold electrodes used in this study may play a role in the occurrence of leakage photocurrents, considering the differences in its interfacial electronic characteristics and band structure as compared to the semiconducting indium tin oxide employed in their work.

4.4 Conclusions

We have demonstrated here that lipid monolayers can be formed on pure ferrocene-terminated C_{11} -alkanethiol SAMs similar to their alkanethiol counterparts. When photoagents are incorporated into such bilayers, modulation of photocurrents is resulted. Such a modulation effect was found to be dependent on the distance between the photoagents and ferrocene moieties in the bilayer. Considering the scope and flexibility of lipid-based amphiphilic assembly, this lipid/SAM hybrid system should be found useful in study of several aspects of photoinduced cross-membrane ET processes, including various physiochemical parameters (e.g., distance and energetics) and other interfacial properties that can influence the ET efficiency.

Reference

1. (a) Allara, D. L.; Nuzzo, R. G., Spontaneously Organized Molecular Assemblies. 1. Formation, Dynamics, and Physical Properties of n-Alkanoic Acids Adsorbed from Solution on An Oxidized Aluminum Surface. *Langmuir* **1985,** *1* (1), 45-52; (b) Bain, C. D.; Evall, J.; Whitesides, G. M., Formation of Monolayers by the Coadsorption of Thiols on Gold: Variation in the Head Group, Tail Group, and Solvent. *Journal of the American Chemical Society* **1989,** *111* (18), 7155-7164.

2. Stolnik, S.; Dunn, S. E.; Garnett, M. C.; Davies, M. C.; Coombes, A. G. A.; Taylor, D.; Irving, M.; Purkiss, S.; Tadros, T. F.; Davis, S. S., Surface Modification of Poly (Lactide-Co-Glycolide) Nanospheres by Biodegradable Poly (Lactide)-Poly (Ethylene Glycol) Copolymers. *Pharmaceutical Research* **1994,** *11* (12), 1800-1808.

3. (a) Esplandiu, M.; Hagenström, H.; Kolb, D., Functionalized Self-assembled Alkanethiol Monolayers on Au (111) Electrodes: 1. Surface Structure and Electrochemistry. *Langmuir* **2001,** *17* (3), 828-838; (b) Chidsey, C. E. D.; Bertozzi, C. R.; Putvinski, T.; Mujsce, A., Coadsorption of Ferrocene-Terminated and Unsubstituted Alkanethiols on Gold: Electroactive Self-assembled Monolayers. *Journal of the American Chemical Society* **1990,** *112* (11), 4301-4306; (c) Eckermann, A. L.; Feld, D. J.; Shaw, J. A.; Meade, T. J., Electrochemistry of Redox-Active Self-Assembled Monolayers. *Coordination Chemistry Reviews* **2010,** *254* (15-16), 1769-1802.

4. (a) Uosaki, K.; Sato, Y.; Kita, H., Electrochemical Characteristics of A Gold Electrode Modified with A Self-assembled Monolayer of Ferrocenylalkanethiols. *Langmuir* **1991,** *7* (7), 1510-1514; (b) Chidsey, C. E. D., Free Energy and Temperature Dependence of Electron Transfer at the Metal-Electrolyte Interface. *Science* **1991,** *251* (4996), 919.

5. (a) Yao, X.; Yang, M. L.; Wang, Y.; Hu, Z., Study of the Ferrocenylalkanethiol Self-assembled Monolayers by Electrochemical Surface Plasmon Resonance. *Sensors and Actuators B: Chemical* **2007,** *122* (2), 351-356; (b) Voicu, R.; Ellis, T. H.; Ju, H.; Leech, D., Adsorption and Desorption of Electroactive Self-assembled Thiolate Monolayers on Gold. *Langmuir* **1999,** *15* (23), 8170-8177.

6. (a) Twardowski, M.; Nuzzo, R. G., Molecular Recognition at Model Organic Interfaces: Electrochemical Discrimination using Self-assembled Monolayers (SAMs) Modified via the Fusion of Phospholipid Vesicles. *Langmuir* **2003,** *19* (23), 9781-9791; (b) Twardowski, M.; Nuzzo, R. G., Phase Dependent Electrochemical Properties of Polar Self-assembled Monolayers (SAMs) Modified via the Fusion of Mixed Phospholipid Vesicles. *Langmuir* **2004,** *20* (1), 175-180.

7. Hosseini, A.; Collman, J. P.; Devadoss, A.; Williams, G. Y.; Barile, C. J.; Eberspacher, T. A., Ferrocene Embedded in an Electrode-Supported Hybrid Lipid Bilayer Membrane: A Model System for Electrocatalysis in a Biomimetic Environment. *Langmuir* **2010**, 5500-5507.

8. Xie, H.; Jiang, K.; Zhan, W., A Modular Molecular Photovoltaic System based on Phospholipid/Alkanethiol Hybrid Bilayers: Photocurrent Generation and Modulation. *Phys. Chem. Chem. Phys.* **2011,** *13* (39), 17712-17721.

9. Zhan, W.; Jiang, K., A Modular Photocurrent Generation System Based on Phospholipid-Assembled Fullerenes. *Langmuir* **2008,** *24* (23), 13258-13261.

10. Jiang, K.; Xie, H.; Zhan, W., Photocurrent Generation from Ru(bpy)(3)(2+) Immobilized on Phospholipid/Alkanethiol Hybrid Bilayers. *Langmuir* **2009,** *25* (18), 11129-11136.

11. Keller, C.; Glasmästar, K.; Zhdanov, V.; Kasemo, B., Formation of Supported Membranes from Vesicles. *Physical Review Letters* **2000,** *84* (23), 5443-5446.

12. (a) Borjas, R.; Buttry, D. A., Solvent Swelling Influences the Electrochemical Behavior and Stability of Thin Films of Nitrated Poly (styrene). *Journal of Electroanalytical Chemistry and Interfacial Electrochemistry* **1990,** *280* (1), 73-90; (b) Buttry, D. A.; Ward, M. D., Measurement of Interfacial Processes at Electrode Surfaces with the Electrochemical Quartz Crystal Microbalance. *Chemical Reviews* **1992,** *92* (6), 1355-1379.

13. Ha, T. H.; Kim, K., Adsorption of Lipid Vesicles on Hydrophobic Surface Investigated by Quartz Crystal Microbalance. *Langmuir* **2001,** *17* (6), 1999-2007.

14. (a) Meuse, C. W.; Niaura, G.; Lewis, M. L.; Plant, A. L., Assessing the Molecular Structure of Alkanethiol Monolayers in Hybrid Bilayer Membranes with Vibrational Spectroscopies. *Langmuir* **1998,** *14* (7), 1604-1611; (b) Plant, A. L., Self-assembled Phospholipid Alkanethiol Biommetic Bilayers on Gold. *Langmuir* **1993,** *9* (11), 2764-2767; (c)

Plant, A. L.; Brighamburke, M.; Petrella, E. C.; Oshannessy, D. J., Phospholipid/alkanethiol Bilayers for Cell-surface Receptor Studies by Surface Plasmon Resonance. *Analytical Biochemistry* **1995,** *226* (2), 342-348.

15. Katz, J. J., Green Thoughts in a Green Shade. *Photosynthesis Research* **1990,** *26* (3), 143-160.

16. Hurley, J. K.; Tollin, G., Photochemical Energy Conversion in Chlorophyll-containing Lipid Bilayer Vesicles. *Solar Energy* **1982,** *28* (3), 187-196.

17. Hubbard, J.; Silin, V.; Plant, A., Self-assembly Driven by Hydrophobic Interactions at Alkanethiol Monolayers: Mechanism of Formation of Hybrid Bilayer Membranes. *Biophysical Chemistry* **1998,** *75* (3), 163-176.

18. Shein, J. B.; Lai, L. M. H.; Eggers, P. K.; Paddon-Row, M. N.; Gooding, J. J., Formation of Efficient Electron Transfer Pathways by Adsorbing Gold Nanoparticles to Self-assembled Monolayer modified Electrodes. *Langmuir* **2009,** *25* (18), 11121-11128.

19. Krysiński, P.; Brzostowska-Smolska, M., Three-probe Voltammetric Characterisation of Octadecanethiol Self-assembled Monolayer Integrity on Gold Electrodes. *Journal of Electroanalytical Chemistry* **1997,** *424* (1), 61-67.

20. Jenkins, A. T. A.; Le-Meur, J. F., Lipid Vesicle Adsorption on Electroactive Self-assembled Monolayers. *Electrochemistry communications* **2004,** *6* (4), 373-377.

21. Rowe, G. K.; Creager, S. E., Redox and Ion-pairing Thermodynamics in Self-assembled Monolayers. *Langmuir* **1991,** *7* (10), 2307-2312.

22. Smith, C. P.; DWhite, H. S., Theory of the Interfacial Potential Distribution and Reversible Voltammetric Response of Electrodes Coated with Electroactive Molecular Films. *Analytical Chemistry* **1992,** *64* (20), 2398-2405.

23. Bertin, P. A.; Georganopoulou, D.; Liang, T.; Eckermann, A. L.; Wunder, M.; Ahrens, M. J.; Blackburn, G. F.; Meade, T. J., Electroactive Self-Assembled Monolayers on Gold via Bipodal Dithiazepane Anchoring Groups. *Langmuir* **2008,** *24* (16), 9096-9101.

24. Silin, V. I.; Wieder, H.; Woodward, J. T.; Valincius, G.; Offenhausser, A.; Plant, A. L., The Role of Surface Free Energy on the Formation of Hybrid Bilayer Membranes. *Journal of the American Chemical Society* **2002,** *124* (49), 14676-14683.

25. Imahori, H.; Azuma, T.; Ajavakom, A.; Norieda, H.; Yamada, H.; Sakata, Y., An Investigation of Photocurrent Generation by Gold Electrodes modified with Self-assembled Monolayers of C60. *the Journal of Physical Chemistry B* **1999,** *103* (34), 7233-7237.

26. Kuhn, H., Classical Aspects of Energy Transfer in Molecular Systems. *the Journal of Chemical Physics* **1970,** *53*, 101.

27. Alivisatos, A.; Waldeck, D.; Harris, C., Nonclassical Behavior of Energy Transfer from Molecules to Metal Surfaces: Biacetyl (nπ∗)/Ag (111). *the Journal of Chemical Physics* **1985,** *82*, 541.

28. Aoki, A.; Abe, Y.; Miyashita, T., Effective Photoinduced Electron Transfer in Hetero-Deposited Redox Polymer LB films. *Langmuir* **1999,** *15* (4), 1463-1469.

29. Matsuo, Y.; Kanaizuka, K.; Matsuo, K.; Zhong, Y. W.; Nakae, T.; Nakamura, E., Photocurrent-generating Properties of Organometallic Fullerene Molecules on An Electrode. *Journal of the American Chemical Society* **2008,** *130* (15), 5016-5017.

Chapter Five

Photocurrent Modulation by the Surface Dipole embedded in Hybrid Bilayer Membranes

5.1 Introduction

Continuing our exploration of lipid-bilayer based molecular photovoltaic systems[1], we report herein that polar alkanethiols included in these bilayers can significantly modulate the resulting photovoltaic responses. We further show that, despite their overall similar constructs and structures, cells using $Ru(bpy)_3^{2+}$ or malonic fullerene (C_{63}) as the photoagent display opposite modulation effects. These results not only allow us to make connections with the practice in organic electronic devices of using polar organic adsorbates to tune the work function of metals and hence the charge injection efficiency, but more importantly, they highlight the intricacy of orientated surface dipole in influencing organic photovoltaic processes, and its subtle interplay with other related factors, such as location, orientation and phase where the photoagents locate.

Of particular relevance is the research in organic light-emitting diodes and other related fields that employs polar organic adsorbates to tune the work function of electrode materials and

hence the charge injection barriers. The fundamental concept[2] here is the use of an organic layer to modify the potential difference of electrons inside and outside a metal, ζ, which is related to the metal work function (ϕ_m) by equation $\phi_m = \zeta - E_F$, where E_F is the Fermi level of the metal. The importance of ζ in affecting the work function of metals was recognized as early as in the 1930s, when a monolayer of alkali atoms was found to reduce ϕ_m of metals by more than half in studies of photoelectric effects[3]. These experimental observations made Bardeen realize that work function is essentially a surface property of a metal that is determined largely by its uppermost atomic layers[4]. In 1996, Campbell and coworkers[5] showed that thiols self-assembled on noble metals could be fruitfully used to systematically tune the work function of these metals. Generally, when a monolayer of thiols is absorbed on a metal, it will either attract or repel electron density from the underlying metal – depending the functional groups attached to and structure of the thiol. In doing so, it sets up a dipole (sometimes called an electrostatic double layer) at the metal/organic interface, which can, electrostatically, impede or ease the extraction of electrons from the metal, thus giving rise to a localized potential. The reason that such an interfacial dipole layer can affect the charge injection from/to organic materials layered further atop, which sometimes are macroscopic, is simply because it is set in the charge injection path. Owing to the ease of preparation and well-defined structures of self-assembled thiols on noble metals, this method has since then evolved into a versatile and powerful strategy[6].

Alkanthiol and perfluorinated alkanethiol of SAMs are known to form opposite dipole directions, which can be used to decrease or increase the work function of electrodes[7]. Wu and co-workers[8] studied a variety of different concentrations of *n*-decanethiol and perfluorinated decanethiol binary mixture SAMs on silver surface, and found that the mixed monolayer serve to tune work function of silver over a wide range by varying the surface composition of the mixed

SAM from 4.1 to 5.8 eV. They used SAMs modified Ag electrode to fabricate the anode of organic LED. It was shown that increasing the ratio of perfluorinated alkanethiol on the Ag surface increased the luminance efficiency that occurred at anode.

In this study, we set to find out how SAMs with well-defined dipoles may influence the photovoltaic responses of HBM systems by comparing C_{12} SAM and heptadecafluoro-1-decanethiol ($C_{10}F_{17}$SAM) (Figure 5.1). These models are one of the simplest models to look at this interesting interfacial phenomenon, with a single dipole layer sandwiched in between an electrode and a photoagent-assembled lipid monolayer. Our results confirm the general trend established by previous studies and in addition, suggest that the polarized photoagent is also involved in such process.

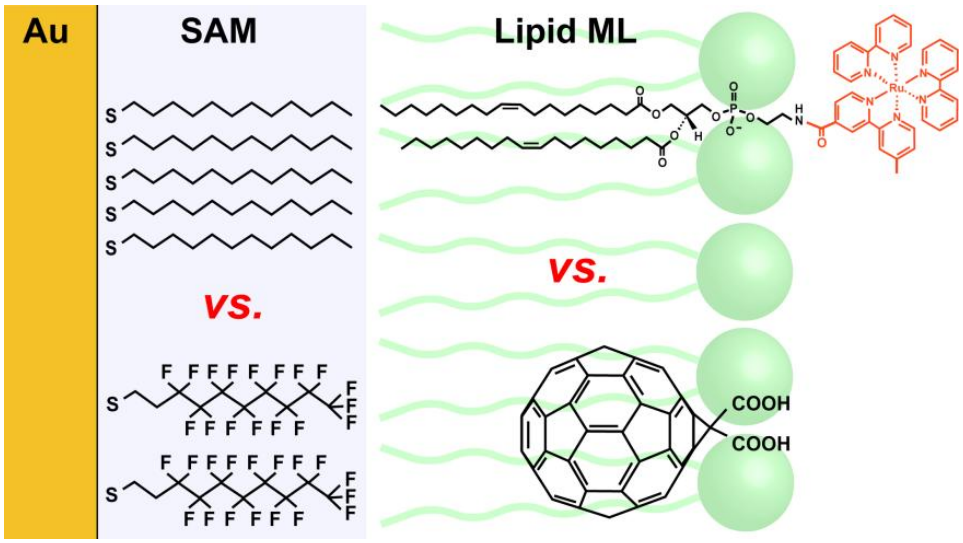

Figure 5.1 shows schematically the structure of lipid/thiol hybrid bilayers and photoactive agents used in this study.

5.2 Experimental Section

5.2.1 Chemicals

Phospholipids such as 1-palmitoyl-2-oleoyl-*sn*-glycero-3-phosphocholine (POPC) and 1,2-dioleoyl-*sn*-glycero-3-phosphoethanolamine (DOPE) were received from Avanti Polar Lipids. DOPE conjugated with $Ru(bpy)_3^{2+}$ ($Ru(bpy)_3^{2+}$-DOPE) and monomalonic fullerene (C_{63}) were prepared according to previously reported procedures[1a, 9]. Potassium hexacyanoferrate(III) ($K_3Fe(CN)_6$) and potassium hexacyanoferrate(II) ($K_4Fe(CN)_6$) were from Riedel-de Haën. Dodecanethiol, 1H,1H,2H,2H-perfluorodecanethiol ($CF_3(CF_2)_7(CH_2)_2SH$), 4-(2-hydroxyethyl) piperazine-1-ethanesulfonic acid (HEPES), methyl viologen dichloride hydrate (MV^{2+}), L(+)-ascorbic acid sodium salt, D-(+)-glucose, glucose oxidase (type X-S from *Aspergillus niger*) and catalase from bovine liver were obtained from Sigma-Aldrich. All solutions were prepared using 18.2 MΩ•cm deionized water (Millipore).

5.2.2 Preparation of SAMs and HBMs

The formation of SAMs on gold substrates was accomplished by immersing gold-coated substrates in 1 mM ethanol solution of alkanethiols at room temperature for at least 15 h. Prior to this step, the gold-coated substrates were thoroughly cleaned in piranha solution[10] (3:1, concentrated H_2SO_4 to 30% H_2O_2 solution, v/v) for 15 min, and rinsed by water and ethanol and dried by an argon stream. The SAM-modified gold substrates were carefully rinsed with ethanol and DI water, dried in argon, and immediately assembled in homemade Teflon cells to be used either for impedance analysis or photoelectrochemical measurements (see below). To form a lipid/alkanethiol hybrid bilayer, typically a 300 μL of phospholipid liposome solution of known concentration was added to the cell. Liposome samples were prepared by a extrusion-based method as detailed previously.[1] Before moving on to further measurements, the unbound vesicle

solution in a cell was replaced by HEPES buffer solution (10 mM HEPES, 100 mM Na_2SO_4, pH 7.7).

5.2.3 Impedance Analysis

All impedance measurements were carried out on a μAutolab Type III/FRA2 electrochemical impedance analyzer system (Metrohm Autolab B.V., Netherlands). The three-electrode setup contains gold substrates (with/without SAM or lipid/SAM bilayer covered) as the working electrode, a Pt wire counter electrode and a Ag/AgCl (KCl saturated) reference electrode. The impedance spectra were measured in the frequency range from 10 mHz to 10 KHz under an *ac* bias of 5 mV. The obtained impedance data were analyzed and fitted by the accompanying software, FRA 4.8, with fitting errors below ±5%.

5.2.4 Quartz Crystal Microbalance (QCM)

QCM measurements were performed on a QCM analyzer equipped with a 5 MHz crystal oscillator (Model QCM25, Stanford Research Systems) at room temperature. All the procedures are as same as in Chapter 4.

5.2.5 Calculation of Dipole Moments

Dipole moments of the neutral radicals of the employed thiol molecules were calculated by *ab initio* quantum chemistry techniques using Gaussian '09. Following a reported method,[10] we first optimized the structures of thiol molecules at Hartree-Fock level using a minimal STO-3G basis set; the hydrogen attached to sulfur was then removed and the dipole moments of the radicals were calculated using the 6-31G basis set.

5.2.6 Electrochemical and Photoelectrochemical Measurements

Electrochemical and photoelectrochemical measurements were carried out with a potentiostat (CHI 910B, CH Instruments) in the above Teflon cells that house three electrodes. Photovoltages and photocurrents were measured at the open circuit potential of each cell. The cells were irradiated with light from a Hg lamp (X-Cite, series 120 PC, EXFO) filtered at 470 ±20 nm for $Ru(bpy)_3^{2+}$-based devices (average intensity: 20 mW/cm^2) and at 417 ±30 nm for fullerene-based devices (average intensity: 40.0 mW/cm^2). A 50 mM ascorbate in HEPES buffer (10 mM HEPES, 100 mM Na_2SO_4, pH 7.7) was used as sacrificial electron donor in the anodic generation; oxygen was removed from the cells by adding 50 mM glucose, 50 units/mL glucose oxidase, and 200 units/mL catalase in the solutions. Under cathodic conditions, the electrolyte solutions contained 50 mM methyl viologen and 100 mM Na_2SO_4 in HEPES buffer.

5.3 Results and Discussion

5.3.1 Characterization of C10F17SH based Hybrid Bilayer Membrane

The blocking ability of C10F12 SAM and related hybrid structure was characterized by cyclic voltmmetry, which reveal behaviors similar to those based on *n*-alkanethiols (C_{12} SAM)[1a]. (Figure 5.2)

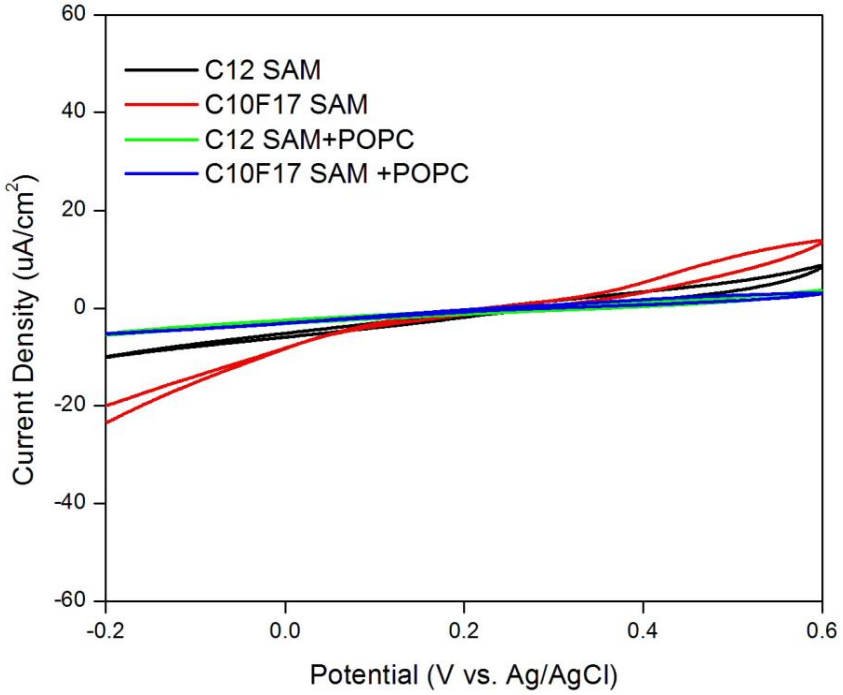

Figure 5.2 Voltammetric characterization of formation of C_{12} and $C_{10}F_{17}$ SAMs on gold electrodes. A deaerated solution containing 1 mM $Fe(CN)_6^{3+}$ in 0.1 M NaCl was probed with gold film electrodes covered with different SAMs. A three-electrode setup with a Ag/AgCl reference electrode and a Pt counter electrode was used; scan rate: 100 mV/s.

Impedance spectroscopy has been used to not only analyze the structures of HBM formed on either C_{12} SAM or $C_{10}F_{17}$ SAM, but also been used to evaluate the heterogeneous charge-transfer constant[11]. Figure 5.3 shows impedance spectroscopy of hybrid bilayer systems in the presence of equal molar $Fe(CN)_6^{3-}$ / $Fe(CN)_6^{4-}$. Randles circuit was used to fit the impedance data[12]. The C_{dl} of bare Au was 25.26 μFcm^{-2}. When Au was modified with C_{12} SAM or $C_{10}F_{17}$ SAM, the C_{SAM} were decreased to 1.52 μFcm^{-2} or 1.44 μFcm^{-2} respectively. C_{HBM} were decreased to 0.97 μFcm^{-2} and 0.81 μFcm^{-2} after lipid monolayer was fused to the SAM layer. According to equation reported in chapter 2, the C_{12} SAM layer has a thickness of 13.42 Å and $C_{10}F_{17}$ SAM layer is 12.92 Å. C_{12} SAM with 12 carbon chain length is not much longer than $C_{10}F_{17}$ SAM with

10 carbon chain length. Both of them can form comparable SAM layers on gold, which is also consistent with CV results. Also, the dielectric thickness of lipid layer can be calculated on C_{12} SAM to 8.92 Å and on $C_{10}F_{17}$ SAM to 12.92 Å. (Table 1).

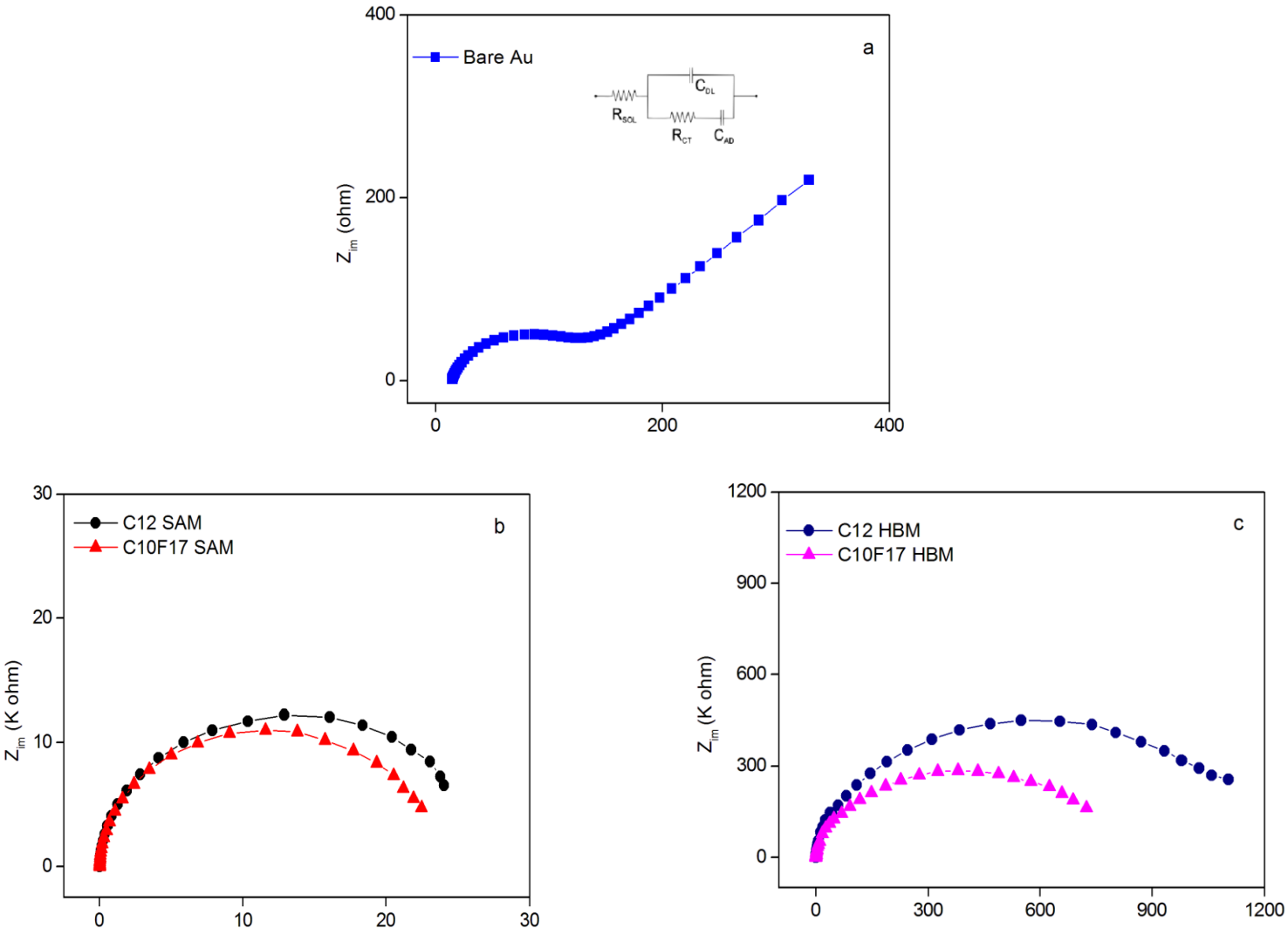

Figure 5.3 Nyquist plots of impedance spectroscopy on Bare Au, C_{12} and $C_{10}F_{17}$ SAMs and their HBMs on Au in the present of 1mM $Fe(CN)_6^{3-}/Fe(CN)_6^{4-}$ 100m M KCl in three electrodes setup with E_{dc} = 0.25 V vs. Ag/AgCl/KCl(sat.), and Pt as counter electrode. Randles equivalent circuit is used to fit the models.

Because the length of POPC is ~ 20Å (including 7Å for the head group and 13Å for the carbon tails)[13], the calculated dielectric thickness is shorter. In comparison the reduced apparent thickness suggest that POPC lipids on C_{12} SAM is an interdigitating conformation[14], while on $C_{10}F_{17}$ SAM, the interdigitation is not as much. The charge transfer resistance (R_{CT}) was obtained for the kinetic study. For the bare Au, R_{CT} is 90.1 Ω, indicating a mass-transfer control during the heterogeneous electron transfer process. When covered with SAM, its R_{CT} increased to 10^3 Ω ranges, adsorption by one lipid layer, its R_{CT} increases to 10^5 Ω ranges. These results indicate that HBMs block electron transfer much more than that by SAMs. The surface coverage was calculated by the equation [15]:

$$\Theta_{IS}^{R} = 1 - \left(\frac{R_{CT}^{bare}}{R_{CT}^{SAM}}\right)$$

The results show that the surface coverage was high enough to induce large decrease in apparent charge transfer constant ($k^{0\ app.}$), and it is dependent on the thickness of each layer (0.996 for both SAMs and 0.9998 for both HBMs). Using equation [16]:

$$K^{0app.} = RT/R_{CT}\ A\ C\ F^2$$

where R=8.314 *J mol* $^{-1}$K $^{-1}$;T= 298K; A= 1.13 cm^{-2} ; C = 10^{-6} mol cm^{-3}; F= 96485 Cmol $^{-1}$

$k^{0app.}$ is calculated in Table 8. The estimated apparent charge transfer constants suggest that the electron transfer of $Fe(CN)_6^{3-/4-}$ in both HBMs is an electron tunneling process[17]. In summary, both C_{12} and $C_{10}F_{17}$ HBM systems appears having comparable features that is worthy of further investigation.

Table 7. Capacitance of SAMs and HBMs with their calculated dielectric thickness

	[a]C_{SAM}: μF/cm^2	[b]dielectric thickness of SAM layer Å	[a]$C_{bilayer}$: μF/cm^2	[b]C_{lipid}: μF/cm^2	[b]dielectric thickness of lipid layer Å
C_{12}	1.52 ± 0.02	13.42	0.97 ± 0.01	2.68	8.92
$C_{10}F_{17}$	1.44 ± 0.01	12.92	0.81 ± 0.01	1.85	12.92

[a]measured values. [b]calculated values. ε values of 2.3, 2.1 and 2.7 were used for polyethylene[18], polytetrafluoroethylene and POPC monolayers in the calculation

Table 8. Calculation of charge transfer constant ($k^{0\ app.}$) and apparent coverage (θ_{IS}^{R})

	[a]R_{CT} Ω	[b]$k^{0\ app.}$ cm s^{-1}	[b]apparent coverage θ_{IS}^{R}
Bare Au	90.1	2.61 x 10^{-3}	
C_{12} HBM	8.97x 10^5	2.62 x 10^{-7}	0.9998
C_{12} SAM	25.14 x10^3	0.986 x 10^{-6}	0.996
$C_{10}F_{17}$ HBM	5.68x 10^5	4.15 x 10^{-7}	0.9998
$C_{10}F_{17}$ SAM	23.73x10^3	0.994 x 10^{-6}	0.996

[a]measured values. [b]calculated values.

5.3.2 Photoelectrochemistry

Figure 5.4 compares the anodic/cathodic photocurrents obtained from hybrid bilayers containing 2 mol% $Ru(bpy)_3^{2+}$-DOPE in the top POPC layer. In the anodic process, a photocurrent of ~60 nA/cm^2 was generated from bilayers having C_{12} SAM as the underlayer, whereas a higher current of ~160 nA/cm^2 was obtained when the underlying SAM is $C_{10}F_{17}SH$ instead. This difference in the anodic currents is not due to different loadings of $Ru(bpy)_3^{2+}$-DOPE on the two SAMs during the hybrid bilayer formation, as an opposite trend was seen from the cathodic photocurrents obtained from the same devices (dashed traces, Figure 5.4a). These responses indicate the photocurrent generation process is instantaneous and relatively stable in these systems. The photovoltages recorded from these devices display a similar trend, i.e., higher voltages accompany with higher currents, and lower voltages accompany with lower currents (Figure 5.4b); but unlike the photocurrents, they increase only gradually upon photoexcitation and cannot reach steady states in a given light on/off cycle (15 s). This sluggish behavior resulting from the technique used in the photovoltage measurement is operated under open-circuit conditions where no external current is allowed to flow. Thus, it shows that a dynamic response of charging/discharging processes respondes from photoexcitation. For example, the relatively steep rise of photovoltage as the light is just turned on reflects the fast initial accumulation of charges in the bilayer as a result of photoinduced electron transfer; as such a process continuously charges up the bilayer, the latter approaches its capacity, causing further charging to slow down.

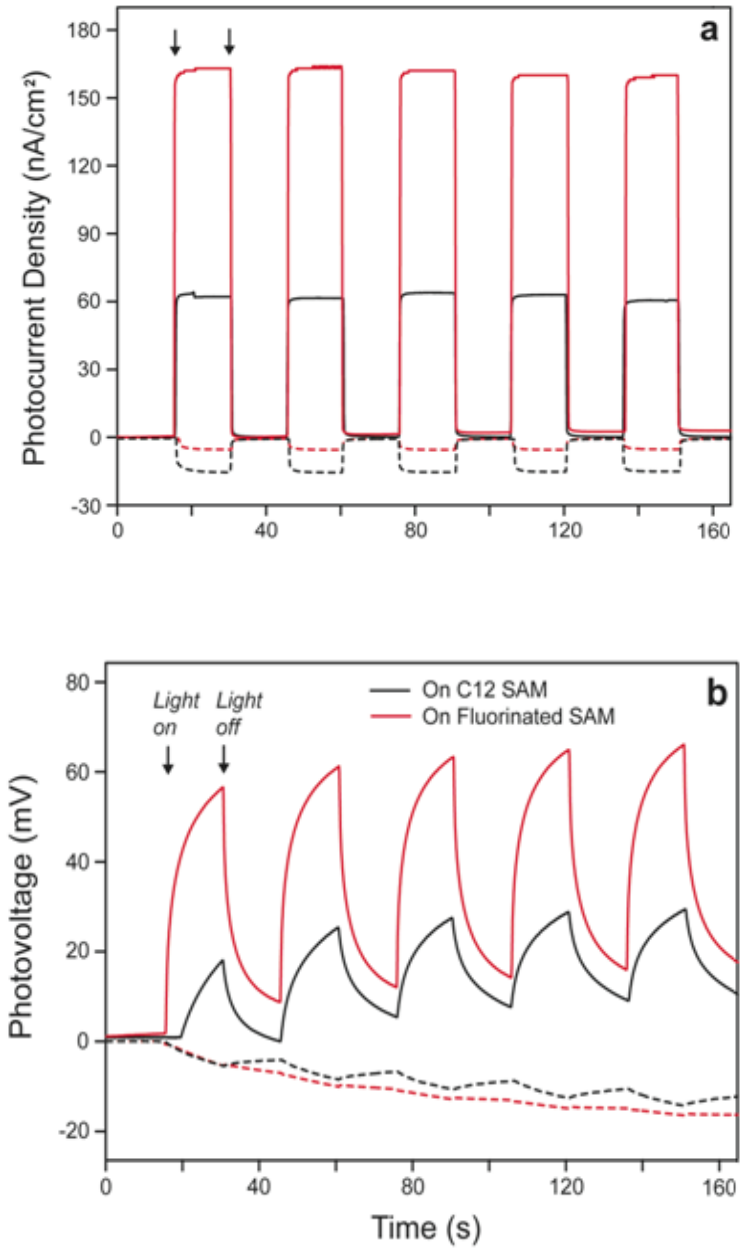

Figure 5.4 Photocurrents (a) and photovoltages (b) generated from 2% $Ru(bpy)_3^{2+}$-DOPE in POPC lipid monolayers on either C_{12} SH SAM (traces in black) or $C_{10}F_{17}$ SH SAM (in red).

When bilayers containing 2 mol% C_{63} in the top POPC layer are subjected to similar photocurrent/photovoltage generation, an opposite trend is observed (Figure 5.5). Here, a lower anodic current (i.e., 60 vs. 85 nA/cm^2) and a higher cathodic current (i.e., 18 vs. 10 nA/cm^2) is

obtained when $C_{10}F_{17}$ SAM replaces C_{12} SAM as the underlying layer in the bilayers. Photovoltages again follow photocurrents.

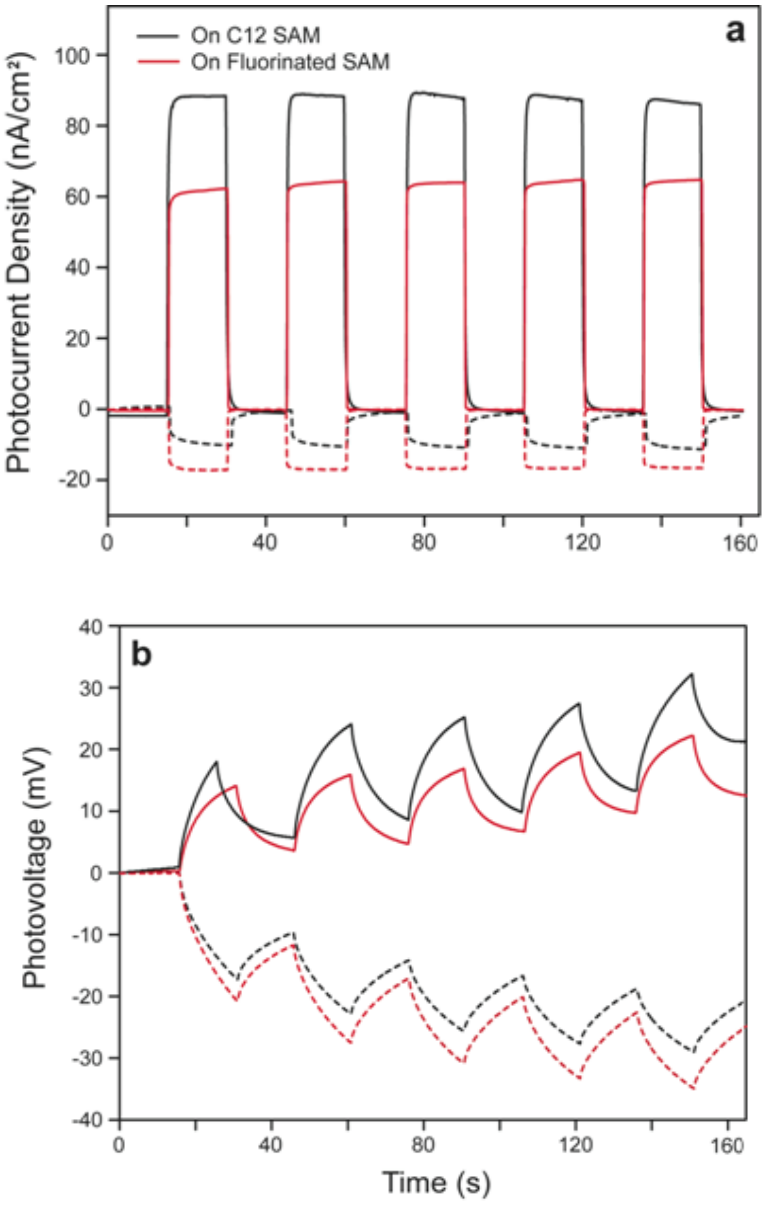

Figure 5.5 Photocurrents (a) and photovoltages (b) generated from 2% fullerene C_{63} assembled in POPC lipid monolayers on either C_{12} SAM (traces in black) or $C_{10}F_{17}$ SAM (in red). Here, the anodic photocurrents are marked by solid traces and the cathodic photocurrents by the dashed traces.

To understand the above modulation effects as well as the different trends of modulation displayed by the two photoagents, we analyzed the interfacial energetic levels of these bilayer structures. For organic electric devices governed by tunneling-based charge injection processes including the present system, the efficiency of hole (/electron) injection is mainly determined by the energy differences between the Fermi potential level of an electrode and the HOMO(/LUMO) levels of the organic layer[19]. As discussed in the Introduction, one exploitable strategy of minimizing the charge injection barriers and thus enhancing the injection efficiency is inserting a SAM layer between the interface of the organic material and the electrode. Depending on its dipole orientation versus the electrode, the SAM layer acts to shift up (or down) the effective vacuum energy level of the electrode, which makes the removal of electrons from the metal more (or less) energetically costly, resulting in an increase (or a decrease) in the effective work function of the metal. For the organic layer, the HOMO/LUMO levels will also be shifted by the inserted dipole layer, since its energy level related to the vacuum is changed.

Following solid-state physics convention, the HOMO/LUMO energies of $Ru(bpy)_3^{2+}$ are calculated from its first oxidation/reduction potentials[1a], respectively, and converted to absolute scale vs. the vacuum (i.e., potential of the latter is taken as 4.5 eV[16] vs. NHE). A value of 4.9 eV is used as the work function of gold under ambient condition[20]. This analysis was further shown by the calculated dipole moments of the two SAMs: 2.08 D for $C_{12}SH$ and −1.79 D for $C_{10}F_{17}SH$.

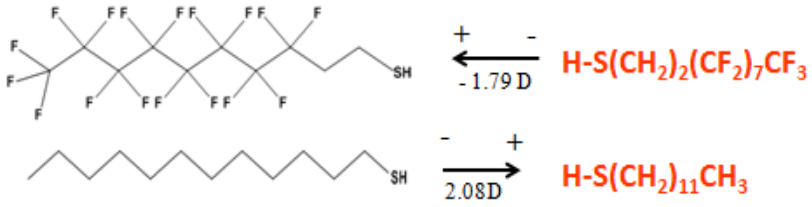

Upon formation of self-assembled monolayers on gold, these polar molecules will yield a collective dipole that contains a non-zero component normal to the gold surfaces. Bert de Boer et al.[21] used Kelvin probe to study the work function tuned by alkanethiol SAMs. From their report, it showed that $C_{10}F_{17}SH$ SAM could increase the work function of gold by 0.6 eV relative to the unmodified gold, whereas the oppositely polarized $C_{16}SH$ SAM effectively lowered the gold work function by 0.8 eV. In our case, we assumed that the shifted potentials of C_{12} SAMs were approximated by using data of C_{16} SAMs, which are taken into the depiction of energetics of $Ru(bpy)_3^{2+}$ based bilayer cells (Figure 5.6). As shown in Figure 5.6b, the C_{12} SAM in between the gold electrode and the $Ru(bpy)_3^{2+}$-containing lipid top layer brings down the HOMO/LUMO levels of $Ru(bpy)_3^{2+}$ in vacuum. In consequence, the gap between the LUMO level (4.0 eV) with the Fermi level of gold (E_F = 4.9 eV) is smaller, whereas the gap between the HOMO and the gold Fermi level is enlarged. These changes accordingly produce a smaller electron-injection barrier (EIB) and a larger hole-injection barrier (HIB) in C_{12} based hybrid bilayer structure. By contrast, the energy levels associated with $Ru(bpy)_3^{2+}$ will be shifted up when $C_{10}F_{17}SH$ is used to form the bilayers, which result in a smaller hole-injection barrier and a larger electron-injection barrier (Figure 5.6c). Ultimately, the underlying polar SAMs in these hybrid bilayers substantially modify the thermodynamic barrier for charge injection to occur, leading to a more efficient cathodic photovoltaic process (due to small EIB) in the case of C_{12} thiol and a facile anodic process (due to small HIB) for the fluorinated thiol.

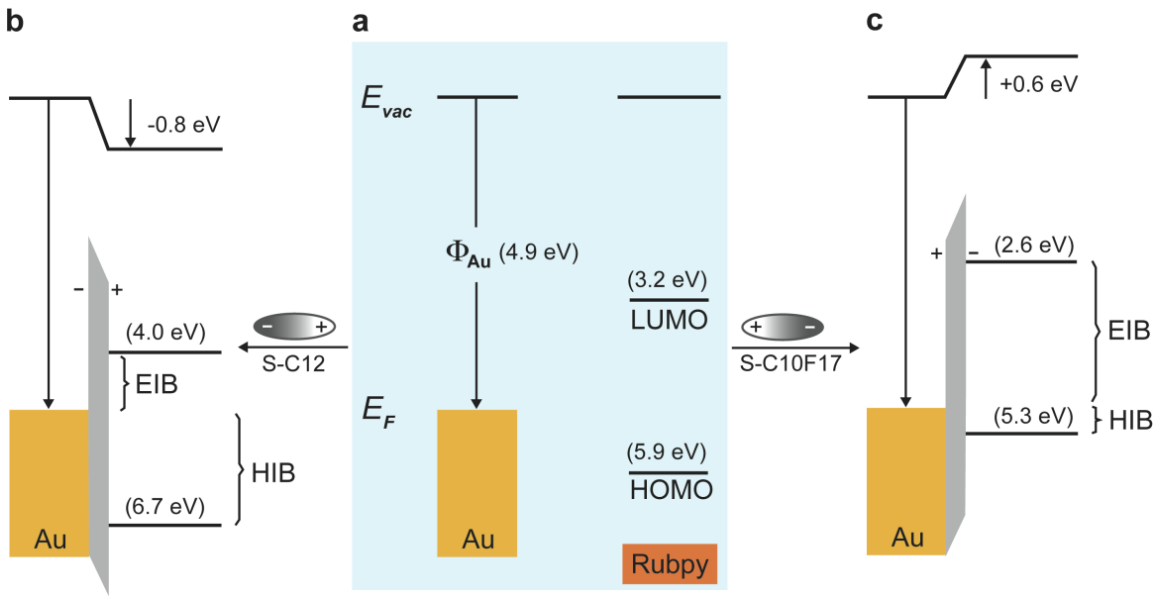

Figure 5.6 Energy diagrams of $Ru(bpy)_3^{2+}$-based photovoltaic systems. In panel a), the gold Fermi energy level (E_F) and the HOMO/LUMO levels of $Ru(bpy)_3^{2+}$ are separated in vacuum. b) Lowering of HOMO/LUMO levels of $Ru(bpy)_3^{2+}$ vs. E_F (Au) induced by the dipole of C_{12} SAM situated in between the electrode and the photoagent. c) Up shifting of HOMO/LUMO levels of $Ru(bpy)_3^{2+}$ vs. E_F(Au) induced by the dipole of $C_{10}F_{17}$ SAM situated in between the electrode and the photoagent.

Similar energy diagrams for C_{63} based hybrid bilayer membranes can be sketched by putting together the respective potential energy levels of each participating component. An immediate prediction that can be made for C_{12} SAM based cells is that a maximal cathodic photocurrent should be seen in this case as the estimated EIB approaches zero, i.e., $4.1 - (-0.8) = 4.9$ eV = E_F(Au) (the middle dashed line, Figure 5.7b). But the fact is that a higher cathodic

photocurrent is observed on $C_{10}F_{17}$ based HBM (Figure 5.5) rather than on C_{12} SAM, however, some other facts may be considered in such case.

In order to satisfactorily account for the opposite photovoltaic behaviors between $Ru(bpy)_3^{2+}$ and fullerene C_{63} in otherwise similarly hybrid bilayer strucutres, we further evaluated the organization, position and orientation of these two agents in the bilayers. In terms of organization, $Ru(bpy)_3^{2+}$ groups are directly linked to DOPE lipids via the amine head group, whereas fullerenes are incorporated into lipids noncovalently. As such, upon lipid assembling on the SAMs, the $Ru(bpy)_3^{2+}$ group is expected to take position at the top of the lipid monolayer facing the water/lipid interface. On the other hand, the malonic group on fullerene C_{63} renders amphiphicity to the sphere-shaped molecule, which should position itself within the surrounding hydrophobic lipid environment, so that the exposure of its hydrophobic bulk (or hydrophilic malonic group) to water (or lipid acyl chains) can be minimized. Recent experimental and simulation results support this analysis. For example, Bortolus et al.[22] found that several singly regio-derivatized fullerenes tend to occupy spaces right below the lipid/water interface in the lipid matrix. In addition, our recent study[1b] on photoinduced electron transfer in hybrid bilayers comprising lipids and ferrocene-terminated SAMs showed a stronger electronic coupling between C_{63} and underlying ferrocenes compared to the case of $Ru(bpy)_3^{2+}$. Thus, all the evidence indicates that, the lipid-associated fullerene C_{63} is situated closer to the SAM as well as the gold surface compared to $Ru(bpy)_3^{2+}$. Considering also the high molecular polarizability (e.g., the ground-state polarizability[23] of C_{60} is $10^{-24}cm^3$ [9]) of fullerenes, this data additionally indicates thus positioned C_{63} can directly experience the withdrawal of its electron density by the fluorinated thiols underneath, i.e., intermolecular polarization; whereas in case of $Ru(bpy)_3^{2+}$, the highly polarizable hydrocarbon chains (e.g., ~30 $Å^3$ for hexadecane[24]) of the lipids will largely

isolate the photoagent from being directly polarized by groups placed still under, i.e., the dielectric screening effect.

More importantly, these fullerenes are directionally oriented in the lipid monolayer, that is, the hydrophilic malonic group tends to point outwards whereas the fullerene bulk preferentially faces the SAM (as illustrated in Figure 5.1). Since the malonic fullerene itself is polar, it produces a non-zero dipole along the normal of the bilayer structure, with its negative pole being the malonic group. Oriented as such in the bilayer, these fullerenes will acquire a dipole potential that can impact the efficiency of the charge-injection processes. As previously observed by other workers,[25] this dipole-induced potential is absent from the potential determined by techniques such as cyclic voltammetry, which only gives macroscopic, orientation-averaged redox potentials of a target. Another fine point worth mentioning in comparing the dipole potentials originated from fullerene C_{63} and SAMs is: The dipole potential induced by the SAMs is global, meaning all components, as long as they are in close proximity to the SAM, will experience such polarization; whereas for fullerenes, because of their low concentration in the bilayer, their influence of polarization is largely localized and on themselves. This in no way implies that SAMs influence the overall charge injection process more strongly than the 2% fullerenes – Because the electron/hole transfer actually originate from these fullerenes, they are expected to shift the energy levels even more effectively.

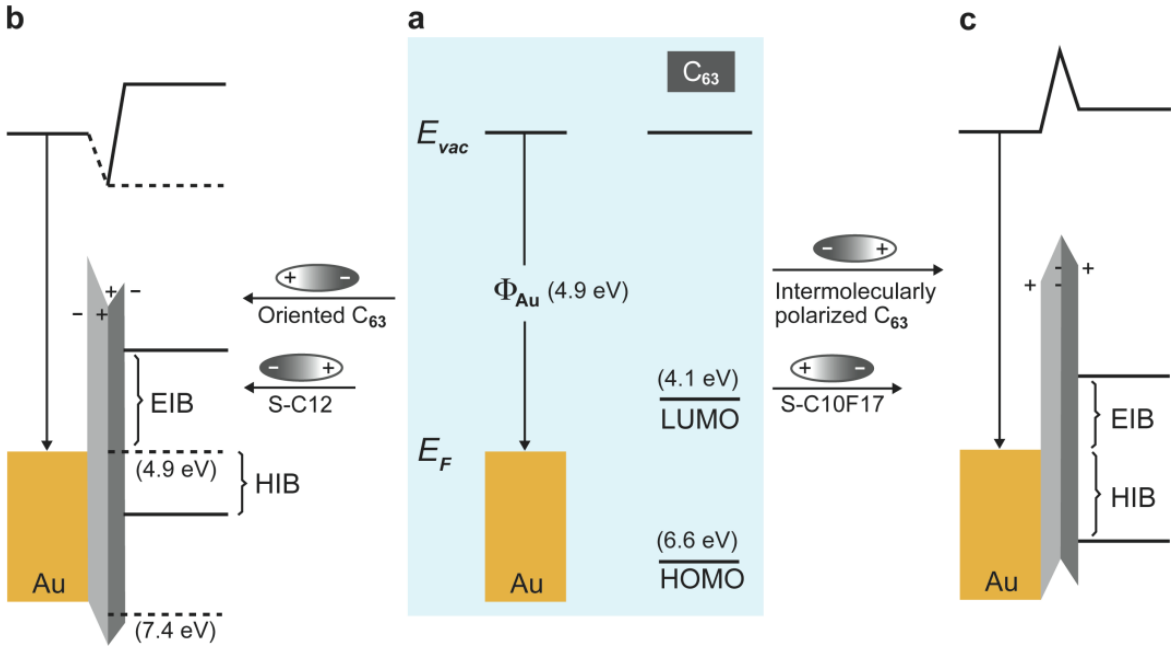

Figure 5.7 Energy diagrams of C_{63}-based photovoltaic systems. In panel a), the gold Fermi energy level (E_F) and the HOMO/LUMO levels of fullerene C_{63} are separated in vacuum. b) Shifting of HOMO/LUMO levels of C_{63} vs. E_F(Au) by a combined modification from the dipoles of C_{12} SAM and C_{63}, with one opposing the other. c) Shifting of HOMO/LUMO levels of C_{63} vs. E_F(Au) by the dipoles of $C_{10}F_{17}$ SAM and C_{63}, where fluoride atoms on the thiol attract electron density both intramolecularly and intermolecularly.

We have thus arrived at a scenario where the dipoles of the photoagent itself and the underlying SAM modify the charge-injection barriers together. As shown in Figure 5.7 b, the presence of the C_{63} dipole shifts the effective vacuum level upwards and in doing so compensates the energy lowering induced by the C_{12} SAM. The resulting EIB/HIB is nonzero. When $C_{10}F_{17}SH$ replaces C_{12} thiol in forming the bilayer, the close proximity between the

perfluorinated chain of the SAM and the buckyball, together with the high polarizability of fullerene, enable the fluorinated SAM to polarize the latter and thus reverse fullerene's direction of dipole moment in the bilayer. The net effect of this intermolecular polarization is a downshift of fullerene HOMO/LUMO levels as compared to the case of C_{12} SAM based bilayers and coming with it, a slightly decreased EIB and an increased HIB (Figure 5.7c), which ultimately lead to higher cathodic and lower anodic responses (Figure 5.5). In both cases, fullerene C_{63} functions as a depolarizer to offset the influence of the SAMs in affecting the charge injection.

5.3 Conclusions

We have found in this work that the intrinsic dipoles of alkanethiols can be used to modulate $Ru(bpy)_3^{2+}$-based photo-induced charge injection processes in alkanethiol/lipid based bilayer photovoltaic systems. These modulation effects can be explained by dipole-induced modification of work function of the metal substrates and hence the Shockley energy barriers[11,12] – a concept well established and broadly exploited in organic light-emitting diodes and field-effect transistors. Our investigation on fullerene C_{63} further revealed an opposite trend of photocurrent/photovoltage modulation, which can be understood from the intrinsic polarity of fullerene C_{63}, its high polarizability and deeper position in the bilayers. Together, our results reveal the intricacy of orientated surface dipole in influencing the photovoltaic processes, and its subtle interplay with other related factors, such as location, orientation and phase where photoagents locate. These findings may be of use in designing new thin-film based photovoltaic and organoelectronic systems.

Reference

1. (a) Jiang, K.; Xie, H.; Zhan, W., Photocurrent Generation from Ru(bpy)(3)(2+) Immobilized on Phospholipid/Alkanethiol Hybrid Bilayers. *Langmuir* **2009,** *25* (18), 11129-11136; (b) Xie, H.; Jiang, K.; Zhan, W., A Modular Molecular Photovoltaic System based on Phospholipid/Alkanethiol Hybrid Bilayers: Photocurrent Generation and Modulation. *Phys. Chem. Chem. Phys.* **2011,** *13* (39), 17712-17721.

2. Kao, K. C. Dielectric Phenomena in Solids. Elsevier Academic Press. San Diego, CA, 2004, Chapter 6.

3. Ives, H. E.; Olpin, A., Maximum Excursion of the Photoelectric Long Wave Limit of the Alkali Metals. *Physical Review* **1929,** *34* (1), 117.

4. Bardeen, J., Theory of the Work Function. ii. the Surface Double Layer. *Physical Review* **1936,** *49* (9), 653.

5. Campbell, I.; Rubin, S.; Zawodzinski, T.; Kress, J.; Martin, R.; Smith, D.; Barashkov, N.; Ferraris, J., Controlling Schottky Energy Barriers in Organic Electronic Devices using Self-assembled Monolayers. *Physical Review B* **1996,** *54* (20), 14321-14324.

6. Natan, A.; Kronik, L.; Haick, H.; Tung, R. T., Electrostatic Properties of Ideal and Non-ideal Polar Organic Monolayers: Implications for Electronic Devices. *Advanced Materials* **2007,** *19* (23), 4103-4117.

7. Tseng, C. T.; Cheng, Y. H.; Lee, M. C. M.; Han, C. C.; Cheng, C. H.; Tao, Y. T., Study of Anode Work Function Modified by Self-assembled Monolayers on Pentacene/Fullerene Organic Solar Cells. *Applied Physics Letters* **2007,** *91* (23), 233510.

8. Wu, K.-Y.; Yu, S.-Y.; Tao, Y.-T., Continuous Modulation of Electrode Work Function with Mixed Self-Assembled Monolayers and Its Effect in Charge Injection. *Langmuir* **2009,** *25* (11), 6232-6238.

9. Zhan, W.; Jiang, K., A Modular Photocurrent Generation System Based on Phospholipid-Assembled Fullerenes. *Langmuir* **2008,** *24* (23), 13258-13261.

10. Love, J. C.; Estroff, L. A.; Kriebel, J. K.; Nuzzo, R. G.; Whitesides, G. M., Self-assembled Monolayers of Thiolates on Metals as A Form of Nanotechnology. *Chemical Reviews* **2005,** *105* (4), 1103-1170.

11. Campuzano, S.; Pedrero, M.; Montemayor, C.; Fatas, E.; Pingarron, J. M., Characterization of Alkanethiol Self-assembled Monolayers Modified Gold Electrodes by Electrochemical Impedance Spectroscopy. *Journal of Electroanalytical Chemistry* **2006,** *586* (1), 112-121.

12. Eckermann, A. L.; Feld, D. J.; Shaw, J. A.; Meade, T. J., Electrochemistry of Redox-Active Self-assembled Monolayers. *Coordination Chemistry Reviews* **2010,** *254* (15-16), 1769-1802.

13. Silin, V. I.; Wieder, H.; Woodward, J. T.; Valincius, G.; Offenhausser, A.; Plant, A. L., The Role of Surface Free Energy on the Formation of Hybrid Bilayer Membranes. *Journal of the American Chemical Society* **2002,** *124* (49), 14676-14683.

14. Peng, Z.; Tang, J.; Han, X.; Wang, E.; Dong, S., Formation of A Supported Hybrid Bilayer Membrane on Gold: A Sterically Enhanced Hydrophobic Effect. *Langmuir* **2002,** *18* (12), 4834-4839.

15. Janek, R. P.; Fawcett, W. R.; Ulman, A., Impedance Spectroscopy of Self-assembled Monolayers on Au (111): Sodium Ferrocyanide Charge Transfer at Modified Electrodes. *Langmuir* **1998,** *14* (11), 3011-3018.

16. A.J. Bard, L.R. Faulkner., Electrochemical Methods, Fundamentals and Application, second ed., Wiley, New York, 2001.

17. Cui, X. L.; Jiang, D. L.; Diao, P.; Li, J. X.; Jia, Z. B.; Tong, R. T.; Wang, X. K., Assessing the Apparent Effective Thickness of the Supported Hybrid Bilayer Membranes consisting of Octadecanethiol and Phospholipid by AC Impedance Spectroscopy. *Journal of the Chinese Chemical Society* **1999,** *46* (4), 571-576.

18. Lanza, V. L.; Herrmann, D. B. *J. Polym. Sci.* **1958**, 28, 622-625

19. Kim, J.; Khang, D. Y.; Kim, J. H.; Lee, H. H., The Surface Engineering of Top Electrode in Inverted Polymer Bulk-Hetero Junction Solar Cells. *Applied Physics Letters* **2008,** *92*, 133307.

20. Rusu, P. C.; Brocks, G., Surface Dipoles and Work Functions of Alkylthiolates and Fluorinated Alkylthiolates on Au (111). *The Journal of Physical Chemistry B* **2006,** *110* (45), 22628-22634.

21. de Boer, B.; Hadipour, A.; Mandoc, M. M.; van Woudenbergh, T.; Blom, P. W. M., Tuning of Metal Work Functions with Self-Assembled Monolayers. *Advanced Materials* **2005,** *17* (5), 621-625.

22. Bortolus, M.; Parisio, G.; Maniero, A. L.; Ferrarini, A., Monomeric Fullerenes in Lipid Membranes: Effects of Molecular Shape and Polarity. *Langmuir* **2011**.*27*(20),12560-13568

23. Renge, I., Solvent Effects on the Absorption Maxima of Fullerenes C60 and C70. *The Journal of Physical Chemistry* **1995,** *99* (43), 15955-15962.

24. www.chemspider.com.

25. Wei, Q.; Tajima, K.; Tong, Y.; Ye, S.; Hashimoto, K., Surface-segregated Monolayers: A New Type of Ordered Monolayer for Surface Modification of Organic Semiconductors. *Journal of the American Chemical Society* **2009,** *131* (48), 17597-17604.

Chapter Six

Summary

6.1 Conclusions

This thesis focuses on studying molecular photovoltaic systems based on phospholipid/alkanethiol hybrid bilayer membranes using self-assembly methods. By incorporating photo-agents either ruthenium tris(bipyridyl) complexes or monomalonic fullerenes, we have successfully generated photocurrent from the models (Chapter 3). By setting the upper phospholipid monolayer to the same experimental condition, we demonstrated that the photocurrent and photovoltage can be controlled by different types of SAMs (Chapter 4&5).

We investigated several analytical methods to study the formation of hybrid bilayer membrane, and demonstrated that both un-substituted alkanthiol SAMs and functionalized SAMs can provide hydrophobic environment for liposome adsorption, rapture and formation of lipid monolayers. However, there is no easy method to directly study the HBM structure. For directly study the HBM structure, more advantaged techniques need to be applied, such as AFM probe in aqueous media[1]. Those are future works.

We have successfully demonstrated a new photocurrent-generation system constructed on the photo-agents incorporated HBM. This system has important technical advantages over the supported lipid bilayers for building artificial photosynthetic systems[2]. By forming a HBM on an

Au electrode, it allows the electrochemical properties of each layer to be tailored separately, so a higher performance on photoconversion can be achieved. Then, a number of improvements have been made to the current system to investigate the photo-induced electron transfer mechanism. We embedded ferrocene into this HBM system and found a modulation effect of photocurrent, which was depended on the distance between the photo agents and ferrocene groups. We also demonstrated that the intrinsic dipole effect of alkanthiols can affect the photo-induced charge injection in the HBM system. These modulation effects can be successfully explained by dipole-induced modification of work function of the metal substrates and hence the Shockley energy barriers[3]. Besides the dipole effect, our results also reveal that the subtle influences by other related factors, such as location, orientation and phase where photo-agents positions may influence the charge transfer rate.

There are still several issues existing in this system. First, because this model is in aqueous media, several aspects such as solvent effect, ion adsorption, double layer formation at the electrode/electrolyte interface may limit its efficiency for photo-induced electron transfer. Second, the orientation of the donor-acceptor in molecular lever is hard to control. The percentage of photo-agent was controlled at the beginning step of liposome preparation. How it is distributed into the liposome and how much exactly quantity involved in the HBM system remains to be determined. Third, during the photo-conversion process in anodic condition, we used a glucose oxidase/ catalase oxygen scavenging system to get rid of oxygen in the system. However, enzyme can non-specifically adsorb on the lipid monolayer, which may introduce another electron transfer pathway to influence the efficiency. However, by continuous study this system, other group members have made several improvements. For example, a degassing system was designed instead of enzyme system, which demonstrated to be more stable and

reproducible. A tandem cell was investigated to build a more advanced photosentizer-donor-acceptor system to improve higher photoconversion efficiency.

6.2 Future Work

Hybrid bilayer membrane will continue to play an important role to investigate electron transfer within biological membranes. More recently, Ma et al[4]. reported the reversible inter-conversion between NADH and NAD^+ at a low overpotential by ubiquinone embedded HBM to mimic the initial stages of respiration in plants, which provided new insights into the mechanism of biological redox cycling. Hosseini et al[5] presented another HBM sytem to study proton-coupled electron transfer (PCET) by controlling the proton flux . Within this system, oxygen reduction by an iron porphyrin was used as a model PCET reaction. By using this system, they observed a different catalytic behavior than obtained by simply changing the pH of the solution in the absence of an HBM.

To fully tap its potential in artificial photosynthesis, our ultimate goal is to build natural photosensitized dye[6] and redox protein immobilized HBM system to fundamental understand the photosynthesis in nature and efficiently capture and store the solar energy.

Reference

1. Meuse, C. W.; Krueger, S.; Majkrzak, C. F.; Dura, J. A.; Fu, J.; Connor, J. T.; Plant, A. L., Hybrid Bilayer Membranes in Air and Water: Infrared Spectroscopy and Neutron Reflectivity Studies. *Biophysical Journal* **1998,** 74 (3), 1388-1398.

2. Li, Y. X. L. Y. X.; Chen, Y. L.; Wang, L.; Fang, Y. P., Ion Transport through A Porphyrin-terminated Hybrid Bilayer Membrane. *Electrochimica Acta* **2011,** *56* (3), 1076-1081.

3. Sushko, M. L.; Shluger, A. L., Dipole-dipole Interactions and the Structure of Self-assembled Monolayers. *Journal of Physical Chemistry B* **2007,** 111 (16), 4019-4025.

4. Ma, W.; Li, D. W.; Sutherland, T. C.; Li, Y.; Long, Y. T.; Chen, H. Y., Reversible Redox of NADH and NAD^+ at a Hybrid Lipid Bilayer Membrane Using Ubiquinone. *Journal of the American Chemical Society* **2011**.133 , 12366–12369

5. Hosseini, A.; Barile, C. J.; Devadoss, A.; Eberspacher, T. A.; Decreau, R. A.; Collman, J. P., Hybrid Bilayer Membrane: A Platform to Study the Role of Proton Flux on the Efficiency of Oxygen Reduction by a Molecular Electrocatalyst. *Journal of the American Chemical Society* **2011**,133, 11100–11102

6. Liu, L.; Zhan, W., Molecular Photovoltaic System Based on Fullerenes and Carotenoids Co-assembled in Lipid/Alkanethiol Hybrid Bilayers. *Langmuir* **2012**, 28, 4877–4882